Air Force Institute of Technology
AFIT Scholar

3-11-2011

Adaptive Imaging Methods using a Rotating Modulation Collimator (RMC)

Daniel T. Willcox

Follow this and additional works at: https://scholar.afit.edu/etd

Part of the Nuclear Commons

ADAPTIVE IMAGING METHODS USING A

ROTATING MODULATION COLLIMATOR

THESIS

Daniel T. Willcox, Lieutenant, USN

AFIT/GNE/ENP/11-M20

DEPARTMENT OF THE AIR FORCE

AIR UNIVERSITY

AIR FORCE INSTITUTE OF TECHNOLOGY

Wright-Patterson Air Force Base, Ohio

APPROVED FOR PUBLIC RELEASE; DISTRIBUTION UNLIMITED

The views expressed in this thesis are those of the author and do not reflect the official policy or position of the United States Air Force, the Department of Defense, or the United States Government. This material is declared a work of the U.S. Government and is not subject to copyright protection in the United States.

ADAPTIVE IMAGING METHODS USING A

ROTATING MODULATION COLLIMATOR

Presented to the Faculty

Department of Engineering Physics

Graduate School of Engineering and Management

Air Force Institute of Technology

Air University

Air Education and Training Command

In Partial Fulfillment of the Requirements for the

Degree of Master of Science in Nuclear Engineering

Daniel T. Willcox, BS

Lieutenant, USN

March 2011

AFIT/GNE/ENP/11-M20

ADAPTIVE IMAGING METHODS USING A

ROTATING MODULATION COLLIMATOR

Daniel T. Willcox, BS

Lieutenant, USN

Approved:

Maj Benjamin Kowash (Chairman)	Date
Ronald F. Tuttle, PhD (Member)	Date
Richard K. Martin, PhD (Member)	Date

AFIT/GNE/ENP/11-M20

Abstract

The Rotating Modulation Collimator (RMC) belongs to a larger class of radiation imaging systems that rely on either temporal or spatial modulation of incident radiation through collimation to map the location of the incident radiation source. The strengths of these detection systems include their low cost and simplicity. A major drawback is the collection time required for low radiation intensities due especially to the loss of radiation information resulting from collimation. One method of addressing this drawback for the RMC is by applying an adaptive imaging approach. As with most system design theory, there are inherent design tradeoffs for the RMC. By using different RMC configurations for the same radiation environment observation, these tradeoffs can be wagered against one another to improve overall performance. This research explores the effect of RMC configuration changes, specifically by changing the mask design, sampling method, and the angle between the image plane and the RMC centerline.

Acknowledgements

This research represents contributions from far too many people to name individually. Anything of substance and real value can be attributed to others contributions while any short comings belong to the author alone. I would like to express appreciation to my advisor for his constant guidance and enthusiasm toward this research. I would also like to express my great appreciation to my wife and daughter for all their sacrifices throughout the course of this research.

<div align="right">

-Daniel T. Willcox

</div>

Table of Contents

List of Figures

x

List of Tables

Adaptive Imaging Methods using a Rotating Modulation Collimator

I.   Introduction

The world in which we live thrives on connections. Be it via internet, transoceanic flight, or simple public transportation these avenues connect neighborhoods, communities, countries and continents. These avenues have also redefined relationships in both personal and professional circles. People, goods, and currency travel on these global and local connections with more ease, frequency, and intensity than at any time in history. These increases in dynamic exchanges force the practice of radioactive material accountability to become even more diligent and effective. In April 2010 a misplaced Co-60 source from the Delhi University Chemistry Department in India was found at a salvage yard after one man died and 8 others suffered from the effects of high radiation exposure. While the source originated at the university, school officials were not aware of the gamma source in the equipment found in the salvage yard [1]. As the traffic of radiation materials increases, both authorized and otherwise, the need for detection systems that can be employed in a variety of environments and with materials that are both easily accessible and affordable increases.

The problem of tracking and maintaining strict accountability of authorized radioactive materials and detecting, locating, and identifying unauthorized radioactive materials is not solved by one radiation detection system. The Department of Homeland Security uses an array of systems in the hopes that a tiered approach will have the versatility and flexibility to maintain accountability and thwart adversary efforts to harm US interests [2]. The Rotating Modulation Collimator (RMC) has been explored as an option to aid in stand-off detection of radiation

1

sources [3]. The RMC is a radiation imaging technique first developed to image far field high energy photons in space without the use of focusing lenses or a position sensitive detector [4]. The intricate principles behind the RMC technique are outlined in chapter 2. The "research RMC" designed by Kowash for stand-off detection successfully applied the RMC technique to image radiation sources in various scenarios [3]. The research completed to date has not only shown the feasibility of the system but uncovered areas that can be further exploited to improve not only the RMC as an option to the stand-off radiation source problem but also other modulation image reconstruction methods as well. This research focuses on applying adaptive imaging techniques to the research RMC to improve the system response to radiation.

I. A. Objectives

The research for this thesis focuses on applying adaptive imaging techniques to a research Rotating Modulation Collimator (RMC). These techniques can be broken into three distinct areas but can be combined to achieve maximum performance:

1. Determine the effect of alternative RMC transmission function sampling techniques. The traditional sampling technique used with the research RMC involves a near continuous rotation in which the position and count number from the detector are recorded at nominal intervals of 0.5 degrees of collimator rotation. This data is then sorted into 1 degree bins, resulting in 360 uniform samples. One alternative sampling technique is to look at the effect of decreasing the number of uniform samples from 360 to allow for a longer duration at each sample angle. Additionally, irregular sampling using fewer than 360 samples is explored. Rather than uniform spacing between samples, irregular sampling samples at random whole degree locations. The desirable effect of increasing the dwell time at each sample angle is the improved counting statistics.

2. Determine the effect on position resolution and RMC absolute detection efficiency of changing the degree of modulation through the masks by altering the mask design parameters. Traditional masks used with the research RMC have had rectangular slits with a slit width equal to half the pitch. The slit shape is changed to a trapezoid and a variety of slit widths are explored while keeping the slat width constant at 0.1 in.

3. Determine the effect of pivoting the RMC on the position variance through the application of *a priori* Cramer-Rao Lower Bound (CRLB) of the position variance. The CRLB provides a maximum performance indicator for an unbiased estimate, and is constant for a fixed

3

RMC system configuration. By pivoting the centerline of the RMC with respect to the origin of the image plane, the position estimate of the variance should follow the CRLB of the position variance.

I. B. Thesis Overview

This thesis is divided into five chapters. The first chapter has provided a brief introduction into some applications of the RMC along with the research objectives.

The second chapter discusses the theory associated with general RMC operations and the theory behind the image reconstruction used with the research RMC. Also included is the pertinent theory used to investigate the research objectives, mainly sampling theory, mask design, and the development of the CRLB on the position estimate variance. Included in the second chapter is a section on the Structural Similarity (SSIM) index. The SSIM is a full-reference image comparison technique developed by Zhou Wang used to measure the relative performance of reconstructed images [5].

The third chapter includes a description of the RMC and processing equipment used in the research along with discussions relating to the experimental processes used for each of the research objectives. Included are explanations of the sources used and calibration processes required prior to executing the experimental processes.

The fourth chapter includes the calibration results, the alternative sampling results, the various mask design results, and the RMC pivot results. Each of these areas presents the results along with an analysis of the pertinent details.

The fifth chapter summarizes the major results of the research and presents areas in which future work with the RMC is recommended.

4

II.   Theory and Background

This chapter discusses the theory relevant to the RMC and the background for adaptive techniques of interest for this thesis. A brief overview of the basic operating principles behind the RMC and a few examples of past applications are provided. The focus is concentrated on three areas of adaptive imaging using the RMC. The adaptive rotation section explores different sampling methods used in the data collection and response of the RMC. This discussion begins with the theory that explains the detector's response and how the RMC response is then used to compute an estimate of the source location and activity. All of the methods are discrete but vary in the number of sampled points, the fixed or random interval between sampling locations, or both. This discussion includes the strengths and weaknesses of each of these methods and when their application might be more beneficial to our RMC application. In the adaptive pivot section a degree of freedom is introduced allowing for the entire detection system to alter its angle relative to the desired image plane. This will include a discussion of how the knowledge of the RMC system response allows for pivot adjustments which in turn change the reconstructed results.   The adaptive mask section explores the theory behind selected mask designs and how their implementation aides in our adaptive approach when different mask combinations are used. Finally, a method for reconstructed image comparison is presented as a tool to compare the results of reconstructed images from various RMC system configurations. This comparison tool is essential when attempting to compare differing RMC system configurations imaging identical radiation scenes. When approaching adaptive methods, this comparison tool allows for benchmarks to be created which provide an indication of a needed change of the RMC system. Through the

5

collection process as these benchmarks are reached and RMC system configuration changes in response to reconstructed image, the collection and reconstruction process becomes adaptive.

II. A. Rotating Modulation Collimator

RMC systems belong to a larger class of radiation imaging systems known as mechanically collimated imaging systems. Mechanically collimated imaging systems are able to determine the location of incoming radiation by systematically collimating the radiation through any number of means. This class of radiation imaging systems includes pin-hole, coded aperture, and the RMC to name a few. While certain mechanically collimated systems are designed quite simple, a critical inherent design tradeoff exists between detection efficiency and the information content received through temporally varied collimation [6].

First developed by astrophysicists in the 1960s as an alternative to using focusing lenses or position sensitive detectors, Mertz is credited with the RMC's development to image cosmic radiation scenes from space [7]. More recently the RMC has been adapted to help solve the orphan source problem associated with standoff detection posed by the Department of Homeland Security in 2008 and in the medical imaging field as part of Neutron Stimulated Emission Computed Tomography (NSECT) [3] [8]. The premise of a rotating modulation collimator is that a non position sensitive detector is able to determine the position of a photon source by rotating a pair of aligned masks that modulate the intensity of the radiation source. Mask design is discussed in detail in II.4.A, but in short each mask is designed to allow a fraction of the incident photons to transmit through mask openings unobstructed. If the masks are perfectly aligned and

6

have identical designs, the reconstructed image will be duplicated about a line of symmetry. As the collimator including the mask pair is rotated, the fraction of photons allowed to transmit through the collimator to the detector varies as shown in fig. 1. Each position in the field of view of the RMC varies the transmission of photons through the collimator uniquely. Multiple methods have been used to solve the inverse problem of image reconstruction based on the collected data. A few examples are CLEAN, Fourier, and Bessel Functions methods [9] [10]. The method used in this research estimates the position using the Maximum Likelihood-Expectation Maximization (ML-EM) method by matching the measured transmission function to an ideal transmission function, an example of which is shown in fig 1.(b). The transmission function will be discussed in further detail in section II.B.1 and the ML-EM will be addressed in section II.2.B. While the RMC technique was initially applied generically to photons, this research will focus specifically on gamma ray radiation and will consider all sources as gamma sources for the remainder of the thesis.

7
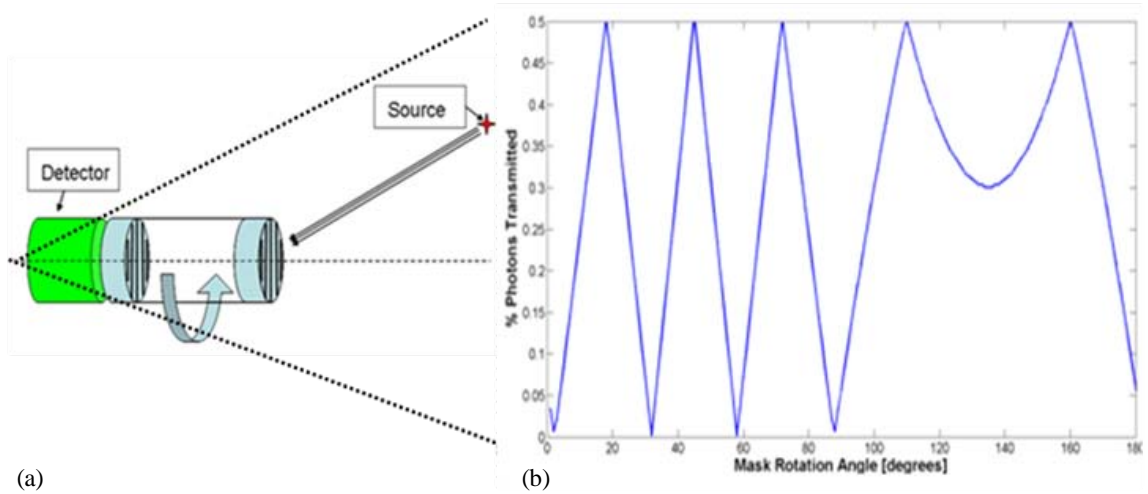
Fig. 1. (a) An overhead view of how an RMC uses a detector without position sensitivity to image the location of a photon source based on the rotation of the collimator. As the collimator rotates the masks allow a different ratio of photons incident the detector to transmit through the collimator to the detector. Provided is a plot of the ratio of transmitted photons vs the collimator rotation angle (b). The plotted result is referred to as the transmission function.

II. B. Adaptive Rotation

This section discusses the background behind the adaptive rotation techniques investigated in this research. Initially the discussion is focused on how the transmission function is generated by the RMC and how it is then used to reconstruct an image. This information is important for all RMC operations, as it provides the necessary foundation of RMC image generation. Adaptive rotation refers to changing the rotation of the collimator in response to collected data. Because the discrete sampling of the transmission function is entirely dependent on the physical rotation of the collimator, this section could just as well be titled adaptive sampling. For clarity, the term adaptive rotation will be used to retain a physical sense of what is being sampled. A discussion of different discrete sampling methods of the transmission function concludes this section.

II. B. 1. Transmission Function Generation

The transmission function for the RMC refers to the number of gammas transmitted through the paired masks of the collimator as a function of collimator rotation angle. As the paired masks rotate together, the number of gammas transmitted unperturbed through the masks changes with the angle of rotation. As a gamma source is observed for a full rotation, the transmission function formed is then used to compute an estimate of the gamma source location and activity based on knowledge of the system response contained in a library of previously computed noiseless transmission functions for each possible position of the source. It is widely known that the decay of radioactive materials can be modeled accurately as a Poisson stochastic process in which each decay event occurs continuously and independently from one another [11]. The equation for the

9

number of counts detected at a particular collimator position from transmission function

of the prototype RMC detector used in this research is

$$y_n = \tau_n \left[\alpha \cdot \varepsilon(E) \cdot \frac{\Omega}{4\pi} \cdot \left[P_n + (1 - P_n) \cdot \lambda(E) \right] + b(E) \right]. \qquad (2.1)$$

This represents the number of counts y at the nth collimator angular orientation for

a dwell time of τ and is dependent on the energy dependent detector efficiency $\varepsilon(E)$,

source activity α, the solid angle from the source incident the detector Ω, the probability

of the a gamma ray transmitting through the masks at the nth angle P_n, the attenuation

factor λ, and the energy dependent background effect $b(E)$ [3]. According to (2.1), for a

collection with a constant background and source activity and a stationary source, the

only change from one angle of rotation to another is the P_n term which is dependent on

the mask design. More specifically, P_n is dependent on the area of the detector face that

is exposed to the source. Figure 2 depicts this relationship between the exposed detector

face to the incident radiation source and the number of counts received at an nth angle of

rotation. The seven points selected are the local minimums and maximums through the

first 180 degrees of rotation. The images below the transmission function provide a sense

of how the masks' geometry determines the exposed detector area. It is important to

note, the masks are assumed to block all radiation incident to the solid portions of the

masks. This is a valid assumption based on the low energy gammas (122 keV) and the

mask material attenuation properties used in this research presented in section II.4.A.
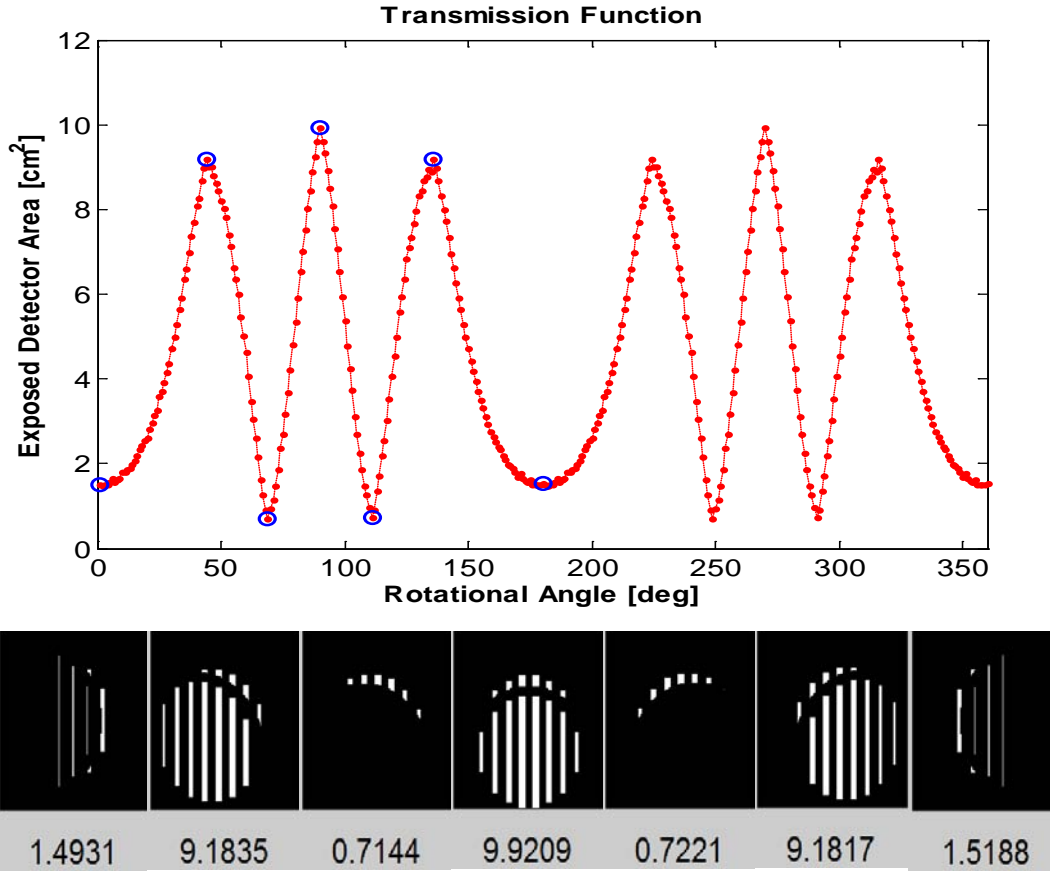
Fig. 2. This shows a plot of a transmission function (top) with seven points circled within the first 180 deg of rotation. The corresponding exposed detector images are shown (bottom) with their calculated exposed areas in cm^2. This shows the relationship of the exposed detector face relative to the source to the number of counts y from (2.1).

Consider a three dimensional space that includes the detector and a gamma source, where the position of the source is (x,y,z) with z as the known distance between the detector and the source as depicted in fig. 3. The source location in the x-y image plane is unknown. A transmission function is collected by the RMC after an observation period in which the collimator is rotated discretely with a fixed step interval and a fixed dwell time. Figure 3 displays the relationship between the source position and the frequency and phase of the generated transmission function.

11
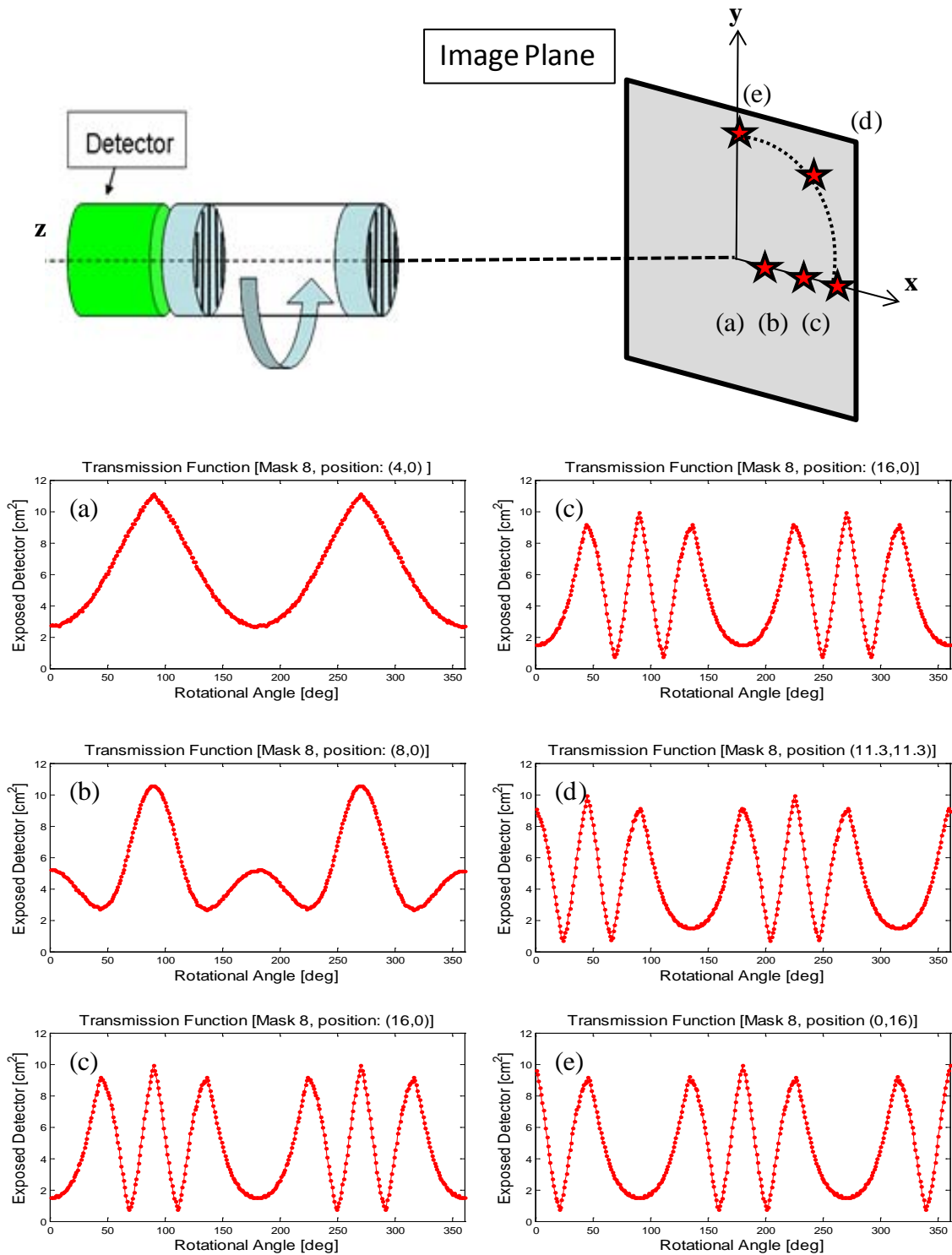
Fig. 3. This shows how the frequency of the transmission function increases as the distance between the source and the RMC centerline increases (a through c) and how the phase of the transmission function shifts based on the degree of rotation from the x axis of the image plane (c through e).

12

Figure 3 provides a detailed development the effect of the source location on the phase and frequency of the transmission function. The relationship can be succinctly shown in fig. 4. The distance away from the centerline determines the frequency of the transmission function and the angle of rotation from the x axis determines the phase of the transmission function. It is recognized that using a polar coordinate system may provide a less cumbersome discussion, but recognizing that all computations were completed using the Cartesian coordinate system, it will remain as the coordinate system of choice for consistency purposes.
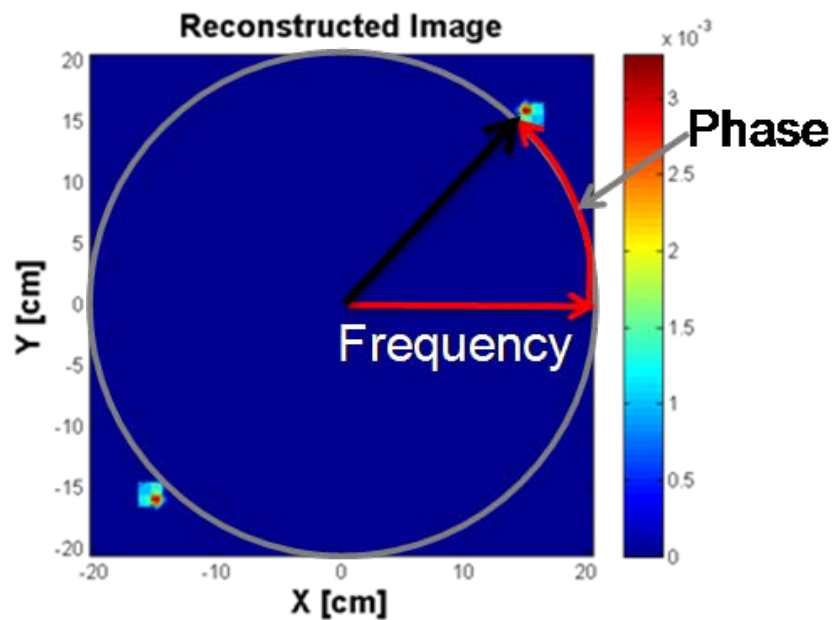
Fig. 4. This is an example of a reconstructed image using two identical masks which results in the source position to be reconstructed not only at its position but also at its mirror or symmetric location as well. The centerline of the RMC orthogonally intersects the origin of the image plane at the origin. It also shows the relationship between the phase and frequency of the transmission function and the source position [12].

13

A few interesting points can be made concerning this relationship. In section II.4.B, the field of view for the RMC is provided, which bounds the limits of the image plane. The maximum frequency expected of a sampled transmission function is easily determined by the field of view and knowledge of the system response for a given RMC configuration. This will be helpful to remember in discussing sampling techniques in section II.2.C.

Figure 3 and 4 provide a host of ideal transmission functions with their respective source locations in the image plane. It also shows a few of the physical source parameters manifest in the associated transmission function. Both figures show the frequency increase as the source is moved radially and the phase shift as the source is rotated from the horizontal axis. The effect of the source distribution is not considered for this research because the same source was used for all measurements and the point source approximation is valid for a disk with a 1 cm diameter over 300 cm away from a detector face with a 7.62 cm diameter. Another effect not shown in figure 3 or 4 is the effect that background has on the transmission function. Provided that the background is constant during the observation of the source, the entire transmission function will simply shift vertically according to the background intensity. Time varying background rates are beyond the scope of this research but may need to be incorporated for applications outside the lab environment. The observation period required to develop a transmission function with both a distinct phase and frequency to compare to the library of transmissions functions is dependent on the parameters from (2.1).

II. B. 2. Image Reconstruction

Upon collection of an "observed" transmission function, the next step is the application of the statistical bootstrap routine. The bootstrapping routine is an iterative process that provides an "averaged" transmission function from a number of created "pseudo" transmission functions. These "pseudo" transmission functions are generated based on the observed data. It is important to note the "observed" transmission function is not the transmission function that is used in the reconstruction process. The "observed" transmission function is nothing more than the summation of the independent transmission functions for every rotation of the collimator. This provides an opportunity to apply a statistical bootstrapping routine in an effort to accurately account for the distribution information available for a single sample angle. For example, fig. 6 (a) shows an "observed" transmission function taken over 150 seconds with ten full rotations. To simplify the example, the points between 120 and 140 are circled for further inspection. Figure 6(b) shows these twenty points with their associated ten independent observations, one for each full collimator rotation. Due to background and the stochastic properties of radioactive decay, not every observation at a given sample angle is equal. To create a "pseudo" transmission function from the example in Fig. 6, ten values, representing the ten rotations, are selected with replacement for each sample angle. One "pseudo" transmission function represents a possible transmission function based on the collected data distribution of each sample angle. To accurately account for the distribution for all sample angles, multiple "pseudo" transmission functions are generated. Once all the "pseudo" transmission functions are generated, their average is calculated, and the "averaged" transmission function is used for further reconstruction.

15

(a)

Observed Transmission Function (150 sec)

(b) **Observed Transmission Function Contributions for each full Rotation**
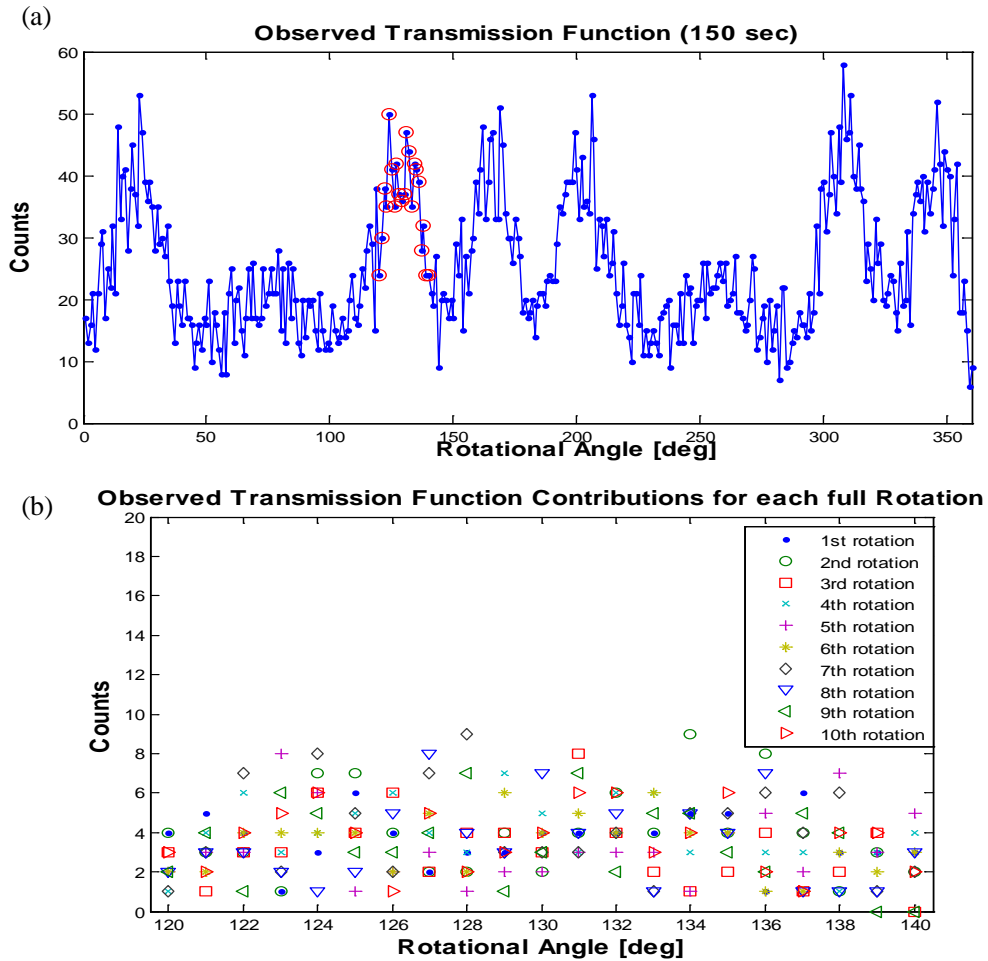
Fig. 5. **(a) This is an example of an observed transmission function, which is the summation of each independent observation at a specific angle for each collimator rotation. The circled points between 120 and 140 degrees provide an example of the summation results for the corresponding sample angles below (b). For this example the observation time was 150 secs, corresponding to 10 full rotations. The statistical bootstrap routine uses the multiple independent observations at each sample angle to more accurately represent the available distribution information in the averaged transmission function.**

Having computed an "average" transmission function, the next step is to reconstruct the image estimate. Having completed the bootstrap routine, the data will simply be referred to as the transmission function. Kowash discusses a few of the benefits of using different estimation methods for computing estimates for source

16

position and activity based on the collection of noisy observations [3]. By using the

Maximum Likelihood Estimate (MLE) of the transmission function given the observed

data, a source position and source activity can be estimated.

The MLE is defined for this problem as,

$$\hat{\theta}_{ML} = \arg{}_{\theta} \max L\left(\underline{y}_n \mid \underline{\theta} \right). \tag{2.2}$$

$\hat{\theta}_{ML}$ represents the parameter values for $\underline{\theta}$ (activity and position in this case) that

maximize the log likelihood L of the transmission function y_n from (2.1). L is defined as

the log likelihood function of the probability density function of y_n given $\underline{\theta}$,

$$L = \ln \left[p\left(\underline{y}_n \mid \underline{\theta} \right) \right]. \tag{2.3}$$

In other words it answers the question, "What value of $\underline{\theta}$ (which contains the

source position and activity parameters) results in the greatest probability of a

transmission function being generated matching the collected data?" The MLE is often

used for obtaining practical results. It can be easily applied to complex estimation

problems and is asymptotically Gaussian, unbiased, and efficient for large enough data

records [13]. While the MLE works for estimating multiple parameters, it becomes either

computationally expensive or altogether impossible to compute the likelihood maximum

using a mapping or first derivative method. The first derivative method fails when a

closed form solution is unattainable, which then requires a mapping of the log likelihood

function L. A search of this map for the maximum accounts for the computationally

expensive drawback. However, an alternative is available. The method of parameter

(source activity and position) estimation used in this research is the Maximum Likelihood

Expectation Maximization (ML-EM). It is an iterative method that is guaranteed to

17

converge albeit to a local maximum in some instances and has a positivity constraint for activity estimates. Various forms of the ML-EM algorithm can be used and for this research the following form was used,

$$\underline{\lambda}_{new} = \underline{\lambda}_{old} .* \left[\underline{\underline{A}}' \cdot \left(\underline{y} ./ \underline{\underline{A}} \cdot \underline{\lambda}_{old} + \underline{b} \right) \right] ./ \underline{a}. \tag{2.4}$$

The new image estimate following a given iteration is $\underline{\lambda}_{new}$. The previous image estimate is $\underline{\lambda}_{old}$ and is equal to unity for the first iteration. The system matrix is $\underline{\underline{A}}$, which along with its transpose $\underline{\underline{A}}'$, comprise the known system response for a given RMC configuration. The transmission function data and recorded background activity are $\underline{y}$ and $\underline{b}$ respectively. Finally a normalization parameter $\underline{a}$ is added to provide stability to the iterative method [3]. The .* and ./ indicate the multiplication and division operations are applied elementally. To help clarify the dimensions of the variables from (2.4), the equation is rewritten with the variables removed and replaced by their equivalent dimensions in column row format;

$$\left[N_p \times 1 \right] = \left[N_p \times 1 \right] .* \left(\left[N_p \times N_s \right] \cdot \left(\left[N_s \times 1 \right] ./ \left[N_s \times N_p \right] \cdot \left[N_p \times 1 \right] + \left[N_s \times 1 \right] \right) \right) ./ \left[N_p \times 1 \right]. \tag{2.5}$$

N_p is the total number of pixels in the image plane and N_s is the total number of samples of the transmission function. The .* and ./ indicate the multiplication and division operations are applied elementally.

There are two different iterations set by the user during image reconstruction; one for the number of bootstrap routines to complete and one for the number of ML-EM iterations to complete. While the number of iterations selected certainly will change the

18

results of the reconstructed image, results can be compared across the board by fixing these iteration parameters.

II. B. 3. Sampling Methods

There are various ways to sample the transmission function by altering the rotational profile of the RMC. Sampling theory is a complex and deep field of study, however, a few simple techniques have been explored for this research to determine whether more efficient sampling provides similar quality position estimates using a shorter measurement time. Figure 7 includes generic examples of the sampling techniques explored on a continuous signal.
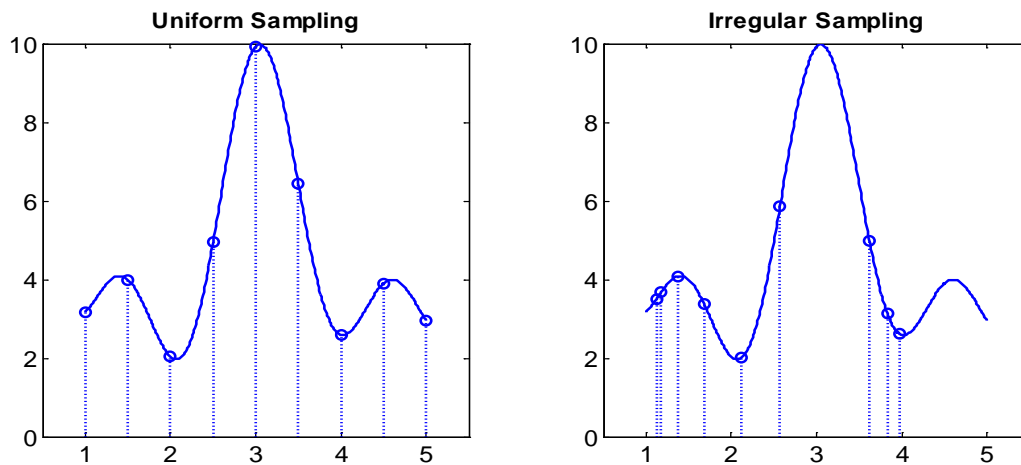
Fig. 6.   This is an example of a uniformly sampled signal (l) and an irregularly sampled signal (r). The irregularly sampled signal shows the potential to have two sample locations much closer together than the uniformly sampled signal with the same number of observations which can help in identifying higher frequency components of the signal but is also susceptible to under sampling certain regions of the signal.

19

The Nyquist rate,

$$f_N \equiv 2 \cdot f_{\max},$$ (2.6)

 determines the lower bound on the sampling rate and is based on sampling at least twice the highest frequency component $f_{\max}$ of the continuous signal. Sampling below the Nyquist rate can introduce aliasing artifacts that distort the digitized waveform from its continuous form. Uniform sampling, applies to the RMC in two ways. Uniform discrete sampling involves rotating the collimator a fixed distance and dwelling for a fixed amount of time. This is repeated until an entire revolution or multiple revolutions are complete. Uniform continuous sampling is sampling at a constant rate, while the RMC continues rotation. This is the method of sampling the transmission function that has been applied for most RMCs presented in literature [3] [4] [8].

Another method is irregular sampling which involves sampling at random intervals between consecutive sample locations as shown by the generic example in fig. 7. Using a collimator rotating discretely with a fixed step and fixed dwell time, radiation scenarios that are difficult to detect would require long collection times to statistically strengthen the sample transmission value at a given rotation angle. By applying the Whittaker- Shannon sampling theorem, which uses the Nyquist Sampling rate as a sampling constraint, we can reduce the collection time by sampling at twice the maximum frequency of the signal, which is equivalent to the field of view of our detector as discussed in section II.4.B [14]. The reduction in the sampling number has two significant benefits that become apparent with an example. Figure 8 shows the transmission functions from a 30 second collection using three different sampling methods. The first two are uniformly sampled with 360 and 20 samples respectively with

20

the same total collection time. The third is irregularly sampled with 20 samples. Because the counts for each sample are Poisson distributed, the standard deviation is,

$$\sigma = \sqrt{x}. \qquad (2.7)$$

Where x is the number of counts recorded at a sample location. The lower plot in fig. 8 shows how the standard deviation for the reduced sample sizes greatly increases the distinction between the minimums and maximums of the transmission function. The sample size of 360 suffers from overlapping standard deviations throughout the transmission function, resulting in ambiguous transmission functions as the source is moved throughout the image plane.

21
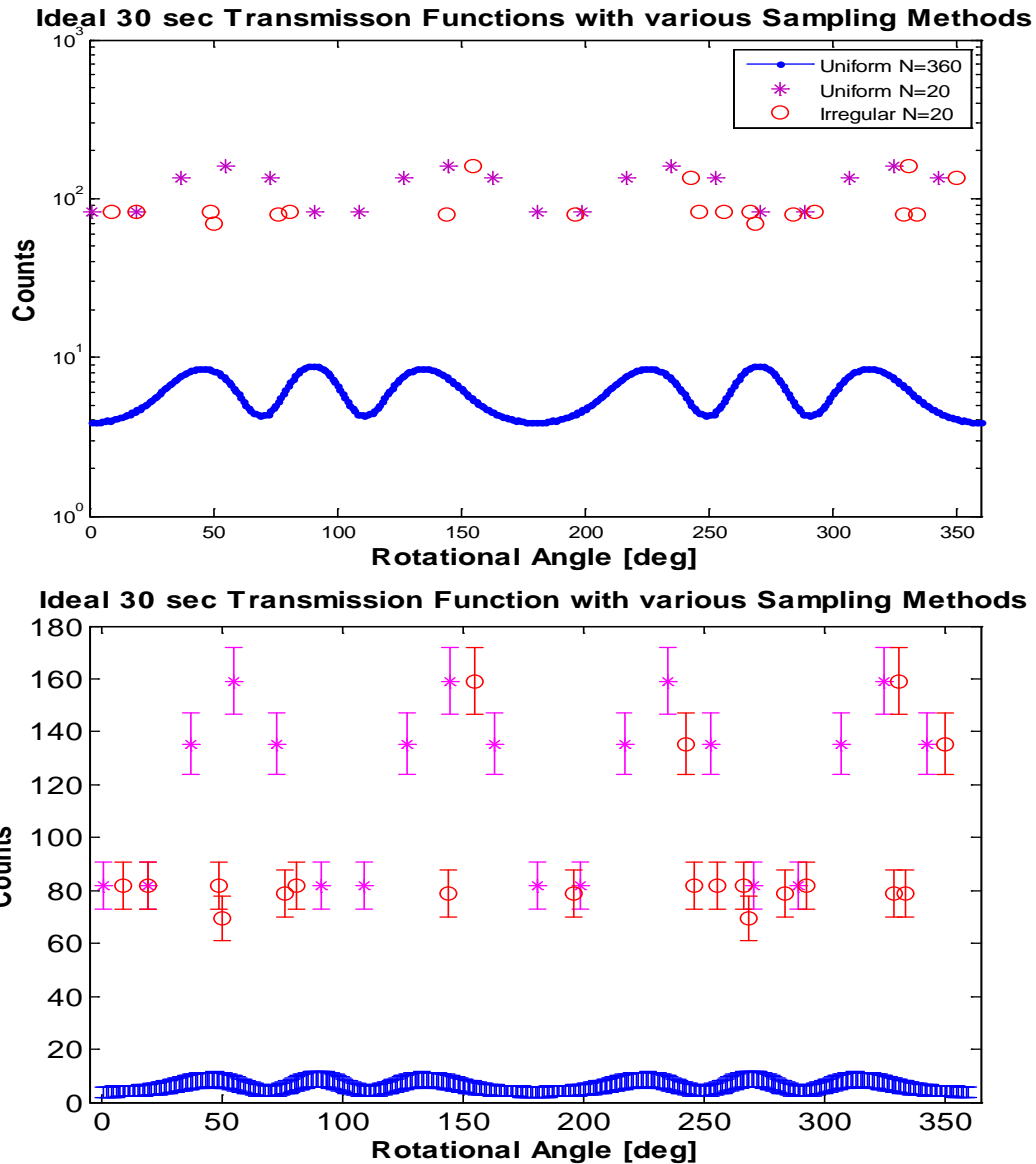
Fig. 7. These plots show three different sampling methods used with the same collection time. The top plot shows the ideal transmission function for each sampling method on a semi log scale. The bottom plot shows the effect of reducing the number of samples for a fixed collection time provides greater distinction between the peaks and valleys of the transmission function. The method using 360 samples have error bars that essentially overlap throughout the function, resulting in ambiguous transmission functions.

22

II. C. Adaptive Pivot

This section discusses an adaptive pivoting method which takes advantage of the RMC system response information gained by computing a mapping of the Cramer Rao lower bound on the variance.

II. C. 1. RMC centerline pivot

The ability to pivot the detector not only introduces an additional degree of freedom which allows for expanded field of view but has the added benefit of potentially improving the reconstructed image by altering the source location relative to the centerline of the RMC by altering the pivot angle of the RMC. Figure 9 illustrates the detector and source location relationship as the RMC pivot angle is adjusted.
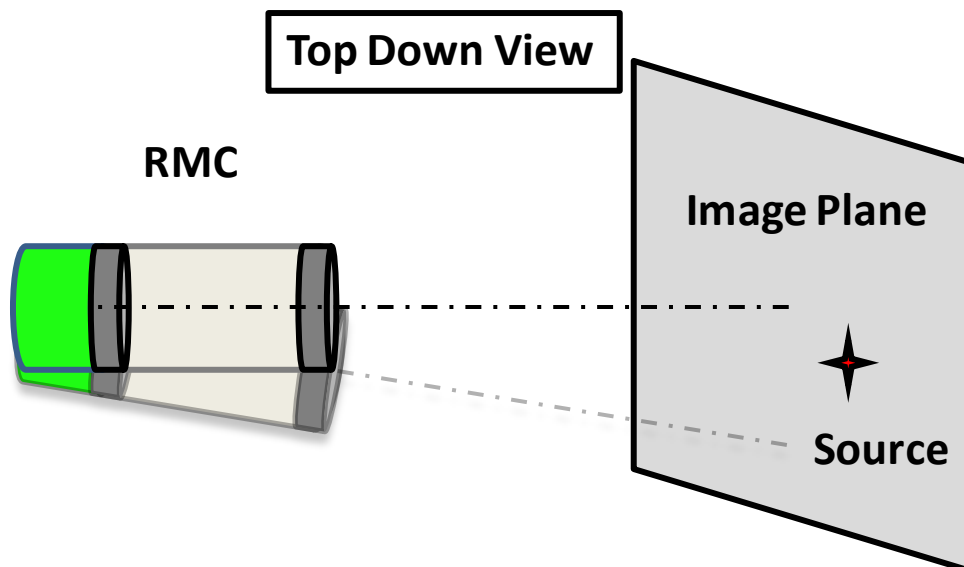
Fig. 8. **This shows an overhead view of how the pivot angle relative to the image plane is adjusted to place the radiation source in a different location relative to the centerline of the detector. Adjusting the pivot angle left or right will also slightly change the distance from the detector to the image plane.**

23

II. C. 2. Cramer-Rao lower bound (CRLB) on position variance

The Cramer-Rao Lower Bound (CRLB) on the variance of the parameter estimate was calculated for the system. The CRLB represents an ideal potential for any estimate of the parameter. For our work our parameter estimate will include both position and activity, which results in a covariance matrix that includes the individual CRLB on the variance for the position and activity individually. Moreover, it represents the lowest variance an unbiased estimator can achieve and provides a benchmark for comparison. While the total error is a combination of the bias and variance, the CRLB provides the lowest achievable variance without any bias. This is not to say, however, that a biased estimate cannot have a lower variance. The CRLB for our problem is derived as,

$$CRLB \equiv \mathrm{cov}\left(\underline{\hat{\theta}}\right) \geq I\left(\underline{\theta}\right)^{-1}$$

$$I\left(\underline{\theta}\right) = \left(-E\left[\frac{\partial^2}{\partial \underline{\theta}^2} L\right]\right)$$

$$L = \ln\left[p\left(y_n \mid \underline{\theta}\right)\right]$$

$$CRLB \equiv \mathrm{cov}\left(\underline{\hat{\theta}}\right) \geq \left(-E\left[\frac{\partial^2}{\partial \underline{\theta}^2}\ln\left[p\left(y_n \mid \underline{\theta}\right)\right]\right]\right)^{-1} \quad (2.8)$$

The Fisher information $I(\theta)$ is defined as the negative expectation of the second derivative of the log likelihood function L [13]. It is important to note that the CRLB is specific to a given RMC configuration.

As previously discussed the radioactive decay process can accurately be modeled as a Poisson random process. The Fisher Information is a quantitative way of measuring the amount of information that an observable random variable carries about an unknown parameter upon which the probability of the random variable depends [13]. For this application that is simply a measurement of the information content the transmission

24

function has about the source position and activity. Because the CRLB is dependent on the Fisher Information, the two are closely related.

The CRLB for RMC systems has some unique features that are worth discussing. In Kowash's study of the CRLB for various RMC configurations he found the Fisher Information of the position estimates were not uniform within the field of view. Subsequently, the CRLB was also not uniform. Figure 10 shows examples of the CRLB of the position variance maps for various RMC configurations. The concentric rings show that the information content of the RMC increases when the source is located in a band of high intensity compared to the regions of lower intensity. Using this information, an initial image can be reconstructed to determine if the RMC is attempting to locate a source in a relative position known to have a high variance based on the CRLB map. By pivoting the detector to the left or right, to a relative location of lower variance the position variance of the reconstructed image decreases.
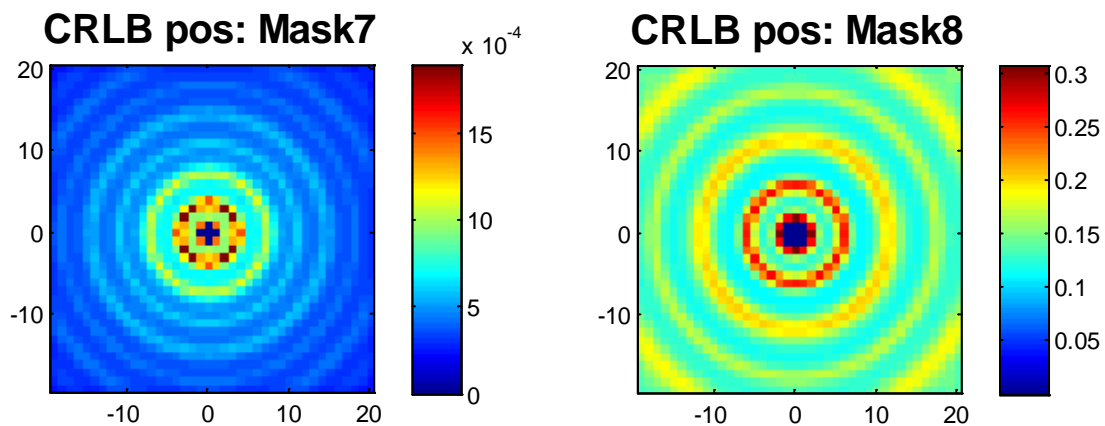
Fig. 9.   Two sample maps of the Fisher Information for the prototype RMC showing concentric circles of intensity. This graphically shows the motivation behind developing an adaptive pivoting method that will be able to increase the information used in the estimate by pivoting the detector to place the radiation source in a ring of higher intensity [3].

25

II. D. Adaptive Mask

This section discusses the effect of the mask designs on the RMC system response and subsequent transmission function generation. The material and geometric properties of these masks determine the efficacy of the RMC at imaging differing radiation environments. By understanding the tradeoff between position resolution and detection sensitivity, masks designed around these competing requirements offer two distinct capabilities.

II. D. 1. Basic Mask Design

From (2.1) P_n is the probability a gamma emitted isotropically from a radiation source is incident on the top mask of the RMC and then successfully passes through the open slits before arriving at the front face of the detector. The physics which determine whether a gamma will be blocked by the masks or will interact within the mask depends not only on the material and geometric properties of the mask but also the radiation type and energy of the incident radiation. As a gamma travels through the solid portions of the mask there are three major types of interaction mechanisms that can occur. These interactions are the photoelectric effect, Compton effects, and pair production. The combination of these interactions leads to the linear attenuation coefficient μ described as

$$\mu = \tau + \sigma + \kappa, \tag{2.9}$$

which is a combination of the probability per unit path length for the photoelectric effect τ, Compton scatter events σ, and pair production events κ of gammas being removed from the incident gamma flux. It follows that the mean free path of a gamma λ is defined

26

as the average distance mono-energetic gammas will travel through a material before encountering an interaction given by the equation

$$\lambda = \frac{1}{\mu}. \tag{2.10}$$

The masks used with the RMC must be able to adequately block the incoming low energy gammas, meaning the thickness of the mask must be several times thicker than the mean free path to account for the distribution of actual lengths traveled by the gammas before an interaction. The linear attenuation coefficient for material is normally listed in a more convenient manner as a ratio of the linear attenuation coefficient μ to the density of the material ρ to allow for applications were non element materials are involved.
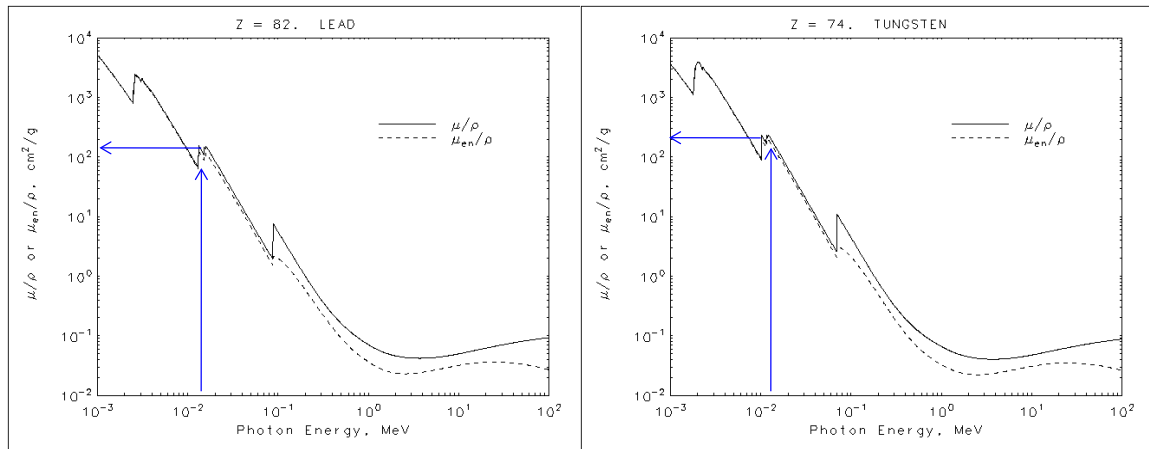
Fig. 10. (L) This is a plot of the ratio of the mass attenuation coefficient over the density for lead with the 122 keV photon energy highlighted. (R) This is a similar plot for tungsten [15].

Details of these three main interactions are widely known and greater details are available through a number of sources [11] [16]. Figure 12 shows that for the high z

27

material of the RMC masks (74 or 82), the photoelectric effect will dominate the gamma

interaction with the mass for low energy gammas up to roughly 500 keV.
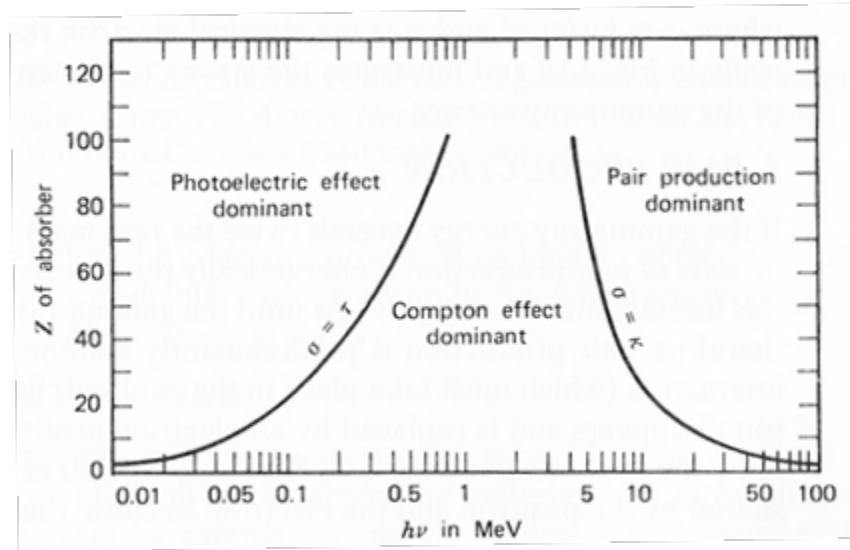
Fig. 11. This figure shows the dependence of the cross-section for the three major types of interactions a gammas ray can undergo as it transits mass. This cross section is dependent on the energy of the gamma ray and the material properties of the mass. This research focuses on low energy gammas and high z materials which is the region dominated by the photoelectric effect [11].

The standard mask design implemented in previous RMC work is the Ronchi

grating. Wilmore explains that the Ronchi grating is a transmission grating with straight,

parallel rulings, the opaque and transmission portions being of equal width [11]. A slight

change in the Ronchi grating is used by allowing the slits (open transmission portion of

the mask) and slats (opaque portion of the mask) to have different widths. As the width

of each grating decreases, the angular resolution increases at a cost of overall detector

sensitivity. This research explores the effect of using masks of varying grate size all of

which are designed after the Ronchi model. If the front and back masks are identical in

28

material and geometric design then the transmission function will be symmetric through 360 degrees of rotation and will provide two source reconstructions. One at the source location and one at the negative complement of the source position as in shown in any of the displayed transmission functions in fig. 2.

Part of the motivation behind changing the mask design was to increase the exposed area of the detector face to allow for improved counting statistics and absolute detection efficiency discussed in section II.4.B. This was accomplished by changing the slit shape from a rectangle to a trapezoid as shown in fig. 13. This improvement is similar to the improvement seen from using the trapezoidal rule in place of the rectangular midpoint rule approximation of a definite integral.
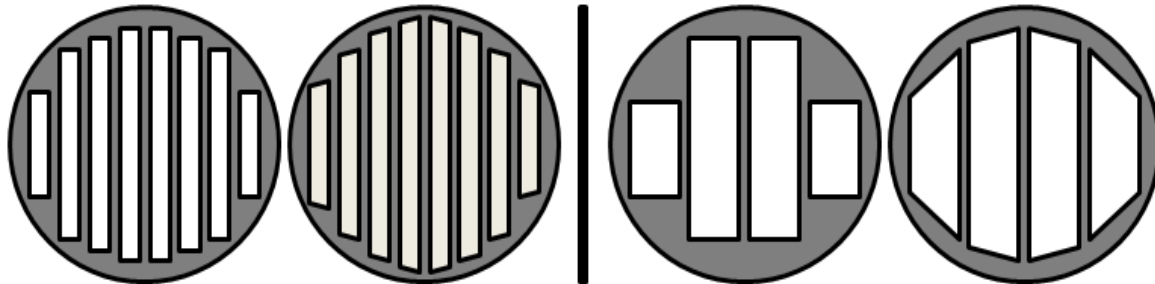
Fig. 12. This is an example of two mask designs with similar pitch. The pitch is measured from the left edge of one slit to the left edge of the next slit. The difference is in the top and bottom shape of the slit. The trapezoid shape (r) allows for more total slit area especially for large slit widths and only a few slits.

II. D. 2. Resolution vs Detection Efficiency

The tradeoff between having very fine slits for the gammas to transmit through and the time required to develop a transmission function that enables an accurate position estimate force the constraints to the novel mask design. This amplifies an issue that RMCs and similar selective transmission techniques must address. Each radioactive

29

decay event radiates information pertinent to determining the presence, activity, geometry, and location of the source. By blocking some of the incident radiation, the information carried by those radiation events is not available.

The resolution of the RMC is determined by not only by the mask design but also the separation between the masks. The equation

$$\Theta = \frac{p}{2L},\tag{2.11}$$

shows the how the resolution Θ is related to the pitch width p and the mask separation L [3]. The pitch width is defined as the distance between two left edges of consecutive slots in the mask. This includes the slot width and the distance between two slots. This provides two degrees of freedom from an RMC design perspective. We can improve the position resolution by increasing the number of slots on the masks or increasing the separation distance between the masks.

Resolution improvement comes with a few tradeoff considerations. As the number of slots increases, we increase the computational cost of the reconstruction process. This occurs because the reconstruction process relies on system responses that must be calculated using numerical geometric modeling. As the number of slots on a mask increases, the slot width and pitch decrease for a fixed mask radius. With geometrically smaller and smaller slot dimensions, the number of points used to define an entire mask must also increase to provide greater fidelity in our computed system response. Computational considerations aside, the lower bound on the pitch limit is the gamma diffraction limit, which is well beyond the scope of this research but provides an interesting concept for potential RMC applications.

30

Another tradeoff that is necessary to consider when improving the position

resolution of the RMC is the mask separation. A competing performance parameter to

improving the position resolution by increasing the mask separation is its effect on the

field of view. The field of view FOV is given by

$$FOV = \frac{d}{L}, \tag{2.12}$$

where d is the diameter of the masks and L is the mask separation. Depending on the

application, the reduction in field of view may not be as much of a consideration

especially for systems designed with the ability to pivot the RMC to multiple areas with a

narrow field of view compared to fixed systems that must rely on one system position

with a wider field of view. The panoramic advantage to a pivoting RMC system is

shown in fig. 14.
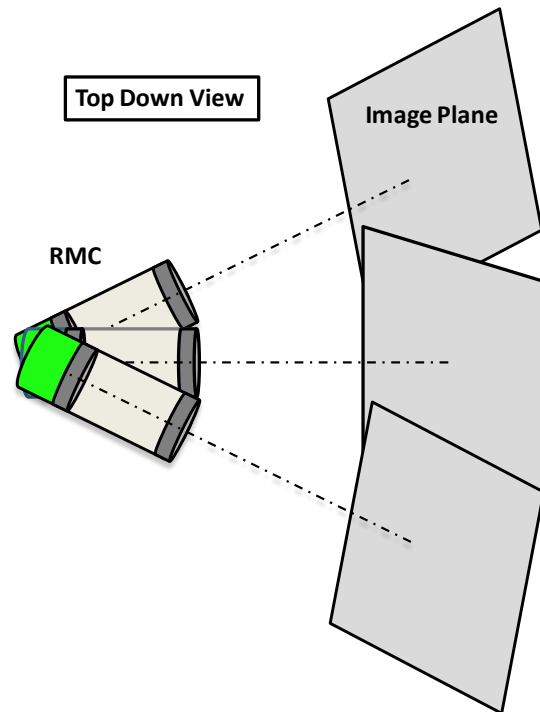
Fig. 13. This depicts the possibility of taking a panoramic image by combing images from different pivot angles.

31

At the heart of the discussion of RMC position resolution is the quantifiable difference in the probability of gammas leaving the source and transmitting through masks to the detector (P_n from (2.1)) as the source is moved within the field of view of the image plane. Small changes in the source position resulting in large differences in P_n have better position resolution compared to the small changes resulting in minuscule differences in P_n. These differences in P_n are measured not only for a single RMC collimator position but for the entire transmission function.

While RMC position resolution is concerned with differences in P_n throughout the phase of rotation to determine one position from another, the RMC absolute detection efficiency is concerned with the magnitude of P_n at each angular position or can be simplified by the average P_n for a revolution. The absolute detection efficiency for any radiation detector ε_{abs} is defined as

$$\varepsilon_{abs} = \frac{N_{recorded}}{N_{emitted}}, \tag{2.13}$$

where $N_{recorded}$ is the number of pulses recorded by the detector and $N_{emitted}$ is the number of gammas emitted by the source [11]. For RMC applications $N_{emitted}$ is a constant value as the collimator is rotated based on the long half-lives of the sources compared to the collection time. Knowing that the source emits isotropically, only the gammas emitted in the solid angle of the detector face have a chance at being detected. This is withstanding effects of the collimator and the intrinsic efficiency of the detector. While the solid angle from the source to the front face of the detector is constant, the overlap of the open area of the two masks which transmit gammas to the detector changes with each new angular

32

position as mentioned in the previous paragraph in the P_n discussion. To improve the RMC system detection efficiency, the detector face exposed area needs to be maximized. Removing the collimator achieves this maximum. All gammas emitted from the source in the direction of the solid angle of the detector travel unimpeded to the detector. While this maximizes the system detection efficiency, it eliminates the ability to estimate the position and intensity of the gamma source within the image plane. As an alternative to removing the collimator, the slot widths can be increased to improve RMC detection efficiency. Herein lays the tradeoff between position resolution and RMC detection efficiency. This tradeoff provides an opportunity to explore an adaptive approach. Masks can be designed to favor a high average P_n at a cost of position resolution but still capable of providing some degree of position information. Alternatively, masks can be designed to favor low position resolution at the cost of system detection efficiency. The masks used independently but with combined results intend to benefit from each of their design strengths.

II. E. Image Comparison

This section discusses the motivation behind an image comparison method as it applies to adaptive imaging, a few of the shortcomings of using descriptive statistics to compare images, and finally the Structural Similarity (SSIM) method that is used as a tool to compare reconstructed images in this research.

II. E. 1. Adaptive Application

Introducing an adaptive method into the data collection of the RMC requires a feedback loop. Essentially, an initial measurement is collected, the collected data is

33

processed to reconstruct an image, the image is analyzed to determine if a system configuration change is desired, an additional measurement is collected, and the additional data is used to reconstruct an updated image. The final image computed using the adaptive technique now needs to be compared to images taken with the same collection time for fixed system configuration to determine the adaptive effect on performance. Here two critical areas have been identified as relying upon an image analysis method to not only determine if system changes are needed during an adaptive measurement but also to assess any performance change between a traditional fixed configuration collection profile and an adaptive collection profile. A quantifiable method for image quality analysis is essential to this research.

II. E. 2. Descriptive Statistics

Descriptive statistics provide a quantifiable means of characterizing a set of numbers. Common examples of descriptive statistics are the mean, median, mode, standard deviation, variance, range, correlation, and linear regression. F. J. Anscombe famously illustrates a significant flaw to singularly relying upon descriptive statistics to characterize data sets. His powerful example computes a handful of descriptive statistics for four separate data sets. All four data sets have identical means in the x and y directions, variances in the x and y directions, correlations between x and y, and linear regression lines computed using double precision. Figure 15 is a plot of each data set, clearly showing the visible differences in distributions undetectable to the statistics mentioned previously [17]. The goal for image comparison is to retain the qualitative value of descriptive statistics but account for what is visibly obvious to the eye without having to manually analyze every image.

34
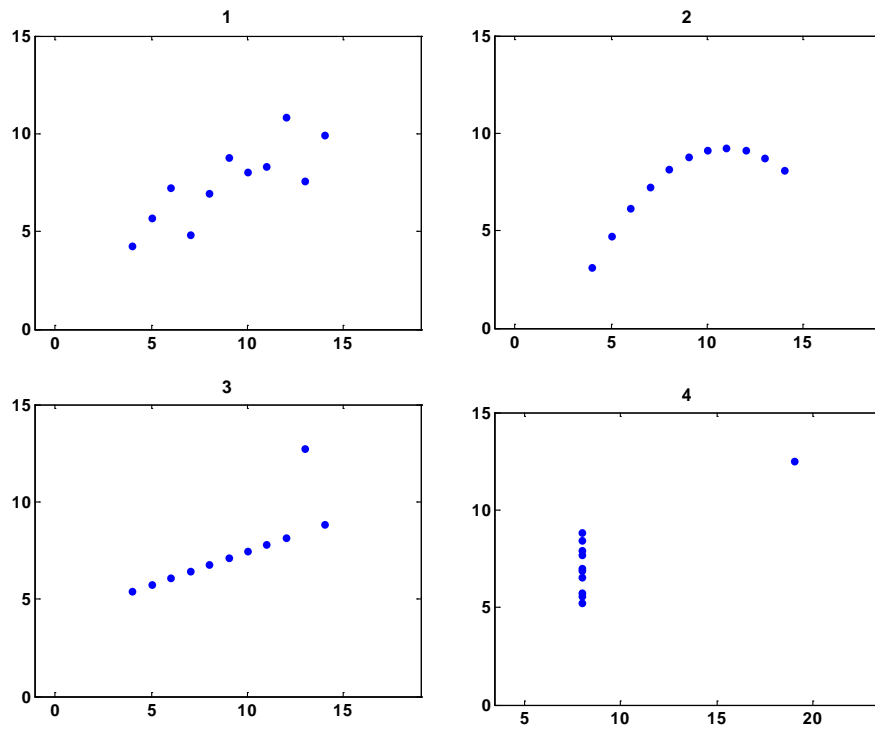
Fig. 14. These plots show the Anscombe's quartet of different distributions with the same values for a handful of descriptive statistics. This is a powerful example of how descriptive statistics can be misleading without visual inspection of the data. The goal for image comparison is to retain the qualitative value of descriptive statistics but account for what is visibly obvious the eye [17].

II. E. 3. Structural Similarity Index

In an attempt to avoid the pitfalls associated with a strictly descriptive statistical image analysis the Structural Similarity (SSIM) method developed by Zhou Wang is applied to reconstructed images in this research [5]. Recognizing that the human eye is quite adept at registering structural content of an observed scene, the SSIM method tried to incorporate structural information into the assessment process. Image assessment methods normally fall into either one of two categories. The first is the blind or no-reference method that requires no information of the original distortion free image. The

35

second is the full-reference method which requires a complete distortion free reference image. Applications are typically concerned with a high resolution digital image with an associated large file size as the reference image used to compare images that have been manipulated in some way for either effects or file size reasons. These altered images are then compared to the original reference image to assess the retained quality of the manipulation. The SSIM method is a full-reference method [5]. In this application, in place of a reference image resulting from data collection and processing, the truth data of the observation environment is used in its place. All comparisons using the SSIM will compare a processed image to the truth image computed by calculating the activity and position of the source and using a background measurement as the value for all other pixels.

The SSIM method combines three image characteristics and compares these characteristics in a combined algorithm to the reference image. The carryover from optical imaging to radiation imaging require only a few definition clarifications. The luminance of an optical image is the same as the activity magnitude of a radiation image which is a combination of the background and source in each pixel. The contrast of an optical image is defined for radiation images as the difference in activity from pixel to pixel. The structural aspects remain essentially unchanged for optical imaging and radiation imaging.

36

The comparative algorithm for the SSIM index is,

$$l\left(\underline{x},\underline{y}\right) = \frac{2\mu_x\mu_y + C_1}{\mu_x^2 + \mu_y^2 + C_1}$$

$$c\left(\underline{x},\underline{y}\right) = \frac{2\sigma_x\sigma_y + C_2}{\sigma_x^2 + \sigma_y^2 + C_2} \tag{2.14}$$

$$s\left(\underline{x},\underline{y}\right) = \frac{\sigma_{xy} + C_3}{\sigma_x\sigma_y + C_3}$$

$$SSIM\left(\underline{x},\underline{y}\right) = \left[l\left(\underline{x},\underline{y}\right)\right]^\alpha \cdot \left[c\left(\underline{x},\underline{y}\right)\right]^\beta \cdot \left[s\left(\underline{x},\underline{y}\right)\right]^\gamma.$$

This equation is broken in the three components previously discussed as luminance, contrast and structure. The reference data set is x which contains the same number of values as data set y the image being compared to the reference. The luminance term contains the mean of x in μ_x and the mean of y in μ_y. The contrast term contains the standard deviation of x and y with σ_x and σ_y respectively. The structural term consists of the standard deviations used in the contrast term in addition to the covariance between x and y in σ_{xy}. Each of the three terms contains a constant (C_1, C_2, and C_3) to avoid instabilities when the denominator in each term is close to zero. The exponential terms α, β, and γ are parameters used to adjust the weight or importance of each of the comparative areas. Their only constraint is that they are positive [5]. For simplification these terms are set to unity for this research. The solution to (2.14) provides an overall index of comparison of the measured or altered image to the reference image [5].

37

A visual example is helpful to understand the application. In fig. 16, an image of a ball cap is distorted in two different manners. Each distorted image blacks out the same number of pixels, one with random pixels selected and the other with random rows selected. The change in luminance is the same for both distorted images while the change in contrast appears to be greater in the middle image.

Fig. 15. This is an example of how the Structural Similarity (SSIM) index can be used to compare two distorted images to an ideal image. The reference image (l) is undistorted. The other two images have the same number of pixels blacked out with the difference being random pixels being black out (m) verse random rows being blacked out (r). From (2.12) with equal exponential weights and the constants removed the computed indexes are 0.9808 (m) and 0.9904 (r).

III. Experiment Setup and Process

This chapter explores the experimental equipment and processes to meet the research objectives. Included are descriptions of the RMC system, the source position mechanism, the radiation sources, and the software used for data processing. Also included are the calibration procedures and the actual data collection procedures. Finally the post processing procedures for the three adaptive research areas are discussed. Two software programs are used to operate the RMC and process the data. National Intruments LabVIEW 8.2 is used to program all the motor control and collection profiles, while MATLAB version 7.10.0.449 R2010a is used to save the collected data and for all post processing.

III. A. Equipment

The RMC is at the center of this research has been used previously in other areas of RMC research. The main tenants of the design remain unchanged from the work Kowash conducted when he designed the RMC in use. A detailed explanation of the design and design theory for the particular RMC used for this research is available in [3].

III. A. 1. RMC

The main components of the RMC are the flight tube, the housing, the position sensing mechanism, the rotating stepper motor, the pivoting stepper motor, and the radiation detector. All these components are combined to produce an electronic pulse that will be further processed and is discussed in the following section. The flight tube is made of aluminum and contains the mask pair. The masks will be discussed in further detail at the end of this section. The back mask is fixed in place using set screws and rests flush against the face of the detector. The front mask is on a slide allowing for easy position adjustments from one measurement to the next. The front mask is fastened into place at the desired mask separation distance up to 50 cm. One

39

end of the flight tube is milled down to fit snugly into an aluminum driver tube contained within the aluminum housing and fixed to the driver tube with set screws. This driver tube fits inside of the housing and is free to rotate with the aid of press fit stainless steel bearing between the housing and the driver tube. The housing acts to hold everything in position and keeps the fixed detector aligned with the rotating driver tube and flight tube assembly. The radiation detector used is a 3 in by 3 in sodium iodide (NaI) scintillation detector using the more common English units for size measurement.
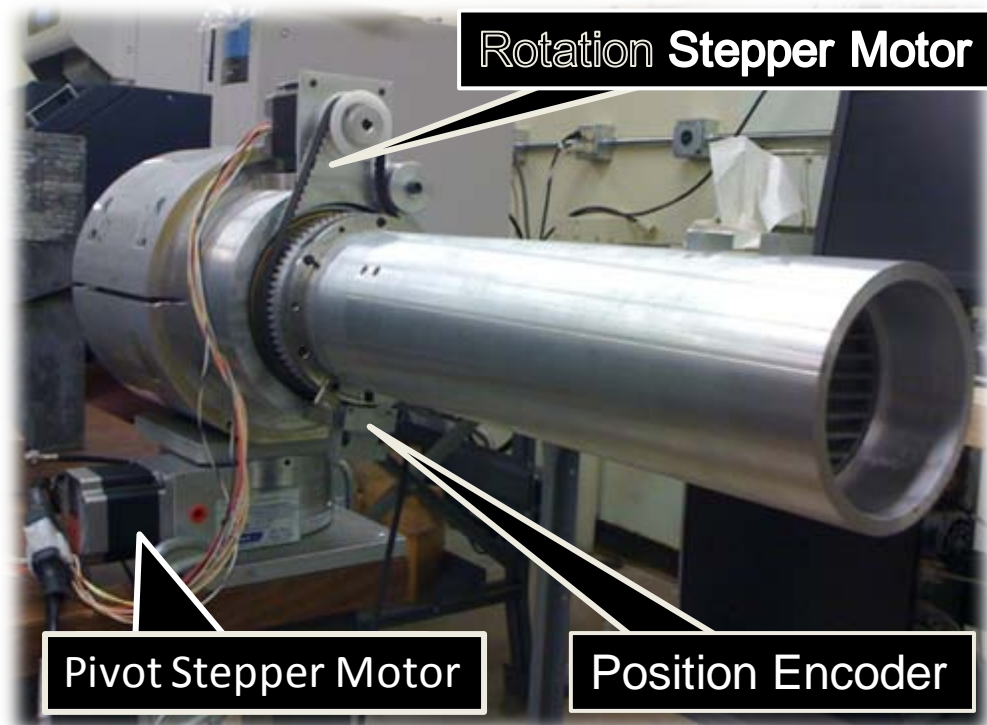
Fig. 16. This is a picture of the RMC used in the research with a few key components labeled. A few of the changes to the RMC from previous research are included. The idler pulley shown near the rotation stepper motor was added to provide improved belt tension for more consistent rotation. The position encoder was upgraded from 16 bits to 32 bits. Finally the RMC was placed on a motorized pivot table to allow for horizontal pivoting.

40

The rotational position of the flight tube must be accurately recorded throughout measurements in order to form the transmission function. This is achieved using a Renishaw optical encoder ring mounted on the driver tube. The encoder ring has 72,000 etched lines equally spaced around the ring with a magnetic reset post mounted at one location on the ring. An optical pick-up is mounted in a fixed position at the bottom of the ring to observe the etching as the flight tube and driver tube rotate. As an etching is observed a square pulse is generated and counted using a 32-bit encoding chip. The counter resets each time the magnetic post passes the optical pick-up. Appendix B.2 includes a picture of the 32-bit encoder chip.

The tube is rotated using a HT23-397 Applied Motion stepper motor that is powered and controlled using an Applied Motion Si3540 control box. The motor is mounted on top of the housing and linked to the driver tube using a half inch timing belt. The timing belt is fed through an idler gear to remove any belt slack and allow the belt to wrap around more of the drive tube. The stepper motor is capable of stepping less than 1 degree per step but can be programmed to step at variable amounts. The gear ratio between the stepper motor to the drive tube is 3.27:1.

The RMC pivots using a Velmex B4836TS rotary table with a Slo-Syn stepper motor. The rotary table includes a magnetic reference point that is used as a homing position. The reference point discontinues power to the motor when passed and therefore must be approached with the same momentum to achieve an accurate starting position. The rotary table has an accuracy of 100 arc seconds. The RMC is fastened to the rotary table using a 1 in aluminum mounting bracket that connects the rotary table to the RMC housing.

The masks used in this research are 3.81 cm radius masks made from lead or tungsten. Each mask pair explored is of the same material and same geometric design. As discussed in chapter 2 one of the objectives of this research was to allow more radiation to be transmitted to

41

the detector while still gaining some valuable position information. In fig. 18 different mask designs provide varying amount of radiation to transmit through to the detector. The ratio of the open surface area to total mask surface area is provided for each mask design. Based on the geometric constraints associated with straight slot edges, the slot width increase does not necessarily coincide with an increase in the computed surface area ratio as seen when comparing masks 2 and 3. Table 1 provides additional mask parameters.
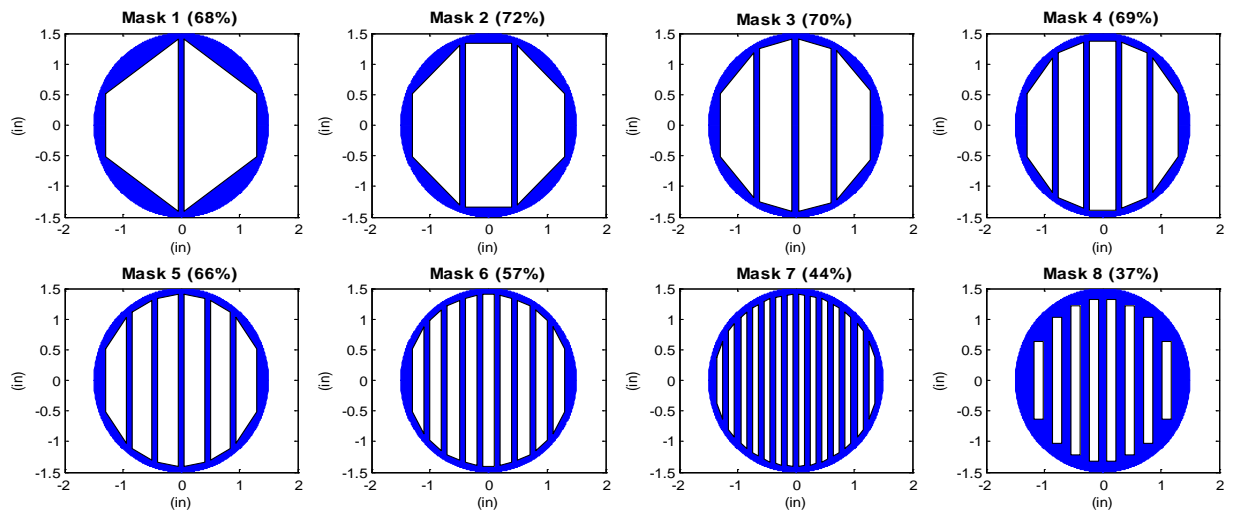
Fig. 17. This a two dimensional plot of the masks used in this research. All masks are have a 3.81 cm radius and 0.635 cm thickness. The percentage next to the mask number represents the ratio of open surface area to total surface area for each mask design.

Table 1.   Mask Design Parameters

Mask Number	Number of Slots	Slot Width (cm)	Slat Width (cm)	Material
1	2	3.175	0.254	Lead
2	3	2.032	0.254	Lead
3	4	1.4478	0.254	Lead
4	5	1.1176	0.254	Lead
5	6	0.889	0.254	Lead
6	9	0.508	0.254	Lead
7	14	0.254	0.254	Lead
8	8	0.4	0.4	Tungsten

III. A. 2. Sources and Scintillation Detector

The radiation sources used in this research are all gamma emitters. To significantly decrease the effects of partial attenuation through the masks low energy gamma sources are used to take advantage of the lead and tungsten mask attenuation properties. The source primarily used for evaluation of the RMC image reconstruction is a Co-57 which emits a 122.1 keV with a branching ration of 85% and a half-life of 271.8 days [15]. The certified source activity was completed most recently on 20 October 2009 as 0.84 mCi. The activity of the source changed slightly over the course of the research but the majority of the measurements were taken when the source activity was 0.33 mCi. The source fits into a bored hole in a block of aluminum which is attached to the source positioning system.

The source positioning system is a Velmex Bi-slide which has two Slo-Syn stepper motors linked to jack screws to control the position of the source platform. These motors are powed and controlled through two Velmex VMX control boxes networked together to allow for control of three motors. Two motors are on the source positioning system and one is attached to

43

the rotary table to pivot the RMC. The source position system is capable of positioning the

source with an accuracy of 5 μ m. Figure 19 shows the source positioning system. To attain

maximum accuracy the system must be leveled at every junction to insure alignment. The range

of motion for the positioning system is 50 cm in the horizontal direction and 25 cm in the vertical

direction. The origin for the source platform was positioned to always place the source within

the forth Cartesian quadrant of the image plane (point (0,0) is in the upper left in fig. 20).
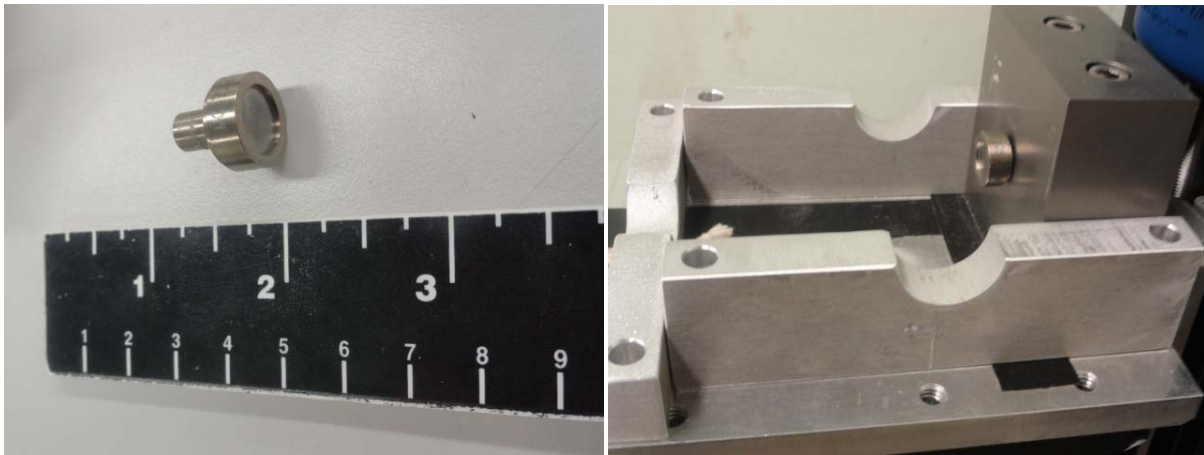
Fig. 18. These photos show the relative size of the point source used in this research (l) and the source platform on the source positioning system. While modeled as a point source, the source is actually disk shaped with a front face of 1cm in diameter. The source platform is connected directly to the Velmex Bi-slide and has aluminum barriers to prevent the source from falling to the ground.

44
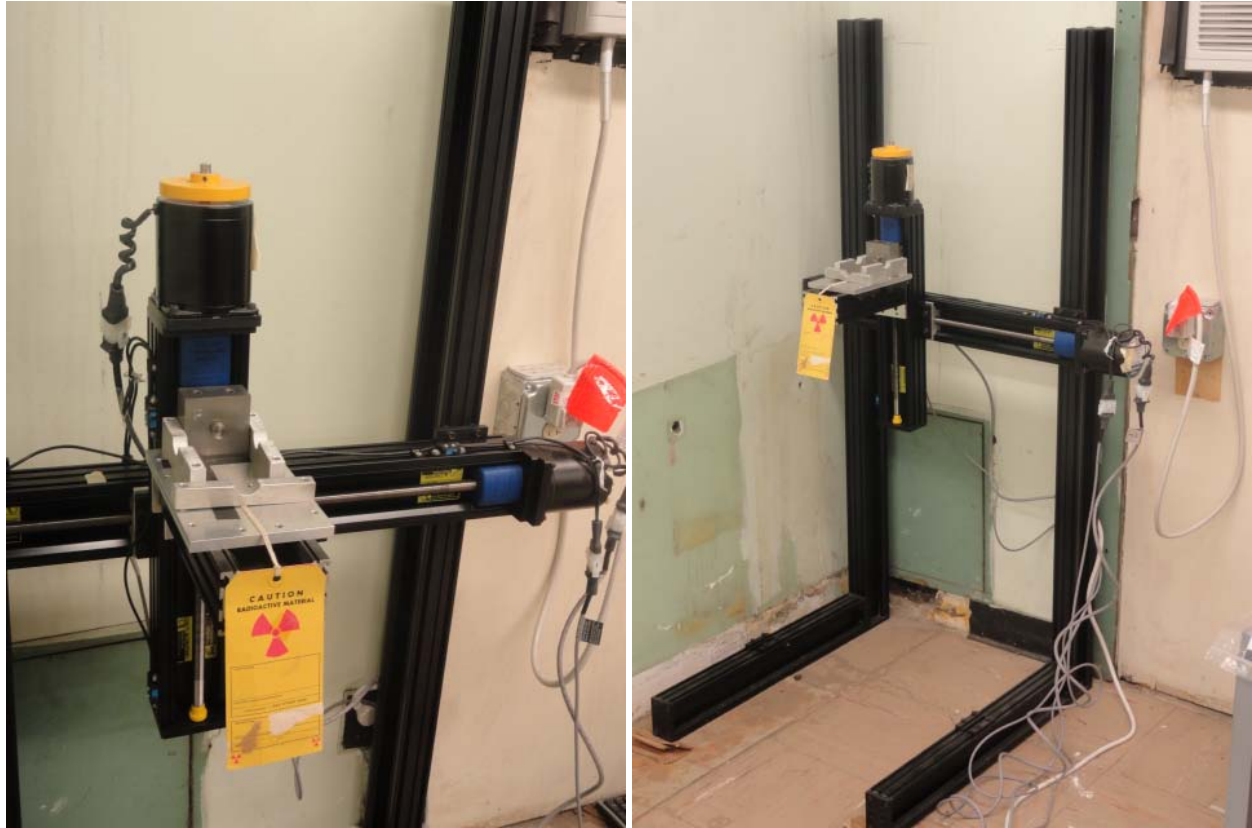
Fig. 19. These photos show the source platform (l) and the Velmex Bi-slide positioning system (r).

One of the advantages of the RMC is the simplistic design which requires only one position insensitive detector. For this research a 3x3" Bicron NaI detector is used. These detectors have long been the cheap work horse of detection applications. As one of the first scintillation materials used for radiation detection the detection properties are well characterized. Known for their relatively high detection efficiency, reliability, and economy, NaI detectors are far inferior to more modern detection systems in their energy resolution. While this research does not include spectroscopic applications, it is essential to narrow the output to those only at the energy level emitted by the source. The energy resolution of the detector is 60% at 122 keV, which will determine the window width used during pulse processing. The detector fits into the housing flush with the back mask of the flight tube and held in place by a polypropylene sleeve to prevent marring or scuffing. Coupled to the detector is a photomultiplier tube (PMT) used to

45

convert the light signal from the scintillating NaI into an electronic pulse. For more details on

scintillation radiation detectors and PMTs refer to Knoll [11].
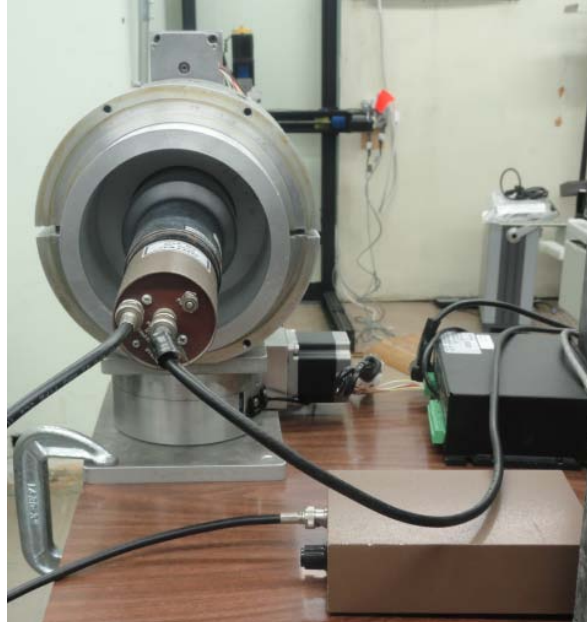
Fig. 20. A photo of the rear view of the RMC showing the sodium iodide (NaI) detector in the RMC housing held in place by a polypropylene sleeve. The output from the photomultiplier tube of the NaI detector is fed into the pre-amplifier. The Velmex source positioning system is visible in the background.

III. A. 3. Pulse Processing

The output from a NaI detector is proportional to the energy deposited in the detector.

For simplified applications the RMC is concerned with the number of pulses leaving the detector

equivalent to a particular energy level. Due to the poor resolution of NaI detector this energy

level becomes an energy window around the energy level of interest. In order to determine how

large to make the energy window an energy spectrum must be taken. Figure 22 shows the block

diagram of the data processing. To acquire an energy spectrum the block diagram uses the

multi-channel buffer to send all pulses received by the detector and shaped by the pre-amplifier

and amplifier to the computer via the data acquisition card. The amplifier is set to ensure that

46

desired energy is well defined by the number of bins in the energy spectrum. The pulse height

information is then processed using Gamma Vision software with 1024 bins to collect an energy

spectrum. A collection is gathered until a visibly recognizable peak is present. The Gaussian

shaped peak should be centered about the channel number corresponding to the energy level of

the selected source. The channel numbers corresponding to the points where the Gaussian curve

meets the flat background on either side of the center of the peak are used to determine the

energy window. Channel numbers are converted to pulse heights by recognizing that Nuclear

Instrument Module (NIM) equipment is being used and the maximum pulse height response is 3

volts on NIM equipment. Once the upper and lower limits of the interested energy window are

determined, the single channel analyzer (SCA) is set accordingly.
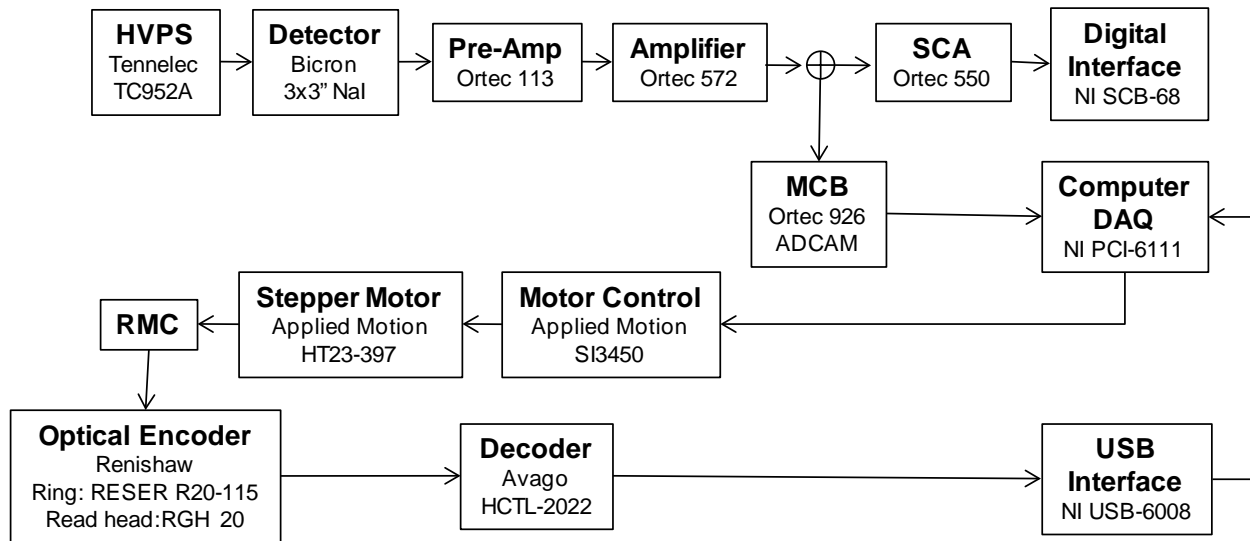
Fig. 21. This block diagram traces the RMC data acquisition process which includes the pulse processing [3].

47

III. B. Calibration

A thorough calibration of all the equipment and experiment area is necessary to fully understand the equipment response to the changed parameters of each RMC experiment. This includes a calibration of the NaI detector. Unless stated otherwise, the source used for detection and imaging is a 0.33 mCi Co-57 source that emits a 122 keV gamma with a branching ratio of 85% and a 136 keV with a branching ratio of 15%. The source is place in the x-y plane a distance of 314 cm away from the detector.

III. B. 1. Pre-Collection

Before calibrating the RMC a few preliminary calibrations must occur. The first calibration required is the energy calibration for the NaI detector response using the Gamma Vision software. It is well known that while NaI pulse height detector response is proportional to deposited energy, the proportionality is not linear across the entire energy spectrum. For this reason an energy calibration is essential when looking at multiple energy levels. While it may not be absolutely necessary in this work where only mono-energetic gammas are being measured, it is necessary when using either a multi-nuclide radiation source or radiation sources emitting gammas with higher energy levels. By observing a known source and recording the channel number of the center of the corresponding peak, a calibration file can be created in Gamma Vision. The Co-57 source was used to identify the 122 keV peak.

The next step includes the source positioning equipment. The calibration needed here consists mostly of leveling all of the travel axes of the positioning equipment. By using a bubble level at various points along the range of travel, two axis motion can be confirmed as truly horizontal and vertical. Adjustments for unlevel ground or misaligned cross beams can be fixed by using shims and readjusting the cross beams (see fig. 20).

48

The RMC must also be carefully calibrated prior to collection. The masks are fixed into position in the flight tube using set screws. The angular alignment is modeled as perfect in phase with each other and this is achieved by sliding a rigid metal guide through corresponding slits of each of the masks. The angle of the front mask is adjusted until the guide rests evenly on both masks, which is verified using a level. The angular uncertainty in the level is 1 degree. Once the masks are aligned the starting position is recorded by again placing the metal guide through both masks while the flight tube is connected to the housing and leveling the guide. The encoder position is read and the home position recorded to ensure all measurements begin from the same position. The final RMC calibration involves the rotary table. During the previous calibration steps, the pivot angle of the RMC can easily have changed. To ensure that the RMC is pointed directly down range to the source positioning system a homing routine is executed. This homing routine uses the RMC control software (Labview v8.2) to pivot the table to the reference position, pivot a set distance away from the reference position, pivot back to the reference position, and then pivot the set distance to point down range from the reference position. The reference position is the magnetic pick-up discussed in the previous section. The reason the RMC pivots to the reference position twice is to account for different positions the RMC may be pointed when the home routine is initiated. To prevent the changes in momentum from having as large an effect on the calibration position, the reference position is found when the RMC is pivoted from the same position at the same speed as the routine homes on the reference position the second time [18].

III. B. 2. Collection

Calibration collection involves collecting data for various source positions to determine how well the reconstructed positions using the RMC correspond with the actual positions of the

49

source using the source positioning system. The fidelity between these two data sets determines how well the RMC is calibrated. If the RMC centerline extends from the RMC and is directly orthogonal to the origin of the image plane the source moves in on the source positioning system then the system is calibrated.

The calibration is conducted using the Co-57 source and after all of the pre-collection calibrations have been satisfied, the source is placed in 18 different locations within the RMC field of view. At each location the RMC collects for 10 minutes with mask 8 and a mask separation of 20 cm. The mask selection was based on the familiarity of the mask 8 response based on previous work and the mask separation ensured high position resolution while still able to span the range of motion of the source positioning system [3]. After data collection, each data set was processed through the reconstruction algorithm to provide an estimate of the 18 source positions. The RMC estimates were compared against the actual source positions. Any discrepancies were noted and appropriate adjustments were made to compensate. The easiest adjustment is to move the origin of the source positioning system the appropriate direction if the discrepancy is consistent for every point.

Another method of calibration involves matching the simulated transmission function with that of a measured one. One mask pair is used to image one source location. A long collection is required to develop a distinguishable transmission function due to the detectable count rate differences from one angular position to the next. The longer the run (or higher the activity of the source) the more unique the transmission function becomes as Poisson decay process is dominated by the mean of the distribution. When the transmission functions match, the simulation has accounted for the critical aspects of the physics, geometry, and material properties of the RMC and background effects.

50

III. B. 3. Encoder Position Validation

Another factor to consider when assessing the calibration of the RMC system concerns the angular position information being processed by the encoder. The first step in ensuring the encoder is set up properly involving slowly rotating the flight tube while observing the encoder status light. The encoder has three status indications lights of green, yellow, and red referring to the amount of information the optical pick-up is receiving. The optical pick-up must be delicately positioned in order to receive the green status light through the entire revolution. The exception to this is when the magnetic reset passes the optical pick-up the light will trip to red indicating the reset of the counter. These steps ensure that the encoding circuitry is receiving valid information.

Once a measurement is taken there is further position validation that is done to ensure the consistent position information will be processed in the reconstruction. Often times throughout the course of runs, particularly long runs, there will be position location that may inhibit accurate reconstruction. The causes of these position anomalies will be discussed further in the next chapter. To correct for these errant position readings two methods are applied. Both look to indentify outliers from the angular position data. The rotation stepper motor is moving with a constant step rate and distance according to a distribution. This distribution is assumed normal and the outliers outside of 3 standard deviations are identified. Upon identification, these points are either corrected back to the best fit line of the remaining data (the mean of the step distance distribution) or removed from consideration entirely along with the corresponding counts.

III. C. Experimental Data Collection

Upon calibration completion an experimental data collection process was identified that provided the flexibility to use the same data for multiple experiments. Recognizing that transmission function generated during a collection is the result of the summation of the

51

transmission functions collected for each revolution of the RMC, one long measurement can be divided into many shorter measurements provided a few conditions are met. The long measurement cannot be broken into a shorter time increment than the time required for one revolution. Additionally, the total measurement must be taken for a discrete number of revolutions otherwise a partial revolution will result in improper equality for all increments of time. For a given mask pair the RMC collected data with the source at a single point (10,-16) for 10 minutes with a constant rotation step size and step rate. Each measurement using the available mask pairs were taken at separation distances of 20, 28, 36, and 44 cm. Whenever the masks were swapped, the calibration procedures for aligning the masks and determining the home position using the encoder were repeated. The source location was chosen at random within the range of the source positioning system, understanding the position sensitivity of the different mask designs and mask separations. These measurements were used in all three adaptive imaging experiments. The adaptive mask experiment compared results for the different mask designs at a fixed separation distance and various corresponding collection times. The adaptive sampling experiment compared results for a mask with all position and counting information included to results including only the desired sample locations and corresponding number of counts. The adaptive pivot experiment used the collected data as a baseline when the RMC centerline was aligned with the calibrated origin of the source positioning system. This experiment did require additional data collection at various RMC pivot angles.

III. D. Post Processing

This section will discuss how the data collected from the RMC is processed to reconstruct an estimate of the source position and activity. The general process is consistently used but each adaptive method requires a tailored method specific to the specific application.

52

III. D. 1. General Processing Procedures

The raw data from every run contains ascending position information in the range of 1 through 72,000 for every revolution of the RMC. It is important to point out that for one revolution there are typically around 800 data points for the nominal rotation speed. For each position point there is a corresponding integer representing the number of counts recorded from the detector at the gated energy level from the beginning of the collection. The number can only increase with time and is not a difference in the number of counts from each triggered position. Again, this speaks to the simplicity of the RMC system. There are two data arrays. The first being the position array which increases in some rotational speed dependent increment up to 72,000 over and over for each full rotation. With the second being the counts array which continuously increases with each position event simple counts the number of events falling in the selected energy window.

The raw data containing the position and count arrays are saved at the end of each collection as a Matlab ".mat" file. Also at the end of a collection, Labview invokes a Matlab function to convert the raw data into a manageable format. First the position information is converted into angular position with the home position as 0 degrees. Next the count array is converted into the number of counts received at each angular position by taking the difference between the total number of counts at each position. Finally, these arrays are compressed into 360 bins each representing a degree of rotation and saved as a separate ".mat" file. A series of Matlab routines which have been created during previous research are used to process the data [3]. An explanation is provided here, while the code is included in Appendix A.

Before processing can begin, the system response file must be created in order to use the ML-EM algorithm discussed in chapter 2. This system response model uses parameters of the

53

RMC system, the source, the background, and image plane to compute a matrix of the transmission probability from (2.1) for every possible source location in the image plane and for each degree of rotation. Once this system response matrix is computed it is stored in a library to expedite future reconstructions with the same parameters. Next the reconstruction routine is invoked, which reconstructs an image estimate based on the collected data using the system response matrix with (2.5) according to the desired computational effort. The number of bootstrap routines and iteration tolerances are input parameters at runtime for this routine. The output is a map of the source position and activity.

III. D. 2. Adaptive Rotation Data Processing

After the initial data collection for a given source position using all eight were acquired, the adaptive experiments could be completed. For the adaptive rotation the objective is to understand the effect of changing the RMC sampling method. For each system configuration the data are binned into the 360 angular position increments. Two sampling methods are explored as described in chapter 2. Using uniform sampling, the number of sampling locations can be reduced to observe the effect of decreasing the number of sample locations. This reduced data sample is achieved by harvesting from the original collection of data only the data located at the desired sample locations. For example, the original data has 360 sample locations. Reducing the number of uniform samples to 120 results in harvesting the data contained in every third bin of the original data. This changes the sampling from 1 sample per degree to 1 sample per 3 degrees. The collection time must be altered to account for the reduction in the number of samples. The collection time is reduced by the same factor that the number of sampling locations were reduced.

54

For irregular sampling a similar process occurs with the exception that once the number of sample locations is identified, a random set of sample locations is selected at varying intervals. The collection time still must be altered based on the ratio of original sample points to the desired sample points.

III. D. 3. Adaptive Mask Data Processing

The adaptive mask data processing is similar to the adaptive sampling process in that the experimental data is similar. Ten minute measurements were collected for each mask of the eight mask design shown in fig. 18 and with a mask separation distance of 20 cm. A Matlab routine was created to divide the 10 minute measurement into 30 second increments to provide reconstructed of images of the progress for each mask design. The incremental data was then processed with 100 bootstrap and ML-EM iterations. The reconstructed images were saved and then run through a Matlab routine to compute the SSIM index based on the truth reference image. These indices were then saved.

III. D. 4. Adaptive Pivot Data Processing

The adaptive pivot data processing begins with the mapping of the CRLB on the position estimate variance. This map provides the indication of whether a RMC pivot adjustment is required. An initial image collection is acquired for 30 seconds with Mask 3 with a separation distance of 20 cm. This data is then used to reconstruct an image as previously discussed with 100 bootstrap and ML-EM iterations. The initial image reconstruction is analyzed and compared to the CRLB map. If the initial image is showing up in a region of high variance, the RMC is pivoted to place the source relative to the detector in a region of lower position variance. This is done by observing the distance and direction required to move the source and calculating the pivot angle required to achieve the shift. It may be useful to refer to fig. 9 to understand the

55

relationship between the stationary source and the change in relative distance between the RMC centerline and the source as the RMC is pivoted.

IV.   Results and Analysis

This chapter includes the results of the calibration and validation processes discussed in section III.2. Also included are the results and analysis of the experiments discussed in section II.3 and III.4.

IV. A. Calibration

The energy calibration for the NaI detector not only provided the energy window limits for the SCA, but also provided an opportunity to collect a background measurement within the gated limits. Figure 23 shows the Gamma Vision results for the energy spectrum of the Co-57 source with the 122 keV peak clearly present. The peak is located between channels 94 and 134 with corresponding pulse heights of 0.92 V and 1.31 V. These are the upper and lower limits of the SCA representing the energy level of interest when using the Co-57 source. The limits provide a valid and repeatable energy window for the Co-57 provided the high voltage power supply and the amplifier settings remain constant. As previously discussed, the poor resolution of the NaI detectors results in relatively larger energy windows compared to more modern detectors like high purity germanium detectors (HPGe). While the resolution suffers with the NaI detector, provided the energy corresponding to the source is accurately bounded, modulation due to mask rotation is sufficient enough to discriminate the probability of detection from one angular position to another. For applications including spectroscopic identification with the RMC, a detector with better energy resolution could easily be included. Using the RMC to properly identify and subsequently preferentially collect the identified peak requires spectrum peak recognition logic not included in this research.

57
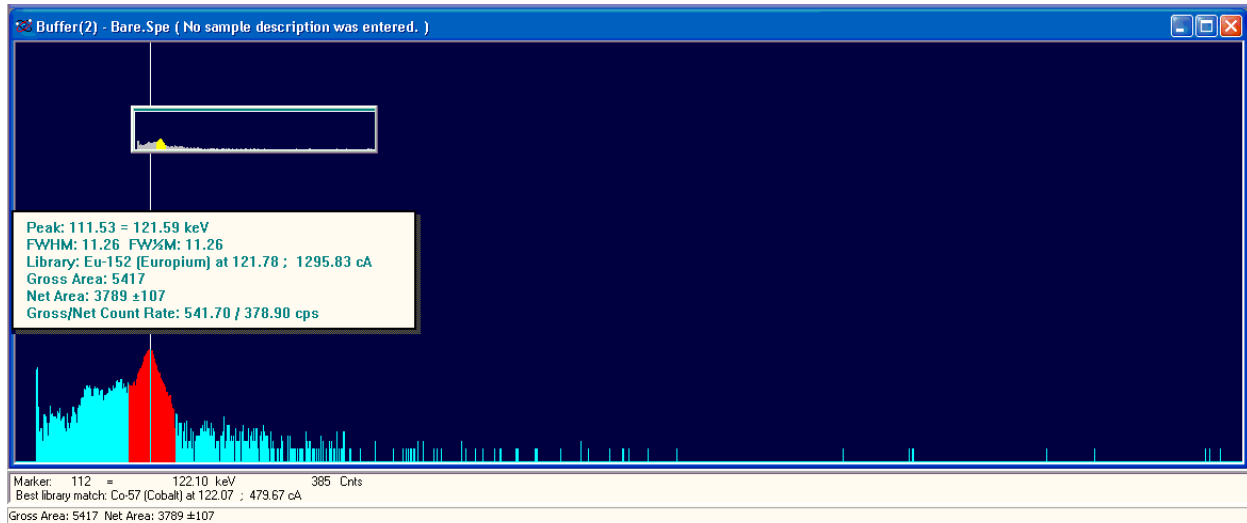
Fig. 22. The energy spectrum collected with the NaI detector used with the RMC with a Co-57 source. The region of interest is the 122 keV gamma peak of Co-57 with an associated resolution of 60%.

The background count rate used in the RMC system response generation includes only the background counts that fall within the gated energy window of the spectrum discussion in the previous paragraph. The application of this number includes a few typical lab assumptions. By setting a fixed count rate, it is assumed that the count rate is time independent. During the collection of data the background, while still being a Poisson stochastic process, the average count rate remains the same. This is fairly accurate in the lab setting but real world applications must accurately account for a potentially changing background for a given scene as vehicles, personnel, and equipment can transit the fixed image plane. Even in the lab the background count rate is subject to change based on the possibility of other experiments being run within the same lab space using radioactive sources. Another assumption that must be considered is the background count rate is not only time independent but also position independent. In the lab we assume that wherever the RMC is pointed the background will be the same. This is a relatively safe assumption, particularly because the image plane is located 314 cm away from the detector and only the RMC is only pivoted a few degrees merely shifting the 40 by 40 cm image plane by

58

10s of cm. Applying the pivoting RMC to homeland security or other radiation accountability scenarios the RMC would be pivoted across a wide angular range, moving the image plane significantly. Each significant shift would require an updated background estimate. The background measurement was obtained by observing the image plane without a source present for 10 minutes. The total number of counts was then divided by the observation time resulting in a background count rate of 14.93 ± 0.15 counts per second. This measurement was taken periodically throughout the course of the research and each measurement fell within the uncertainty of the initial background count rate estimate. The background count rate inputted into the code during data processing was rounded to 15 counts per second.

Additionally the NaI detector efficiency was calculated in order to accurately model the response of the RMC. This simple detection efficiency is important because it is energy dependent. As discussed in the previous chapter, RMC applications attempting to estimate the energy level of the emitted radiation through peak recognition of a collected energy spectrum require a more thorough detection efficiency calculation for the entire energy spectrum of interest. In this research, the detection efficiency for the NaI detector at 122 keV is all that is needed. The intrinsic detection efficiency for the NaI detector used was calculated to be 30%.

Upon completion of the pre-collection calibration, the relative positioning between the RMC and the source positioning system can move forward. Accurately knowing the physical position of the source relative to the RMC is essential in assessing the performance of the RMC reconstructed image, particularly the position estimate. Figure 24 shows the results of the final calibration. Previous measurements were taken with less agreement indicate an adjustment to the origin of the source position system was required to properly align the RMC centerline and the source positioning system origin. Figure 24 also shows the disagreement between the

59

reconstructed position estimate and the actual position estimate near the origin. As discussed in section II, this is the blind spot where the RMC is unable to accurately provide an estimate. This is due to the lack of modulation when the radiation is steaming directly down the centerline of the RMC as the flight tube rotates. The modulation of the radiation has to be larger than the noise of the collected data in order to provide an accurate estimate. The location of the source selected for the majority of the experimental measurements is at (10,-16), an area of the image plane in which the RMC accurately estimates the position.
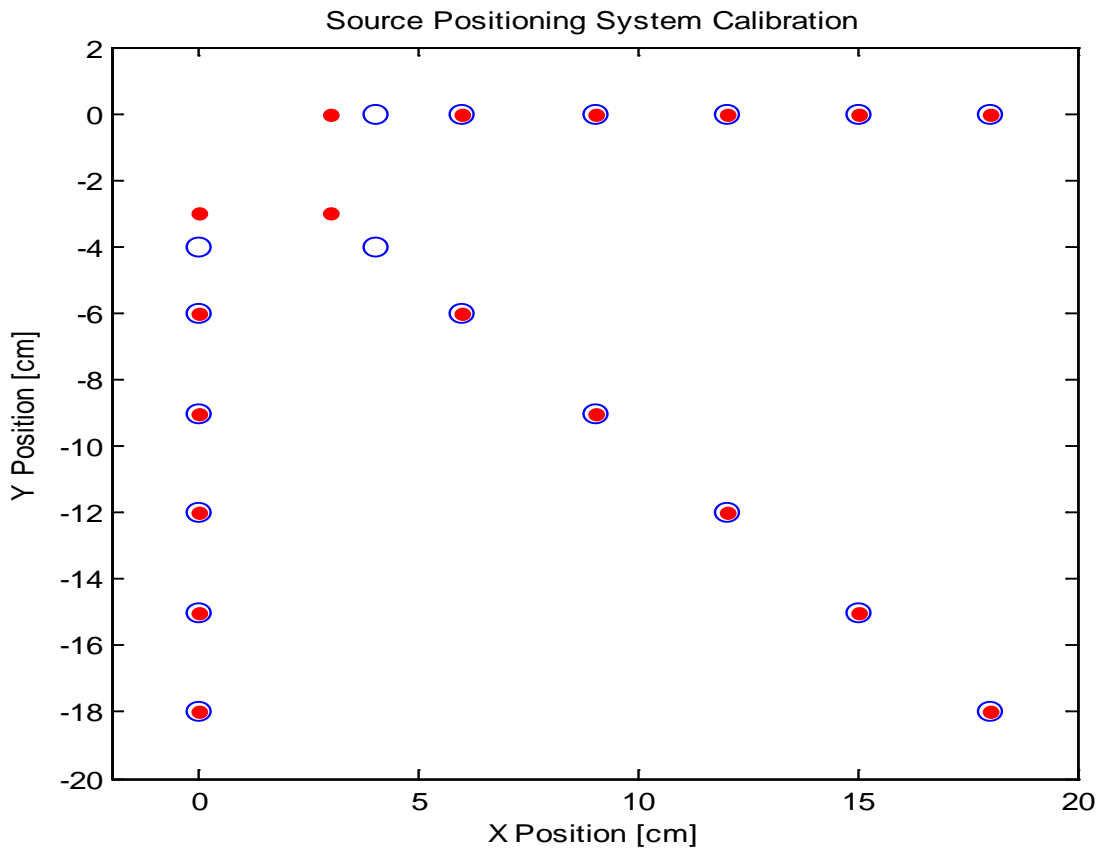
Fig. 23. This plot shows the results of the position calibration for the RMC. The actual source location is shown in red, while the blue dots indicate the RMC reconstructed image position.

60

IV. B. Fidelity

Fidelity refers in this section refers to the degree in which the computed RMC system response agrees with the actual RMC system response from the collected data. The higher the fidelity the closer the two agree. Ideally there is a perfect match between the simulated and experimental response, however a few things prevent that from occurring. The most obvious is the randomness associated with the radioactive decay process. Two subsequent responses for either the simulated or experimental data will not agree entirely due to the random nature of the process. To account for this much longer observation times are utilized to compare the simulated data to the collected to suppress the effects of the random noise. Specifically, the transmission functions are compared between an experimental collection and simulated collection. Provided all the material, geometric, and physical properties are accurately accounted for, the key parameters of the transmission functions would match. The key transmission function parameters include the frequency, phase, amplitude, and DC shift from the x axis.

The transmission function of the experimental data is analyzed first. In fig. 25, two areas of the transmission function exhibit erratic behavior. Both these areas occur in the last 180 degrees of rotation, and are quite unexpected. Multiple collections with multiple masks, separation parameters, source locations, and sources retain these oscillations in the same position within the transmission function. This eliminates a physics based explanation for the anomalies. These anomalies are therefore an artifact of the mechanical collection process either due to inconsistent belt tension due to hysteresis or inaccurate rotational position accountability from the decoder. The belt hysteresis is a plausible concern because the belt was taut around the RMC gearing in the same position for over a year. Due to the fact that identical mask pairs are used, the first 180 degrees of the ideal transmission function matches the second 180 degrees of

61

rotation. By invoking this symmetric property, the last half of the experimental transmission

function is a repeat of the first half because the anomalies are only in the second half, they are

discarded. Figure 26 shows the effect of replacing to the second half of the transmission function

with the first half due to symmetry.
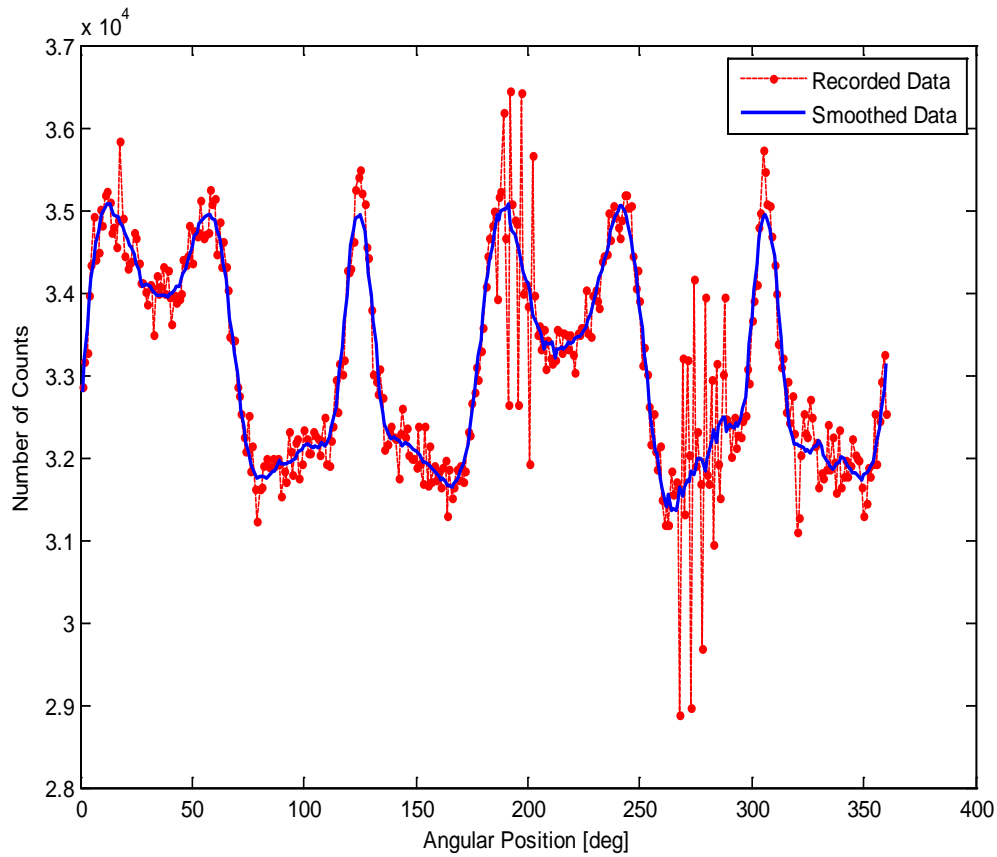
Fig. 24. This is a plot of the collected data using mask 3 with a 20 cm mask separation distance and the source located at (-16,8). Looking at the raw data there are two oscillation regions between 180 and 210 degrees and between 260 and 290 degrees. The smoothed data is the result of applying a third degree Savitzsky-Golay filter with a span of 21. The smooth data enables all but eliminates the erratic behavior in the last 180 degrees, providing better symmetry between the first 180 degrees of rotation and the last 180 degrees of rotation.

62
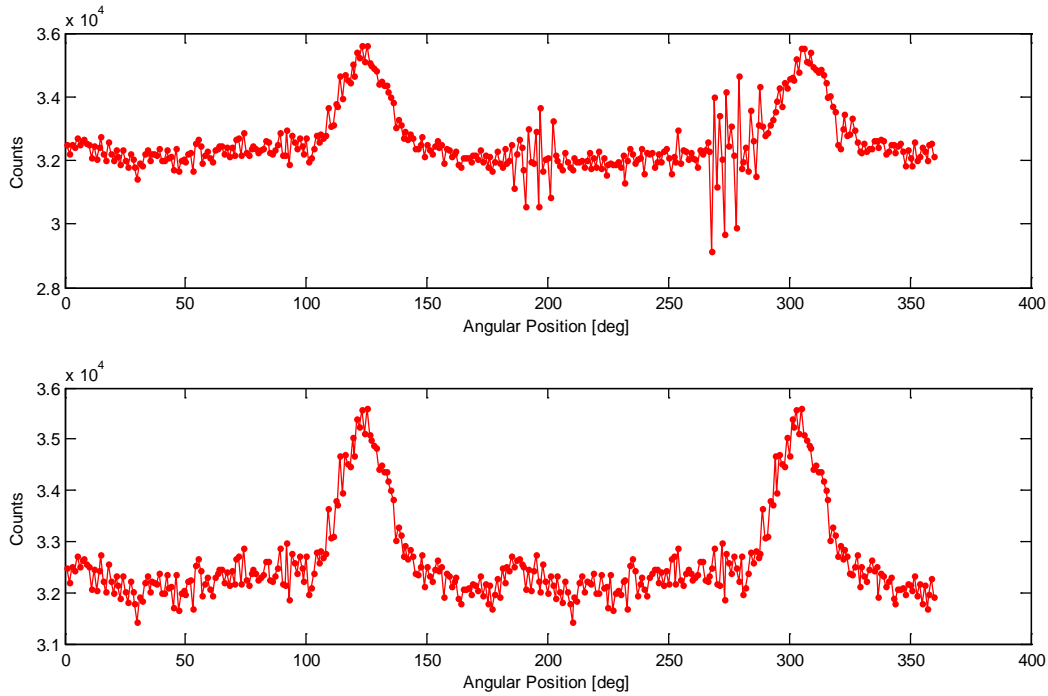
Fig. 25. This shows the symmetry that is invoked to handle anomalies found in the second half of all of the experimentally collect transmission functions. The upper plot is the original transmission function, while the lower plot is the first 180 degrees of the original data concatenated twice. This collection was for mask 3 with a separation distance of 20 cm for 15 hours with the source located at (-10,7).

With the symmetric application applied to the experimental transmission function, the fidelity comparison is essentially narrowed to comparing the first 180 degrees of each function. Figure 27 displays how well the simulated and experimental transmission functions match. This good agreement is misleading however, because the input values were altered to compensate for significant differences between the simulated and experimental transmission functions. In other words, the simulation is modeled using physical parameters from the research RMC. The discrepancy implies that there is some unresolved issue when modeling the new masks that will unfortunately skew the results when using the model as a basis for image reconstruction. Table 2 includes all the simulated values that needed to change to account for differences between the

experiment and simulation. It is important to note, changing the input parameters of the detector efficiency, source activity, and the background led to identifying the cause of the discrepancy between simulation and experiment. The simulation was only accounting for radiation that was transmitted through both masks in the flight tube. This is only a fraction of the radiation the detector senses from the source when the source is located outside the blind spot of the RMC centerline. The radiation can be transmitted through the side of the flight tube and through the back mask of the detector bypassing the front mask entirely. The further away from the origin the source is located the greater the solid angle between the source and the face of the detector which only includes the back mask.
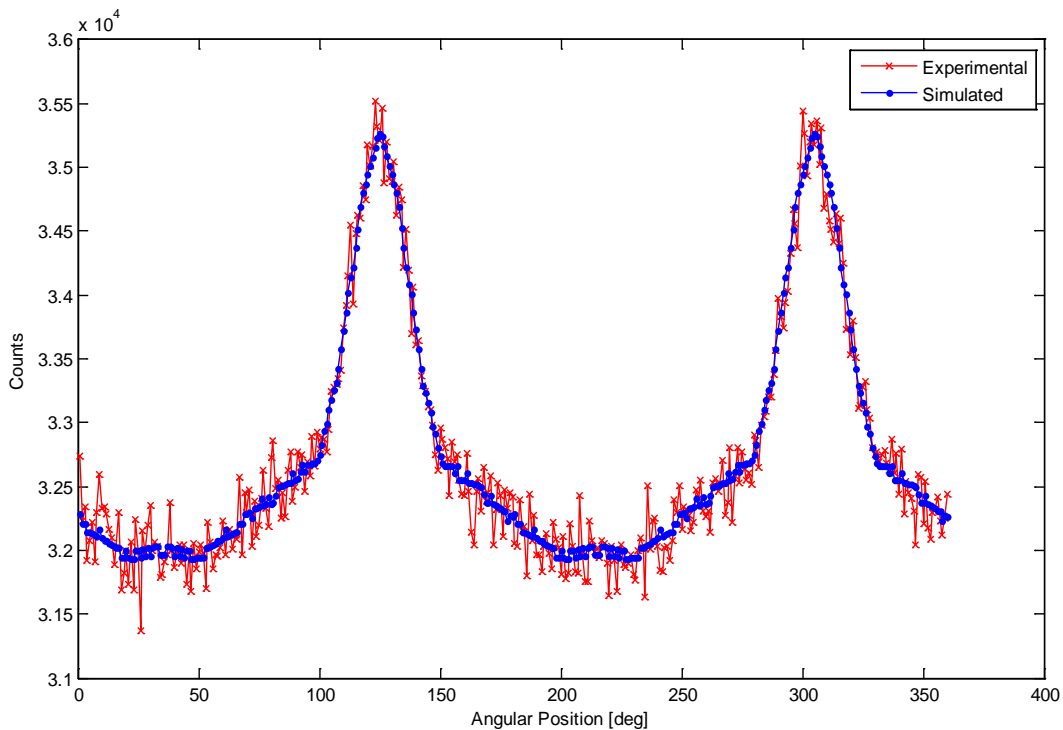
Fig. 26. This plots shows the fidelity comparison between the experimental and simulated transmission function results. Table 2 includes the alterations required to bring the simulated results to align with the experimental. This collection was for mask 3 with a separation distance of 20 cm for 15 hours with the source located at (-10,7).

64

Table 2.   Parameter Changes (corrects simulation to match experimental transmission function)

	detector efficiency	source activity	background
	%	mCi	cnt/sec
actual	0.3	0.33	14
correction	0.35	0.4	101

IV. C. Adaptive Rotation

The results for the adaptive rotation section are all based on simulated information. Based on the results of the calibration, implementing a reliable data collection process for the reduced sampling locations was not possible. Instead, various observations scenarios are simulated in an attempt to understand the effect of reducing the number of samples. Figure 28 shows an example of the simulated measured data compared to an ideal transmission function for each of the sampling techniques. As mentioned in section II.2.C, when the number of samples decreases for a fixed observation time, the number of counts per sample increases based on the increase in dwell time at each sampling location. Figure 28 again depicts this with the increase in the average number of counts from the top plot of roughly 11 for 360 sample locations compared to the middle and lower plots with an average near 200 counts for 20 sample locations. The middle and lower plots show the difference in shape of the transmission function when sampled uniformly versus irregularly for the same number of sample locations. The effect on the uncertainty measurement can be reviewed by referring to fig 8 in section II.2.C.

65
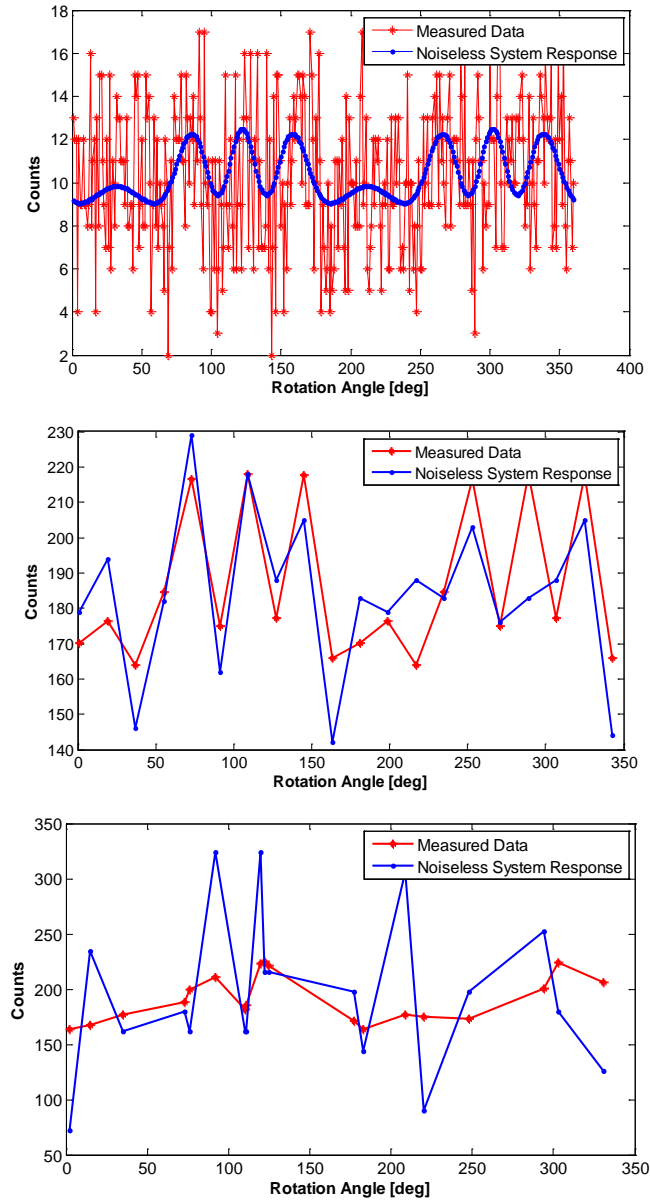
Fig. 27. These are plots of the same transmission function sampled three different ways for a collection time of 60 seconds and a source position of (16,10). The top plot shows a uniform sampling of 360 points. The middle plot is uniformly sampled at 20 locations. The bottom plot is irregularly sampled at 20 locations. The increase in dwell time at a sampling location when the number of sampling locations is decreased is apparent when looking at the same point in all three plots.

In fig. 29, the plots show various simulated image reconstructions using uniform

sampling. In this example the collection time was fixed at 30 seconds using Mask 8 with a

source position of (16,0) and the ML-EM and bootstrap iterations fixed at 1000 and 100 hundred

respectively. The results show the between images (d) and (e) false positives or ghost images begin to appear as the sample size decreases from 30 to 10. Additionally (f) shows more ghost images than (e) but they are not intense indicating a degree of improvement as the sample size is decreased from 10 to 8. Images (g) through (i) provide visual results of under sampling of the transmission function.
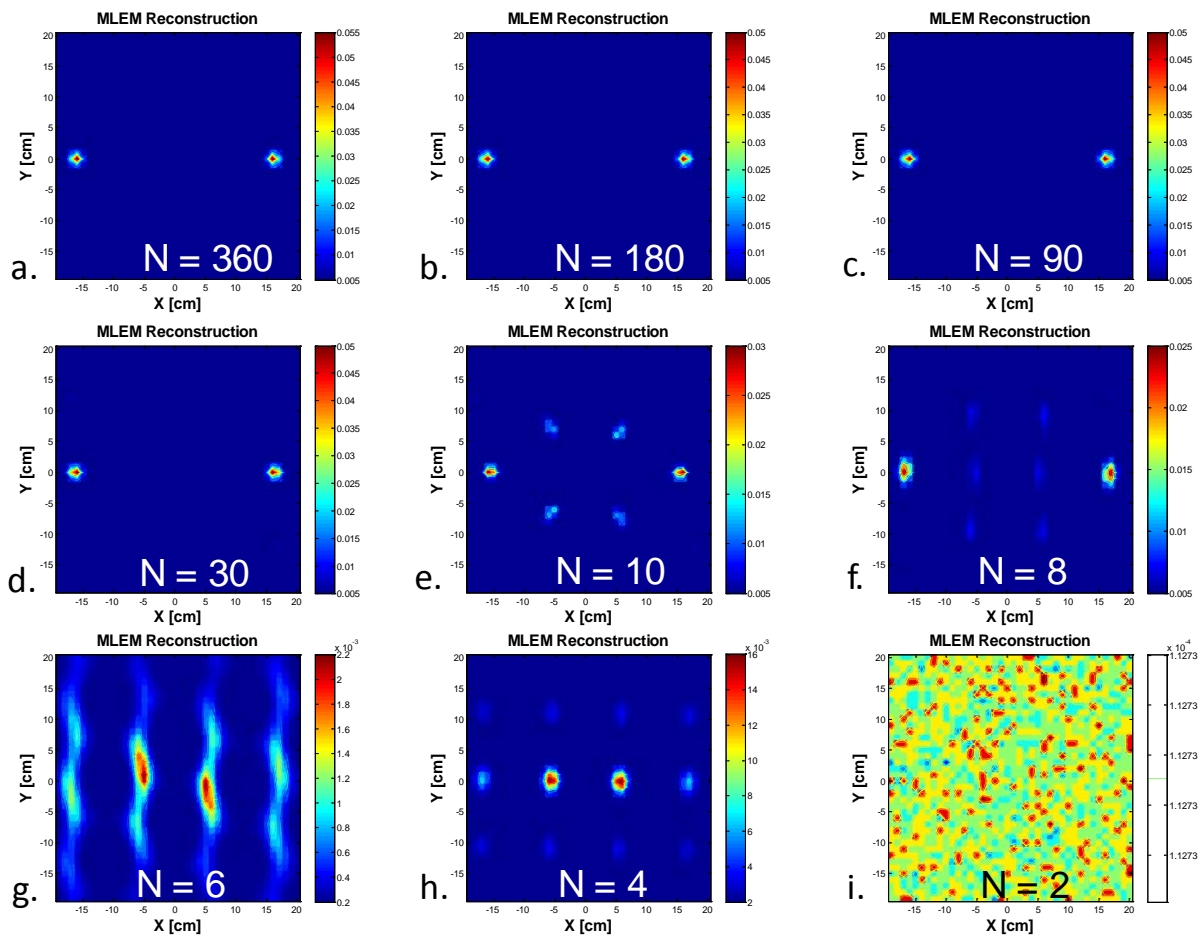
Fig. 28.   Simulated image reconstructions for various uniform sampling sizes of the transmission function observed for 30 seconds using mask 8 with a 330 µCi point source at (16,0). The number of ML-EM and bootstrap iterations were fixed at 1000 and 100 respectively.

67

By applying the SSIM to the reconstructed images in fig. 29, the images can be compared to identify the effects of reducing the sample size. Figure 30 shows the SSIM indices for various sample sizes for the point source located at three different locations. For all three source positions the trend as the sample size is reduced is the same. Because the radial distance for all three points from the RMC centerline is 16 cm Nyquist sample size limit for all three remains 29. Figure 30 shows how the SSIM index remains relatively steady until getting below a sample size of 30. Below a sample size of 30, the SSIM index for all three positions oscillates below plummeting orders of magnitude lower. It should be noted that the SSIM indices for the position (16,0) are negative based on the negative covariance used to compute the SSIM index and therefore do not appear on the log plot in fig. 30.
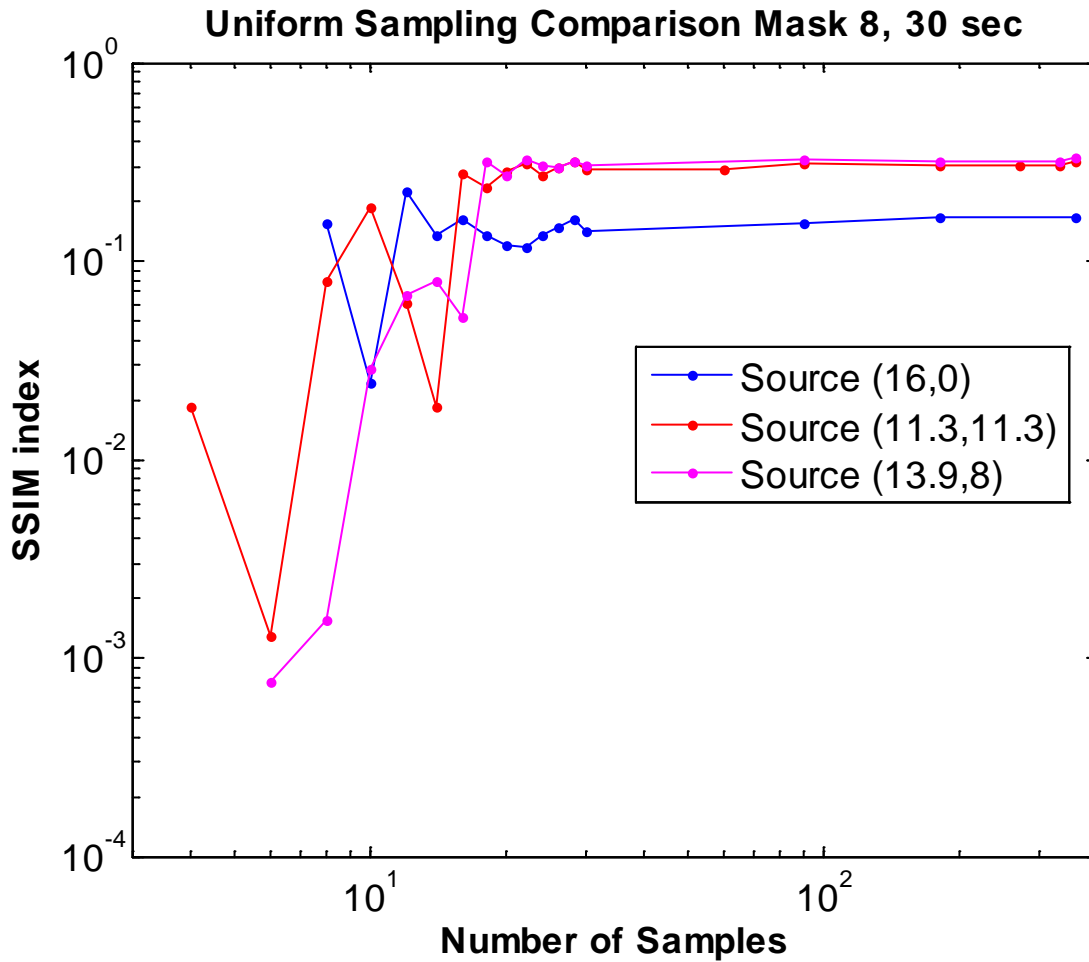
Fig. 29. This plot shows the SSIM index for various uniform sample sizes for a 330 µCi point source using mask 8 observed at three different locations for 30 seconds. The number of ML-EM and bootstrap iterations were fixed at 1000 and 100 respectively.

Figure 31 shows the Nyquist calculation for the transmission function for a source located at (16, 0). By taking the fast Fourier transform of the transmission, the highest meaningful frequency can be identified. Highest meaningful in this case refers to frequency components that contribute to the general overall shape of the transmission function not high frequency noise components. As shown in fig. 30 the minimum sample size to satisfy the Nyquist sampling rate for the ideal transmission function at the point (16,0) is 29. This also helps to explain why ghost images begin to appear in fig. 29 for sample size less than 30.

69
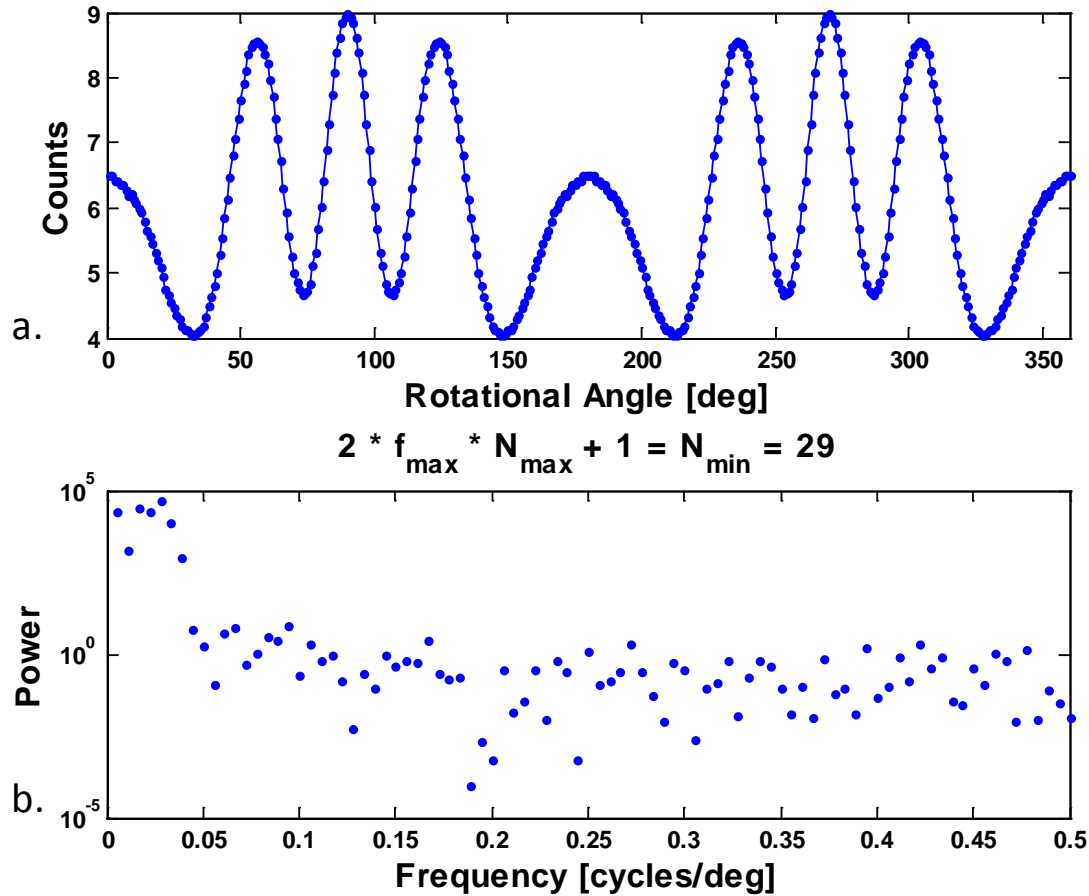
Fig. 30. This shows the calculation for the minimum number of samples required to satisfy the Nyquist sampling criteria for the signal of interest. Plot (a) shows the ideal transmission function for a point source at (16,0) recorded for 30 seconds. Plot (b) is the fast Fourier transform of the transmission function. The highest meaningful frequency is at approximately 0.04 cycles/deg.

Another sampling method explored is irregular sampling as described in fig. 28. The problem with irregular sampling when using randomly sampling locations is the image reconstruction results vary considerably from subsequent runs due to the different sampling locations change. The quality of the image reconstruction is sensitive to not only the total number of samples but also their location. Figure 32 illustrates this problem by comparing multiple runs for various sample sizes using both uniform and randomly selected irregular sampling methods. As the sample size decreases and the number of possible randomly selected sample locations increases, the variation from one run to next using randomly selected irregular

70

sampling increases. Meanwhile, because the sample locations using uniform sampling are fixed

for a given sample size, the variation between one run to the next is not an issue.
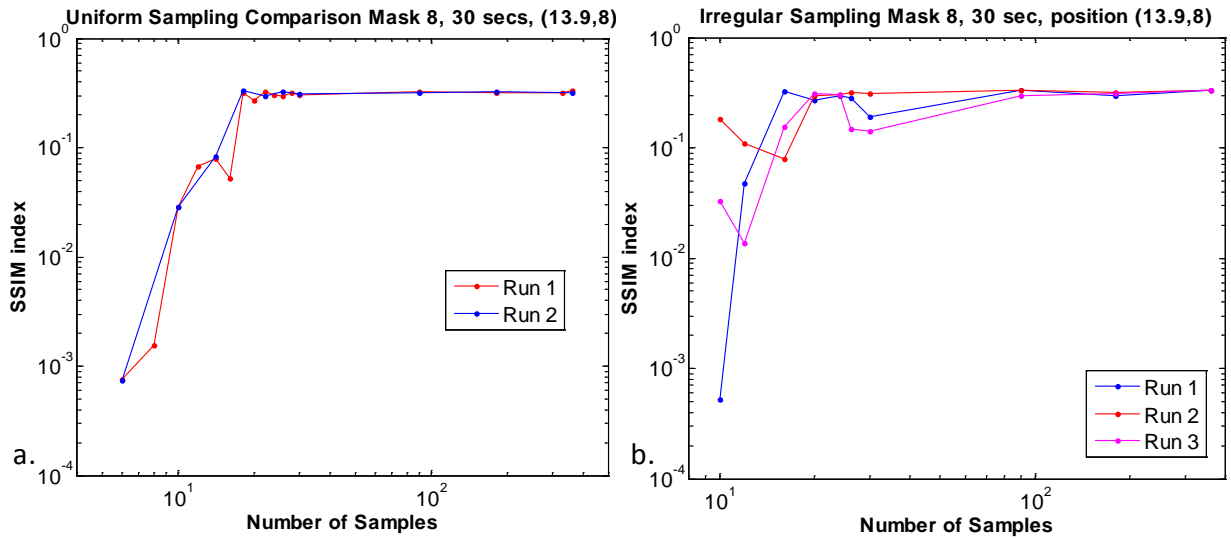
Fig. 31. These SSIM index comparisons illustrate the difficulty in getting the same results for subsequent runs using irregular sampling relying on randomly selecting a fixed number of collection locations compared to the repeatability of uniform sampling. Plot (a) shows the SSIM indices for two subsequent uniform sampling runs where the points are overlapping for the same sample size. Plot (b) shows the SSIM indices for three subsequent random irregular sampling runs where the indices vary for the same sample size.

Based on the information provided in fig. 32, it may be difficult to understand the

usefulness of irregular sampling. There is another was to apply irregular sampling that can

provide more predictable results. Rather than randomly select the sampling locations based on

the desired sampling size, the sample locations are selected based on knowledge of the

transmission function. This may seem a bit backwards because it means the source location is

already known, otherwise how is the transmission function corresponding to the source position

realized. This method could be applied in looking in a specific area within the field of view of

the RMC to determine the radiation content. Figure 30 shows the manually selected sample

locations for the sample sizes of 12 from a transmission function for a point source located at

71

(16,0). These points are selected because they represent the local minima and maxima within the

transmission function and capture the transmission function's phase and frequency required to

identify the source position. This will be referred to as critical irregular sampling to differentiate

it from random irregular sampling.
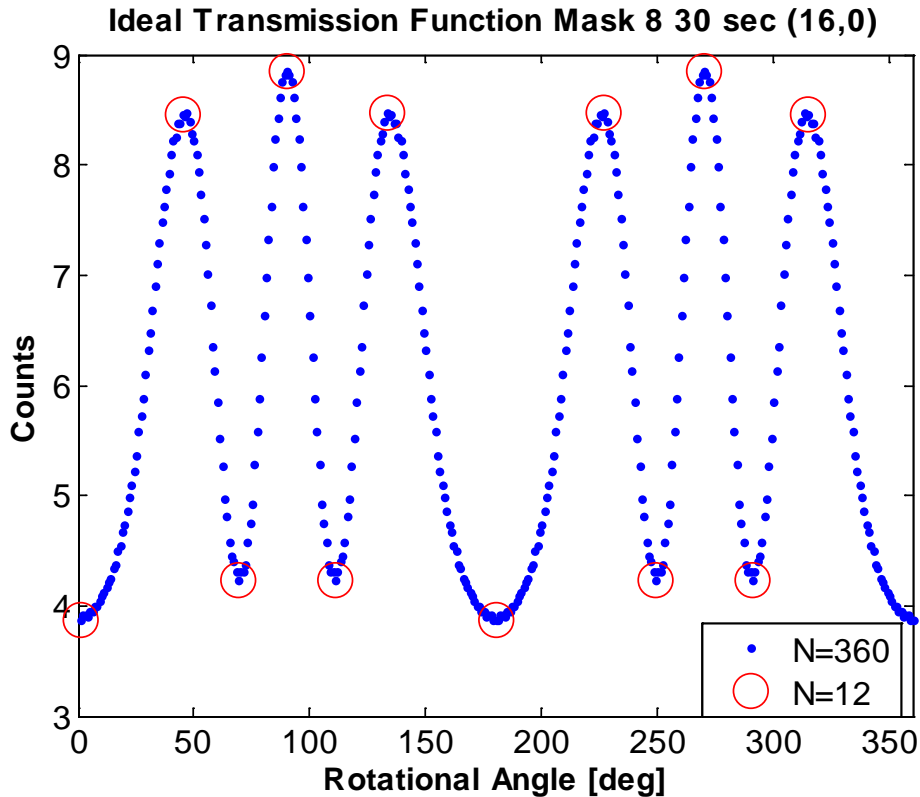
Fig. 32. This plot shows the ideal transmission function along the 12 sample locations carefully selected to capture the frequency and phase information of the transmission function.

Figure 34 shows the effectiveness of using critical irregular sampling compared to

uniform sampling for two different sample sizes. The performance improvement for the critical

irregular sampling is subtle when the point source activity is relatively high as shown in images

(a) through (c). When the source strength is reduced from 330 μCi to 11μCi, the critical irregular

sampling method clearly outperforms the both uniform sampling examples both in the computed

72

SSIM indices and through visual inspection of the reconstructed images. This essentially shows

how critical irregular sampling can reduce the minimum detectable activity, or for this

application minimum activity required for reconstruction at a desired threshold. Again, critical

irregular sampling is only possible when a known transmission function is available or at least

identified as the specific area of interest within the field of view.
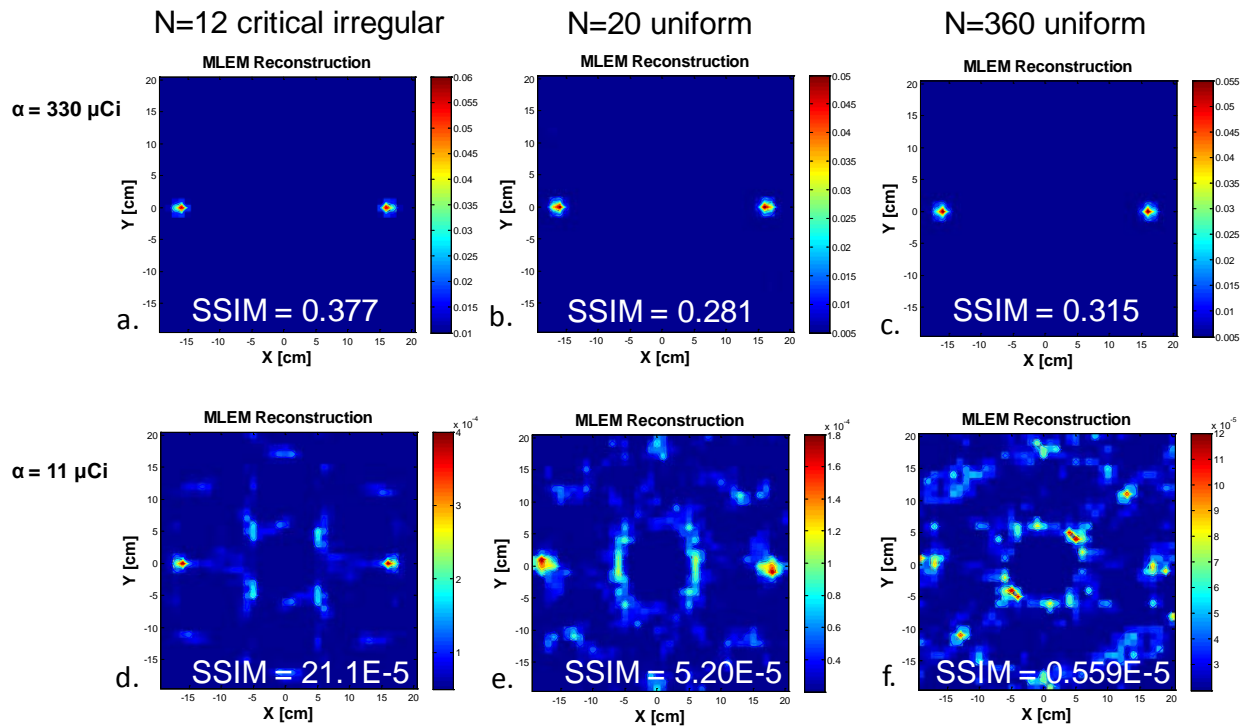
Fig. 33. These simulated reconstructed images show the impact of applying critical irregular sampling. For a source strength of 330 µCi there is only minor differences between the critical irregular and uniform sampling reconstructions (a through c). As the source strength is decreased, the performance of critical irregular sampling is more apparent as the SSIM index becomes nearly four times larger than the uniform sample size of 20 and more than an order of magnitude larger than the uniform sample size of 360.

73

IV. D. Adaptive Mask Design

Each of the eight mask designs were used to image a source for ten minutes. By dividing up the collected data into one minute increments, a time lapse profile for the image formation for each mask design is made. Fig. 35 provides an illustrative example of how the images develop as collection time increases. This figure shows only the position estimate, but clearly shows how the position resolution deteriorates as the as the mask design becomes more and more permissive. Another interesting observation is the apparent lack of change using mask 8. A few 'ghost' pixels are eliminated from the 60 second reconstruction to the 600 second, but overall the image remains unchanged. Another interesting observation is the result of mask 1. After ten minutes of collection with a 0.33 mCi source with a background of 15 counts per second, mask 1 cannot resolve the frequency component of the transmission function indicating the radial distance from the origin as discussed in chapter 2. While the phase information of the transmission function is correct at 600 seconds, mask 1 does not consistently display the correct phase information throughout the incremental development. Many other observations can be made by visually analyzing the images in fig. 35, but most of these observations are qualitative and relative. Where quantitative measures are needed to construct fair and consistent comparisons, the SSIM index discussed in section II.E.3. is applied.

By transferring each reconstructed image matrix into an array, the time lapse images for each mask design can be plugged into (2.14). The reference array contains the calculated activity of the source at its known position with the value of the background in every other location. Using identical masks, even a perfect reconstruction would not exactly match the truth information in the reference image because the symmetric masks reconstruct the source location

74

and its symmetric complement. Figure 36 includes the quantitative comparison of the time lapse

reconstruction for each of the eight masks.
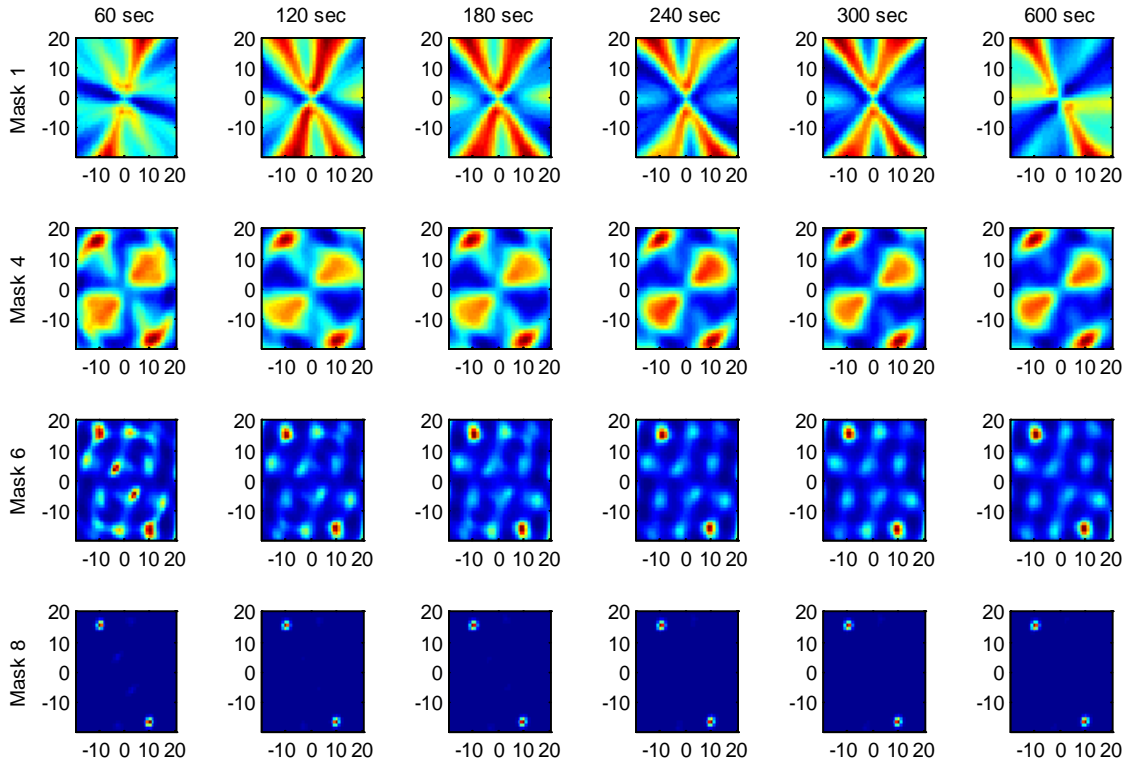
Fig. 34. These plots show the time lapse image formation for four of the mask designs. The plots are organized in rows by mask design and columns by collection time. The image plane is 40 by 40 cm with source located at (10,-16). All mask separations are 20 cm apart and the reconstruction used 100 bootstrap and MLEM iterations. All images are each scaled individually.
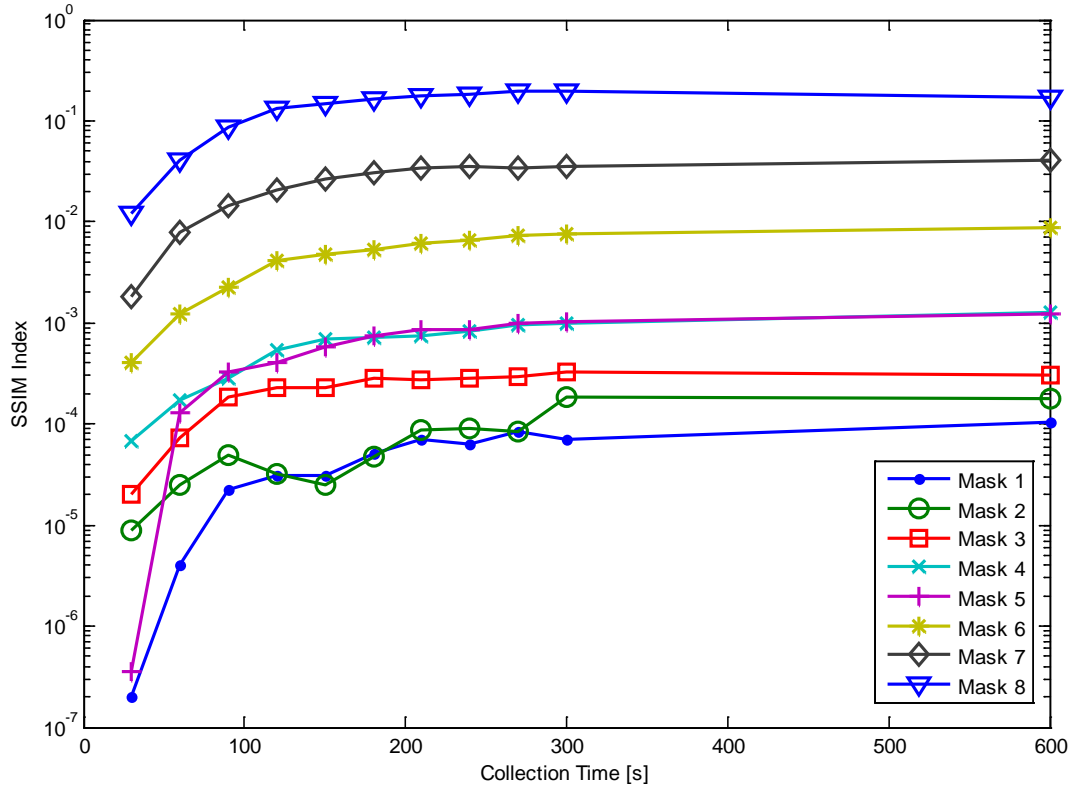
Fig. 35. This plot shows the SSIM results of reconstructing data for time increments up to ten minutes for each of the mask designs. From the SSIM algorithm (2.12) the constants were set to zero and the exponential parameters were unity. The computation reconstruction effort was the same for every computation using 100 bootstrap and MLEM iterations.

Opposed to the strictly position estimate comparison in fig. 35, fig. 36 includes accounts for differences in activity estimates as well. All masks appear to exponentially approach some asymptotic limit of image quality, shown by the leveling off of the SSIM index. The implications of this feature is that by after approximately 120 seconds each mask design has reached its maximum SSIM index under these collection conditions. This may be useful to understand that further collection time will not yield more favorable results without some change to the RMC system. This indicates a maximum achievable performance for a given mask design for a given imaging scenario. An additional feature that is of interest is the sudden increase in the SSIM index for mask 5 between 30 and 60 seconds. This is by far the largest increase for a

76

single mask over a 30 second increase in collection time. This may indicate that the mask 5 design is somehow optimized for these collection conditions between the 30 and 60 second time intervals. Additional experiments would need to be run to verify these feature and to attempt to duplicate is for the other mask designs by altering the collection conditions.

This plot provides one part of the information necessary to understand the tradeoff between position resolution and detection efficiency for a mask design. As would be expected, the mask design that provides the greatest change in exposed area of detector from one rotation to the next provides the best image estimate results.

The other part of the mask selection tradeoff is the detection efficiency. The detection efficiency, as mentioned in section II.D.2, is a function of the number of counts recorded. The efficiency does not change when the number of total counts is divided by the collection time to provide the count rate. The count rates for each mask, using the total number of counts detected in 30 second increments for 600 seconds, were recorded. While the count rate for a specific angular position is different for each angle, this total count rate includes all the counts from the full rotations.

The mean count rate for each of the masks is shown in fig. 37. The trend of the count rates follows the expected theory with a few exceptions. Referring back to the mask surface area ratio in section III.A.1, the ratios did not steadily decrease with the mask design identification numbers. The average count rate, however, falls off steadily from mask 1 to mask 8. None of the count rate uncertainties overlap indicating that the surface area ratio is not the ideal indicator of mask detection efficiency.
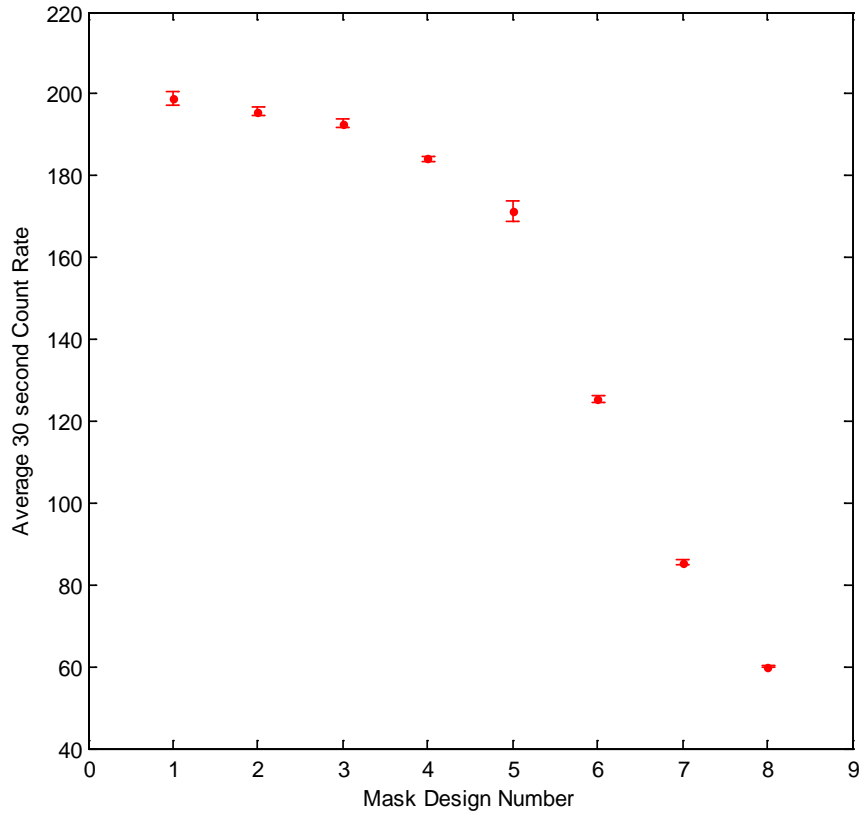
Fig. 36. This is a plot of the average count rate for each mask design over a 30 second collection period.

By combining the information in fig. 36 and fig. 37, the tradeoff between resolution and detection efficiency is apparent. An adaptive mask selection approach can then be used by selecting a mask with a high detection efficiency to observe an unknown scene for a particular energy line. With prior knowledge of the background, the RMC will be able to detect the presence of a source earlier with a lower mask design number. This initial collection provides limited position information, but does provide a crude estimate not provided by a bare detector. The initial position estimate can then be refined by switching the mask design to a higher number which has a better estimate performance based on fig. 36.

78

IV. E. Adaptive Pivot

The CRLB of the source position variance provides critical system performance information. The CRLB map in fig. 38, indicates vulnerabilities of the RMC system performance before any collections are acquired. Obviously regions of poor performance would preferably be avoided. An intermediate image reconstruction indicates if the source potentially is located in a vulnerable region relative to the RMC centerline. The most intense areas of the initial reconstruction overlap the areas of the CRLB cross section where the variance is at a maximum. By pivoting the RMC 1.7 degrees in the opposite direction of the image plane origin located 314 cm away, the source is not located in CRLB variance trough. The image of the pivoted RMC shows the improvement in relative variance. The collection times for each of the reconstructed images are equal. Additionally, the combined results of the two images provide a better position estimate than either of the configurations with equivalent collection times.

Another advantage of using the rotary table is the ability to expand the field of view. While the FOV indeed follows (2.12), the idea of taking a panoramic picture by splicing multiple narrow field pictures together can be applied as shown previously in fig. 14.
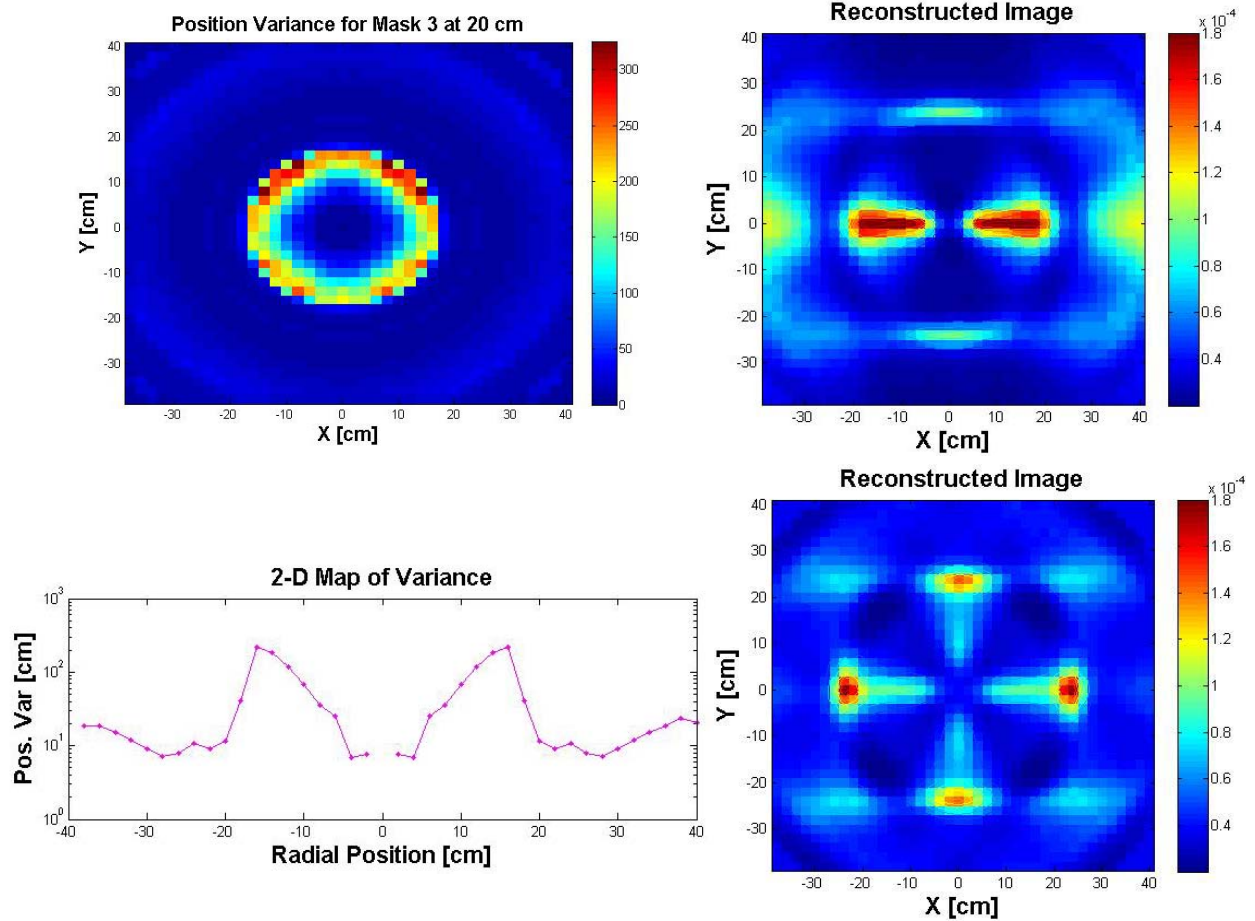
Fig. 37. The initial reconstructed image (upper r) showing a high degree of radial distance variance for the source location. Using the CRLB position variance map (upper l) which is fixed for given RMC system configuration, the pivot angle is slightly adjusted to avoid areas of high variance. The pivoted reconstructed image (lower r) shows the improvement of position resolution. The initial source location relative to the RMC centerline is (16,0) and (22,0) after pivoting the centerline. The cross-section of the CRLB map (lower l) shows a decrease in the CRLB of the position variance of an order of magnitude between 16 and 22.

V.   Conclusions and Future Work

V. A. Conclusions

The fidelity results present a fairly significant problem in making any hard and fast conclusions concerning the experimental results. Specifically, the disagreement between the experimental and simulated transmission functions and the erratic behavior of the experimental transmission function in the two areas of the last 180 degrees of rotation discussed in section IV.B. While duplicating the first 180 degrees of rotation was used as a work around for the erratic contributions, the experimental and simulated transmission functions remain unmatched. Fortunately, this mismatch is not in the phase, frequency, or general shape of the transmission function and is simply DC offset from each other. Essentially a constant scaling factor is all that separates the experimental and simulation transmission functions, the erratic behavior notwithstanding. Because the shape of the experimental and simulated transmission functions are the same, reliable image reconstructions are possible.

The effect of decreasing the number of uniform samples for a transmission function was identified. Provided that the Nyquist limit does not exceed the sampling rate, the number of uniform samples can be decreased from 360. This can improve the time to collect a well established transmission function because the dwell time for each sample can be increased. Irregular sampling can provide greatly improved collection time performance but is difficult to implement due to the need to identify the critical points of the transmission function. While much fewer points can be used to accurately estimate the frequency and phase of the transmission function, the location of these critical points is only identified once the source position is known. It was shown that by decreasing the number of sampling locations by either uniform sampling or critical irregular sampling the minimum activity required to reconstruct an

81

image to a desire SSIM index threshold can be reduced. Additionally, the critical irregular sampling method can further reduce the minimum activity even when compared to a reduced uniform sample size. As discussed, critical irregular sampling can only be applied to a specific transmission function prior to collection. While a purely adaptive approach was not identified, the preliminary understanding of the effect of reduced uniform sampling and irregular sampling provides a starting point moving forward.

The mask designs explored in this research provide some enlightening results in the area of mask design. While the open trapezoid masks have quite low position resolution, they provide general directional information of the source. This can be quite useful in applications needing detection sensitivity over a wide field of view. The tradeoff between position resolution and detection efficiency is readily recognizable when analyzing the SSIM image quality assessment and looking at the count rate for all the mask designs. These results show a potential application in developing a collection profile to improve detection efficiency and position resolution rather than a purely adaptive collection sequence. The feedback loop required in adaptive applications requires SSIM index (or any other image quality assessment) benchmarks to be established for each mask configuration. During collection, these images need to be analyzed against the benchmark to determine which RMC configuration change is necessary. The information presented here concerning these mask designs provides better characterization of the different RMC configurations.

While the bulk of the research focused on sampling techniques and mask design evaluation, the RMC pivot experiment provided a proof of concept for adaptive pivoting. For the specific cases explored, pivoting the mask to a relative location with a lower CRLB on the position variance provided improved performance based on the SSIM index results.

82

V. B. Future Work

There are a number of directions this research could follow. One of the most promising directions is in the area of sampling theory. Significant improvements in compressed sensing in recent years have shown considerable reduction in the lower sampling limit, challenging the historical Nyquist limit. By drastically reducing the number of sampled locations the RMC may be able to overcome the loss of information due to collimation. As one of the long standing drawbacks to RMC application has been the long collection times necessary to image sources with activities near the background. The transmission function in the frequency domain may be sparse enough to take advantage of the principles behind compressed sensing introduced in the following papers [19] [20]. This would allow for fewer samples to be recorded.

Following the characterization of the effects of changing the sampling profile, the mask design, and RMC pivot angle, an ideal collection profile can be determined. By adding variable mask separation distances to the flexible RMC system parameters, ideal collection profiles can be plotted for various image scenarios. While these collection profiles are not adaptive, they benefit from a single image reconstruction process whereas adaptive methods require multiple image reconstructions for the same radiation scene observation.

An additional direction concerns mask design. This research explored masks having a constant slit pitch. Rather than having to change a mask configuration with a different slit pitch, the mask design could include a variable slit pitch. A larger slit pitch in the middle of the mask with smaller slit pitch on the edges of the mask could potentially provide an ideal compromise between the position resolution and detection efficiency. This would combine the position resolution strength of the finer slit pitches with the detector sensitivity of the larger slit pitches.

83

Appendices

Appendix A. Matlab Script

A.1 Create_RMCLib_Systems.m

```matlab
%RMC Library Creator

%By: Ben Kowash
%Date: 21 Jun 08
%Update: 28 Jun 08
%
%Description: This routine Generates RMC system matrices for later uses in
%ML-EM, Likelihood-Function, and fmincon image reconstruction routines.
%
%System matrices 'A' contain the probability that a source emitted from a
%pixel in the source plane is transmitted through the RMC to the detector.

%v1.0: Assumes black masks
%      Assumes two mask systems
%      Naming convention:
%      'Sz_L_t_x_max_dx_gridRes.mat'
%
%v2.0: Creates libraries for multiple RMC measurements/simulations
%v3.0: Utilizes Mask Parameter .mat files to load specific mask information
%and build grids according to slit shape selection




close all
clear all
clc

simulation = 'yes'; %Simulation or Measurment
filename = 'Mask8-20cm'; %Insert name of measurement or simulation

%*********************For Measurements Only*************
Home_Address = 'F:\Lab RMC\';
RMC_data_path = [Home_Address,'Results\24 hr run\'];
RMC_data_files = [RMC_data_path,'RMC_54000 - Mask8-20cm'];
RMC_raw_files = [RMC_data_path,'data_54000.mat'];
RMC_home = 8805; %Encoder Position for Home
%*****************************************************

%Set RMC System Parameters****************************
num_sys = 1; % # of RMCs or measurements made at different positions

RMC_CL_coord = [0 0]; %Cartesian coordinates of RMC centerline
num_grids = [4]; % # of grids . must be >=2
grid_size = [2E3]; % Grid resolution
R_det = [3.81]; %Radius of detector [cm]
mask_path = [Home_Address,'RMClib\Mask Parameters\'];
mask_file = ['Mask8'];
mask_coord_path = [Home_Address,'MaskDesign\',mask_file,'.mat'];
```

84

```matlab
mask_coord = importdata(mask_coord_path);

mask_sep = [21.13]; %Mask separation [cm]
N_samp = [360]; %Number of samples in the transmission function

% samp = sort(randi(360,1,N_samp));  %picks N_samp number of random sampling
points between 1 and 360. "Compressed Sensing"
samp = 1:360/N_samp:360; %picks N_samp at a fixed interval. N_samp muct be a
factor of 360.
samp_diff_var = var(diff(samp)); %if this is zero then it is a fixed interval
if ~= 0 then random interval

runtime= [30*18];  %[sec]
tau = [ones(1,N_samp(1,1)).*(runtime(1,1)/N_samp(1,1))]; %Dwell time per bin
[sec]
epsRMC = [.6]; %Detector Intrinsic Efficiency

%Set Source plane grid parameters***************************
num_src =1;
Sxyz = [16 0 314]; % location of source with detector at (0,0,0) (x, y, z)
[cm]
act = [330e-6*3.7e10]; %source activity [Bq] Co-57 as of 19Oct2010
bkg = [15]; %background [cps]

%Set RMC System Matrix Parameters*************************
x_max = 40; %Number of pixels in x
y_max = 40; %Number of pixels in y
dx_base = 1; %Pixel resolution in x [cm]
dy_base = dx_base; %Pixel resolution in y [cm]
x_expect = 0; %Used to center window to zoom in Measurement
y_expect = 0; %Used to center window to zoom in Measurement
z_max = 1;
z_0 = 314; %location of reconstructed image plane.
dz = 100; %Resolution in z [cm]

%Corrects the repetitive sys parameters for the correct num of sys
if num_sys > 1;
    RMC_CL_coord = correct_for_num_sys(num_sys,RMC_CL_coord);
    num_grids = correct_for_num_sys(num_sys,num_grids);
    grid_size = correct_for_num_sys(num_sys,grid_size);
    R_det = correct_for_num_sys(num_sys,R_det);
    mask_file = correct_for_num_sys(num_sys,mask_file);
    mask_sep = correct_for_num_sys(num_sys,mask_sep);
    N_samp = correct_for_num_sys(num_sys,N_samp);
    samp = correct_for_num_sys(num_sys,samp);
    runtime = correct_for_num_sys(num_sys,runtime);
    tau = correct_for_num_sys(num_sys,tau);
    epsRMC = correct_for_num_sys(num_sys,epsRMC);
end;

%Reads in mask parameter information for each RMC system
slot_len(1:30,1:num_sys) = 0;
for i = 1:num_sys;
    mask_name =[mask_path,mask_file(i,:),'.mat'];
    load (mask_name);
```

85

```matlab
    a(i,:)=slit_pitch;  %slit pitch [cm]
    w(i,:)=slit_width;  %slit width [cm]
    c(i,:)=left_edge_1st_slit;  %location of left edge of furthest left slit
[cm]
    t_mask(i)=mask_thickness;   %mask thickness [cm]
    mask_min(i)=slit_to_radius; %minimum distance between slit and edge of
mask [cm], this determines the slot length unless specified
    slot_type(i,:)=slit_shape;  %describes the shape of the slit as string
variable (trapazoid, rounded, rectangle, or specified)
    if strcmp(slot_type(i,:),'specified');  %'specified' allows for specific
slot length dimensions as input for a rectangle slit
        slot_len(1:length(slot_length),i)=slot_length;
    end;
    mu(i)=mass_atten;   %mass attenuation coefficent based on the material
type and energy of gammas
end;




%Define physical properties of the masks
atten = exp(-mu.*mean(t_mask,2));



%*** Compute mask separation parameters 'L' for each grid ***
for i=1:num_sys

    if (num_grids == 2)
        L(i,:) = [0, mask_sep];
    else
        mask_pos = 0;
        for j=1:num_grids(i)

            L(i,j) = mask_pos;
            if (isEven(j) == 0)
                mask_pos = mask_pos + t_mask(i);
            else
                mask_pos = mask_pos + mask_sep(i);
            end
        end

    end
end
clear mask_pos



%Corrects the repetitive source parameters for the correct num of sys
if num_src > 1;
    Sxyz = correct_for_num_sys(num_src,Sxyz);
    act = correct_for_num_sys(num_src,act);
    bkg = correct_for_num_sys(num_src,bkg);
end;
```

```matlab
    %Saves input into appropriate library file
    if (strcmp(simulation,'yes')==1)
        sim_system = [Home_Address,'RMCLib\Sim_System\'];
        sim_src = [Home_Address,'RMCLib\Sim_Src\'];
        sim_sys_name = [sim_system,filename,'_simsys.mat'];

save(sim_sys_name,'num_sys','RMC_CL_coord','num_grids','grid_size','R_det','a
','w','c','mask_min','t_mask','mask_sep','L','slot_len','slot_type','N_samp',
'samp','tau','epsRMC','mu','atten','mask_coord')

        sim_src_name = [sim_src,filename,'_simsrc.mat'];
        save(sim_src_name,'num_src','Sxyz','act','bkg')

    else %Measurement Data
        meas_system = [Home_Address,'RMCLib\Meas_System\'];
        meas_sys_name = [meas_system,filename,'_meassys.mat'];

save(meas_sys_name,'Sxyz','num_sys','RMC_CL_coord','num_grids','grid_size','R
_det','a','w','c','mask_min','t_mask','mask_sep','L','slot_len','slot_type','
N_samp','tau','epsRMC','mu','atten')

        meas_data = [Home_Address,'RMCLib\Meas_data\'];
        meas_data_name = [meas_data,filename,'_measdata.mat'];
        save(meas_data_name,'RMC_data_files','RMC_raw_files','RMC_home')
    end


    %**********************************************************************
    %****************Generate System Matrix********************************
    %**********************************************************************

    %Sets up the number of image planes to look at seperated by dz
    z = zeros(z_max,1);
    for i=1:z_max
        z(i) = z_0 + (i-1)*dz;
    end

    tic

    for k=1:num_sys

        %sets up image plane grid
        dx = zeros(z_max,1);
        dy = zeros(z_max,1);
        x_tot = zeros(x_max,z_max);
        y_tot = zeros(y_max,z_max);

        for q = 1:z_max

            %adjusts image plane grid magnification based on distance from
            %reference plane z_0
            dx(q) = dx_base * ((q-1)*dz+z_0) / z_0;
            dy(q) = dy_base * ((q-1)*dz+z_0) / z_0;
```

87

```matlab
        %Build RMC Filename -
        %'num_sys-RMC_CL_coord-num_grids-grid_size-R_det-mask_file-mask_sep-
N_samp-runtime-tau-epsRMC-x_max-y_max-dx_base-dy_base-x_expect-y_expect-
z_max-z_0-dz.mat'
        A_name =
[num2str(z(q)),'_',num2str(mask_sep(k)),'_',num2str(min(t_mask(k))),'_',num2s
tr(x_max),'_',num2str(y_max),'_',num2str(dx(q)),'_',num2str(dy(q)),'_',num2st
r(x_expect),'_',num2str(y_expect),'_',num2str(grid_size(k)),'_',num2str(N_sam
p(k)),'_',num2str(samp_diff_var(k)),'_(',num2str(RMC_CL_coord(k,1)),'_',num2s
tr(RMC_CL_coord(k,2)),')','_',num2str(mask_file(k,:))];

        %Read RMC filename to see if library exists.  For random sampling
        %it will re-compute A matrix for new pints even though the number
        %of sampled spoints is the same.

        %checks to see if the TF is sampled randomly or at a constant
        %interval and recomputes system matrix every time for random
        if var(diff(samp))<1;
            [A,x,dummy,dummy,y] = Read_RMCLib(A_name,Home_Address);
        else
            A=-1;
        end;

        if (A == -1)

            %Initialize x & y
            x = zeros(x_max,1);
            y = zeros(y_max,1);

            %************************************** Compute RMC grid size
            for i=1:grid_size
                grid_dim(i) = (2*R_det(k)*(i-1)/(grid_size(k)-1)) - R_det(k);
            end

%**********************************************************************
            %*** Compute grid magnification factor 'M'
            M = z(q) ./ (z(q)-L(k,:));
            %*********************************

            %Get the grid patterns
            R_grids = R_det(k)./M;
            R_slits(k) = R_det(k) - mask_min(k); % Sets the an inner radius
as a contraint on the slit dimensions
            grids =
get_RMCgrids_v2(a(k,:),w(k,:),c(k,:),M,grid_dim,R_slits(k),slot_type(k,:),slo
t_len(:,k));

%
            % Calculate the system matrix 'A'

            A = zeros(N_samp(k),x_max*y_max);
            h = waitbar(0,['Pre-computing A - ',num2str((k-1)*z_max+q),' of
',num2str(num_sys*z_max)]);
            for i=1:x_max
```

88

```matlab
                x(i) = (i-round(x_max/2)-(x_expect/dx(q))) * dx(q);
                Sx = x(i)-RMC_CL_coord(k,1);

                for j=1:y_max

                    y(j) = (j-round(y_max/2)-(y_expect/dy(q))) * dy(q);
                    Sy = y(j)-RMC_CL_coord(k,2);

                    A(:,(i-1)*y_max+j) =
calcA_RMCgrids_v3(grids,num_grids(k),grid_size(k),Sx,Sy,z(q),L(k,:),R_grids,g
rid_dim,w(k,:),M,N_samp(k),samp(k,:),mask_sep(k),mask_coord);
                    A(:,(i-1)*y_max+j) = (A(:,(i-1)*y_max+j) + (1-A(:,(i-
1)*y_max+j)).*atten(k)).*RMC_Omega(R_det(k),z(q)-
max(L(k,:)),sqrt(Sx^2+Sy^2))./(4*pi);
                end
                waitbar(i/x_max)

            end
            close(h)
            Write_RMCLib(A_name,A,x,x_max,dx(q),y,y_max,dy(q),Home_Address)
        end

        if (q == 1)
            A_z = A;
            x_tot(:,q) = x;
            y_tot(:,q) = y;
        else
            A_z = [A_z,A];
            x_tot(:,q) = x;
            y_tot(:,q) = y;
        end

    end
    A = A_z;
    clear A_z;

    if (k ==1)
        A_tot = A;
    else
        A_tot = [A_tot;A];
    end

    clear A

end

Write_RMCLib(filename,A_tot,x_tot,x_max,dx,y_tot,y_max,dy,Home_Address)
```

A.2 RMC_Toolbox.m

```
%RMC Toolbox

%By: Ben Kowash
%Date: 27 Jun 08
%v: 1.0
%
%Description:
%1. This program brings together many of the RMC analysis
%concepts I have developed and puts them into a single package.  The
%program begins by asking whether the input data will be provided
%by measured data or by simulated data. If the data is measured, two files
%are read for each measurement made: (1) Measured data for each measurement
%and (2) System configuration for each measurement.  If the data is to be
%simulated, a pair of files is read that contains: (1) Location and activity,
%of all sources as well as the system background. (2) The system
configuration
%for each measurement.  To avoid confusion, the source plane is used to
%define the coordinate system used for each of the measurements

%2. Once the problem is defined a system model is generated for each new
%measurement.  The user defines the model resolution as well as number of
%pixels to be used.
tic
close all
clear all
clc

num_meas = 1; %Number of independent measurements
simulate = 'yes'; %Use simulation vs measured data
filename = 'Mask8-20cm'; %Name of case to run
Home_Address = 'F:\Lab RMC\';
[A,x,x_max,dx,y,y_max,dy] = Read_RMCLib(filename,Home_Address);
plot_num = 3;

run_LL = 'no'; %Source estimation with log-likelihood model
run_fisher = 'yes'; %Compute Fisher Information map
run_MLEM = 'no'; %Image reconstruction using ML-EM algorithmE;\
    iter_MLEM = 100; %# of MLEM iterations
    iter_BS = 1; %# of bootstrap iterations
    MLEM_bkg = 15; %# background to use for MLEM algoritm
    MLEM_tol = 1e-5; %Tolerance for MLEM convergence
    z_max = 1; %# of z planes in problem

if (strcmp(simulate,'yes') == 1)
    sim_system = [Home_Address,'RMCLib\Sim_System\',filename,'_simsys.mat'];
    sim_source = [Home_Address,'RMCLib\Sim_Src\',filename,'_simsrc.mat'];
    load(sim_system)
    load(sim_source)
else
    meas_system =
[Home_Address,'RMCLib\Meas_System\',filename,'_meassys.mat'];
    meas_data = [Home_Address,'RMCLib\Meas_data\',filename,'_measdata.mat'];
    load(meas_system)
    load(meas_data)
```

```matlab
    end

%**********************************************************************
%******************Set up Data Vector T_sys************************
%**********************************************************************
%***************Get Simulated System**********************************

if (strcmp(simulate,'yes') == 1)

    T_sim = [];
    for k=1:num_sys

        %*** Compute RMC grid size
        for i=1:grid_size(k)
            grid_dim(i) = (2*R_det(k)*(i-1)/(grid_size(k)-1)) - R_det(k);
        end

        %*** Compute grid magnification factor 'M'
        M = Sxyz(1,3) ./ (Sxyz(1,3)-L(k,:));
        R_grids = R_det(k) ./M;
        R_slit = R_det(k) - mask_min;
        %First get the grid patterns
        grids =
get_RMCgrids_v2(a(k,:),w(k,:),c(k,:),M,grid_dim,R_slit(k),slot_type(k,:),slot
_len(:,k));%(a,w,c,M,x,R_slit,slot_type,slot_len)
        grids(1,:) = 0;
        T_multsrc = [];
        for i=1:num_src
            T_sngl =
calcA_RMCgrids_v3(grids,num_grids(k),grid_size(k),Sxyz(i,1)+RMC_CL_coord(k,1)
,Sxyz(i,2)+RMC_CL_coord(k,2),Sxyz(i,3),L(k,:),R_grids,grid_dim,w(k,:),M,N_samp
p(k),samp(k,:),mask_sep(k),mask_coord);
            T_sngl = ((T_sngl + (1-T_sngl).*atten(k)).* act(i) .*
epsRMC(k).*RMC_Omega(R_det(k),Sxyz(i,3)-
max(L(k,:)),sqrt((Sxyz(i,1)+RMC_CL_coord(k,1))^2 +
(Sxyz(i,2)+RMC_CL_coord(k,2))^2)).(4*pi) + bkg(i)).*tau(k);
            T_multsrc = [T_multsrc,T_sngl];
        end

        T_sim = [T_sim;sum(T_multsrc,2)];
        T_sys = poissrnd(T_sim);
    end
    figure(plot_num)
    plot(samp,T_sys,'g*-')
    hold on
    plot(samp,T_sim,'b.-')
    %plot(T_sim./4.3245e+003,'b.')
    plot_num = plot_num + 1;

    clear T_multsrc
    clear T_sngl
%***************Load Measured Data**********************************
else

    T_sys = zeros(360,1);
```

91

```matlab
    %T_sys = [];
    num_sys=1;
    for k=1:num_sys

        load(RMC_data_files(k,:));
        %T_sys = [T_sys; cnt'];
        T_sys = T_sys + cnt';
    end

    num_sys = 1;

    figure(plot_num)
    plot(T_sys,'r.-')
    plot_num = plot_num + 1;

end

%*******************************************************************
%*******************************************************************

%**************Log-Likelihood Function****************************
if (strcmp(run_LL,'yes') == 1)

    act_ref = act; %source activity [Bq]
    bkg_ref = bkg; %background [cps]
    tau_tot = tau(1,:);
    for k=2:num_sys
        tau_tot = [tau_tot, tau(k,:)];
    end

    %Set up and Run the bootstrap algorithm
    if (strcmp(simulate,'yes') == 1)
        %Set up T_BS for simulated data
        T_BS(:,1) = T_sys;
        for j=2:iter_BS;
            T_BS(:,j) = poissrnd(T_sim);
        end
    else
        %Set up T_BS for measured data
        T_BS = Resample_RMC(RMC_raw_files(k,:),RMC_home(k),iter_BS);
    end

    LL = zeros(x_max*y_max,iter_BS);

    h = waitbar(0,'Mapping RMC Cost Function');
    for i=1:iter_BS
      LL(:,i) =
get_LLRMC(T_BS(:,i),A,x_max,y_max,epsRMC,act_ref,bkg_ref,tau_tot,num_sys,N_sa
mp);

        waitbar(i/iter_BS)
    end
    close(h)
```

92

```matlab
    LL_mean = mean(LL,2);
    LL_im = reshape(LL_mean,x_max,y_max);

    figure(plot_num)
    subplot(4,3,1)
    imagesc(x,y,LL_im)
    axis image
    axis xy
    colorbar
    plot_num = plot_num+1;

%     map = zeros(x_max*y_max,1)
%     P_sum = sum(A,1);
%     for i=1:x_max*y_max
%         for k=1:360
%             map(i) = map(i) + T_sys(k) * log(A(k,i)/P_sum(i));
%         end
%     end

%     figure(plot_num)
%     imagesc(x,y,reshape(map,x_max,y_max))

end

%***************Fisher Information*********************************
if (strcmp(run_fisher,'yes') == 1)

    act_ref = 3.7E10 * 100E-6; %Reference activity used for Fisher
Information and LL
    bkg_ref = 8; %Reference background used for Fisher Information and LL
    [F_act,F_x,F_y,CRLB_act,CRLB_x,CRLB_y] =
get_FisherRMC(A,x,y,x_max,y_max,N_samp,act_ref,bkg_ref,tau,epsRMC,num_sys,R_d
et,Sxyz(1,3));

    figure(plot_num)
    subplot(3,2,1)
    imagesc(x,y,reshape(F_act,x_max,y_max))
    colorbar
    axis xy
    axis image
    title(['F_a_c_t - N =
',num2str(sum(N_samp))],'fontsize',16,'fontweight','b')
    subplot(3,2,3)
    imagesc(x,y,reshape(CRLB_act,x_max,y_max))
    colorbar
    axis xy
    axis image
    title(['var_a_c_t - N =
',num2str(sum(N_samp))],'fontsize',16,'fontweight','b')
    subplot(3,2,2)
    imagesc(x,y,reshape(F_x + F_y,x_max,y_max))
    colorbar
    axis xy
    axis image
```

93

```matlab
    title(['F_A_B - N =
',num2str(sum(N_samp))],'fontsize',16,'fontweight','b')
    subplot(3,2,4)
    imagesc(x,y,reshape(CRLB_x + CRLB_y,x_max,y_max))
    colorbar
    axis xy
    axis image
    title(['var_A_B - N =
',num2str(sum(N_samp))],'fontsize',16,'fontweight','b')

    %Plot position variance with large value at zero removed
    tmpA = CRLB_x;
    tmpB = CRLB_y;

    for qq = 1:5;
    loc(qq) = find(tmpA+tmpB == max(tmpA+tmpB));
    tmpA(loc(qq)) = 0;
    tmpB(loc(qq)) = 0;
    end;

    subplot(3,2,6)
    imagesc(x,y,reshape(tmpA + tmpB,x_max,y_max))
    colorbar
    axis xy
    axis image
%     title(['var_A_Bother - N =
',num2str(sum(N_samp))],'fontsize',16,'fontweight','b')
    title(['varAB -
N=',num2str(sum(N_samp))],'fontsize',16,'fontweight','b');

    subplot(3,2,5)
    tmpABsq = reshape(tmpA + tmpB,x_max,y_max);
    for i=1:x_max
        for j=1:y_max

            if (j==round(y_max/2))
                tmpAB(i) = tmpABsq(j,i);
            end

        end

    end
    semilogy(x,tmpAB,'m.-')
    plot_num = plot_num + 1;

    stats = [max(CRLB_act); min(CRLB_act); mean(CRLB_act); max(CRLB_x +
CRLB_y);  min(CRLB_x + CRLB_y);  mean(tmpA + tmpB)];
    %save(['C:\Users\Ben\Documents\PhD
    %Research\RMC_Simulations\Fisher_Information\N=',num2str(N_samp),' -
L=',num2str(mask_sep),'cm.mat'],'F_act','F_alpha','F_beta','var_act','var_alp
ha','var_beta','x','y');

end
```

94

```matlab
%***************ML-EM Image Reconstruction with
Bootstrap************************
if (strcmp(run_MLEM,'yes') == 1)

    % load('C:\Axy_W.mat')
    % x_max = 180;
    % y_max = 180;

     tau_tot = tau(1,:);
     for k=2:num_sys
         tau_tot = [tau_tot, tau(k,:)];
     end

    %Set up and Run the bootstrap algorithm
    if (strcmp(simulate,'yes') == 1)
        %Set up T_BS for simulated data
        T_BS(:,1) = T_sys;
        for j=2:iter_BS;
            T_BS(:,j) = poissrnd(T_sim);
        end
    else
        %Set up T_BS for measured data
        T_BS = zeros(N_samp(1),iter_BS);
        num_sys = 1;
        for k=1:num_sys
            T_BS = T_BS +
Resample_RMC(RMC_raw_files(k,:),RMC_home(1),iter_BS);
            %T_BS = T_sys;
        end

    end

    T_size = size(T_sys,1);
    %load('C:\Extended-T.mat')
    %b = T_bkg; %ones(T_size,1) .* MLEM_bkg .* tau_tot';
    b = ones(T_size,1) .* MLEM_bkg .* tau_tot';
    lambda = ones(x_max*y_max*z_max,iter_BS); %Initialize the guess for
lambda

    A = A.*epsRMC(1)*tau_tot(1);

    h = waitbar(0,'Performing bootstrap analysis');
    for i=1:iter_BS

        %Run the iterative ML-EM

        a = A' * ones(T_size,1);

        lambda_old = lambda(:,i);
        gate = 1;
        q_MLEM = 1;

        while (gate==1) || (q_MLEM < 10)
```

95

```matlab
            lambda(:,i) = RMC_MLEM(lambda(:,i), A, T_BS(:,i), b, a);
            pct_chg_lam = (lambda(:,i) - lambda_old)./lambda_old;
            lambda_old = lambda(:,i);
            if (sum((pct_chg_lam > MLEM_tol)) > 0 && (q_MLEM <= iter_MLEM))
                q_MLEM = q_MLEM+1;
            else
                gate = 0;
                if (q_MLEM < 10)
                    gate = 1;
                    q_MLEM = q_MLEM + 1;
                end
            end

        end

        lambda(:,i) = lambda(:,i) ./ (3.7E7); %Converts lambda from Bq to mCi

        k=1;

%            [img_max(i,1), img_max(i,2)] = max(lambda(:,i));
%            img_max(i,3) = x(floor((img_max(i,2)/x_max(k))));
%            if (floor(img_max(i,2)/x_max(k)) == img_max(i,2)/x_max(k))
%                img_max(i,4) = y(y_max(k));
%            else
%                img_max(i,4) = y(img_max(i,2)-
(floor((img_max(i,2)/x_max(k))))*y_max(k));
%            end

        waitbar(i/iter_BS)

    end
    close(h)

%   lambda = lambda ./ (epsRMC(k).*sum(sum(tau)));

    lambda_mean = mean(lambda,2);
    lambda_std = std(lambda,1,2);
    lambda_pkvar = lambda_mean ./lambda_std;

    lambda_tmp = lambda_mean;
    for i=1:x_max*y_max*z_max
        lambda_tmp(i) = [];
        lam_mn(i) = mean(lambda_tmp);
        lambda_SNR(i) = lambda_mean(i) / lam_mn(i);
        lambda_tmp = lambda_mean;
    end

    lambda_SNR = lambda_mean ./ lambda_pkvar;

%     BS_stats(k,1) = mean(abs(img_max(:,3))); %x mean
%     BS_stats(k,2) = std(abs(img_max(:,3))); %x err
%     BS_stats(k,3) = mean(abs(img_max(:,4))); %y mean
%     BS_stats(k,4) = std(abs(img_max(:,4))); %y err
%
```

96

```matlab
%      BS_stats
    if (k == 1)
        clear k
    end

    for q=1:z_max
        figure(plot_num);
        plot_num = plot_num + 1;
%         subplot(2,2,1)
        lambda_im = reshape(lambda_mean((q-
1)*x_max*y_max+1:q*x_max*y_max),x_max,y_max);
        set(gca,'YDir','normal');
        imagesc(x(:,q),y(:,q),lambda_im)
        axis xy
        axis image
        title('MLEM Reconstruction');
        colorbar
        hold on
        contour(x(:,q),y(:,q),lambda_im)
        title('MLEM Reconstruction','fontsize',16,'fontweight','b')
        xlabel('X [cm]','fontsize',16,'fontweight','b')
        ylabel('Y [cm]','fontsize',16,'fontweight','b')
%         subplot(2,2,3:4);
%         hist(reshape(lambda_im,x_max^2,1),100);


%         subplot(2,2,2)
%         lambda_im = reshape(lambda_mean((q-
1)*x_max*y_max+1:q*x_max*y_max),x_max,y_max);
%         sig = max(max(lambda_im(1:length(x)/2,(length(x)/2)+1:length(x))));
%         noise =
(sum(sum(lambda_im(1:length(x)/2,(length(x)/2)+1:length(x)))) -
sig)/(length(lambda_im(1:length(x)/2,(length(x)/2)+1:length(x)))^2-1);
%         SNR = sig / noise;
%
imagesc(x((length(x)/2)+1:length(x),q),y(1:length(y)/2,q),lambda_im((length(x
)/2)+1:length(x),1:length(x)/2)')
%         axis xy
%         axis image
%         img_title = strcat('MLEM Reconstructed Image: SNR=',num2str(SNR));
%         title(img_title);
%         colorbar
%         hold on
%         contour(x(:,q),y(:,q),lambda_im')
%         title(img_title,'fontsize',16,'fontweight','b')
%         xlabel('X [cm]','fontsize',16,'fontweight','b')
%         ylabel('Y [cm]','fontsize',16,'fontweight','b')

%         subplot(2,2,2)
%         lambda_imstd = reshape(lambda_pkvar((q-
1)*x_max*y_max+1:q*x_max*y_max),x_max,y_max);
%         imagesc(x(:,q),y(:,q),lambda_imstd)
%         axis xy
%         axis image
%         title('Standard Deviation of MLEM Image')
%         colorbar
```

97

```
%
%          subplot(2,2,3)
%          lambda_imSNR = reshape(lambda_SNR((q-
1)*x_max*y_max+1:q*x_max*y_max),x_max,y_max);
%          imagesc(x(:,q),y(:,q),lambda_imSNR)
%          axis xy
%          axis image
%          title('Signal to Noise Ratio')
%          colorbar
%          if (z_max > 1)
%              plot_num = plot_num + 1;
%          end
%
%          subplot(2,2,4)
%          plot(x(:,q),lambda_im(21,:),'b.-')
    end
end

toc
```

A.3 correct_for_num_sys.m

```
%%This eliminates the needs to replicate the same values repetitively for
%%each system parameter.

function [corrected_parameter] = correct_for_num_sys(num_sys,sys_parameter)

if size(sys_parameter,1) ~= num_sys

    for i = 1:num_sys;
        corrected_parameter(i,:)=sys_parameter;
    end;

else

    corrected_parameter = sys_parameter;

end
```

A.4 Read_RMCLib.m

```
function [A_rd,x_rd,xmax_rd,dx_rd,y_rd,ymax_rd,dy_rd] =
Read_RMCLib(lib_title,Home_Address)

%By: Ben Kowash
%Date: 17 Jun 08
%
%v 1.0
%Description: This function takes in data about a system run and determines
%if a file already exists in the library.  If it does the library file is
%opened and returned.  Otherwise an empty data set is returned.

lib_path = [Home_Address,'RMCLib\System_Matrix_1\'];

lib_vol = [lib_path,lib_title,'.mat'];
```

98

```matlab
if (exist(lib_vol,'file') == 2)
    load(lib_vol);
    A_rd = A;
    x_rd = x;
    xmax_rd = x_max;
    dx_rd = dx;
    y_rd = y;
    ymax_rd = y_max;
    dy_rd = dy;

else
    A_rd = -1;
    x_rd = -1;
    xmax_rd = -1;
    dx_rd = -1;
    y_rd = -1;
    ymax_rd = -1;
    dy_rd = -1;

end
```

A.5 get_RMCgrids_v2.m

```matlab
function [grids_out] = get_RMCgrids_v2(a,w,c,M,x,R_slit,slot_type,slot_len)

% Title: get_RMCgrids
% By: Ben Kowash
% Date: 20 May 08
% version: 2.0
%
% Description: This function is used to set up the various masks that are
% used to model a rotational modulated collimation detector.  The final
% output is a vector called 'grids_out' that contains the raw grid
% information for 'N' masks.  This new version uses heaviside functions to
% generate the masks.

num_grids = size(M,2);
grid_size = size(x,2);
num_slots = ceil(-c*2/a);%size(slot_len,2);
grids_out = zeros(grid_size,num_grids);

for i=1:num_grids

    for k=1:num_slots

        if strcmp(slot_type,'trapazoid');
            %comptues the secant line that forms the slanted ends of a
trapaziod
            x_start = c(i)+a(i)*(k-1);
            x_end = c(i)+w(i)+a(i)*(k-1);
            y_start = sqrt(R_slit^2-x_start^2);
            y_end = sqrt(R_slit^2-x_end^2);
            slope = (y_end-y_start)/(x_end-x_start);
            y_int = y_start - slope*(x_start);
```

99

```matlab
            trap_slot_len = slope*(x) + y_int;

            for j=1:grid_size

                H1 = heaviside(x(j)-(a(i)*(k-1)+w(i)+c(i))/M(i));
                H2 = heaviside(x(j)-(a(i)*(k-1)+c(i))/M(i));
                grids_out(j,i) = grids_out(j,i) + (H2'-
H1')*trap_slot_len(j)/M(i);

            end
%               subplot(4,1,1);plot(x,grids_out(:,1),'b.-');

        elseif strcmp(slot_type,'rounded');

            round_slot_len=sqrt(R_slit^2-x.^2);

            for j=1:grid_size

                H1 = heaviside(x(j)-(a(i)*(k-1)+w(i)+c(i))/M(i));
                H2 = heaviside(x(j)-(a(i)*(k-1)+c(i))/M(i));
                grids_out(j,i) = grids_out(j,i) + (H2'-
H1')*round_slot_len(j)/M(i);

            end
        elseif strcmp(slot_type,'rectangle');

            x_start = c(i)+a(i)*(k-1);
            y_start = sqrt(R_slit^2-x_start^2);
            H1 = heaviside(x-(a(i)*(k-1)+w(i)+c(i))/M(i));
            H2 = heaviside(x-(a(i)*(k-1)+c(i))/M(i));
            grids_out(:,i) = grids_out(:,i) + (H2'-H1')*y_start/M(i);

        elseif strcmp(slot_type,'specified');

            H1 = heaviside(x-(a(i)*(k-1)+w(i)+c(i))/M(i));
            H2 = heaviside(x-(a(i)*(k-1)+c(i))/M(i));
            grids_out(:,i) = grids_out(:,i) + (H2'-H1')*0.5*slot_len(k)/M(i);

        end

    end

end

% subplot(4,1,1)
% plot(x,grids_out(:,1),'b.-')
% subplot(4,1,2)
% plot(x,grids_out(:,2),'b.-')
% subplot(4,1,3)
% plot(x,grids_out(:,3),'b.-')
% subplot(4,1,4)
% plot(x,grids_out(:,4),'b.-')
```

100

A.6 calc_RMCgrids_v3.m

```
function [A_out] =
calcA_RMCgrids_v3(grids_in,num_grids,grid_size,Sx,Sy,Sz,L,R_grids,grid_dim,w,
M,N_samp,samp,mask_sep,mask_coord)

% Title: calcA_RMCgrids
% By: Ben Kowash
% Date: 12 Dec 07
%
% Description: This function computes the transmission probability that is
used
% by the ML-EM algorithm to reconstruct an image based on measured RMC
% data.  Tprob uses the project and shift method to find the transmission
% factor given a particular source location.

%This sets the algorithm up for values that fall outside of the RMC FOV
T_prob = zeros(N_samp,1);
phi_crit = -1;
FOV_RMC = 0.5*(6.7/mask_sep)*Sz;
FOV_mask = abs(w(2)/(M(2)*(1-M(2))));
if (sqrt(Sx^2+Sy^2) > FOV_RMC)
    %Phi crit is the width of the cone of acceptance for the masks
    phi_crit = 2*abs(90-acosd(FOV_mask/sqrt(Sx^2+Sy^2)));
    if (Sy == 0)
        phi_phase = 90-0.5*phi_crit;
    else
        phi_phase = atand(Sx/Sy)-0.5*phi_crit;
    end

end

%If the masks are symmetric, k can go from 1:180 and the second half is
%just the same pattern repeated. This conditional tests the masks and if
%they are symmetric speeds up the calculation.

if (sum(diff(w)) == 0)
    num_pts = round(N_samp / 2);
else
    num_pts = N_samp;
end

%Compute area of intersection between the two masks
[grid_center,Sx_mov,Sy_mov] = rotate_source(num_grids,Sx,Sy,1,M,N_samp);

%define distance between detector plane mask and top RMC mask in x-y plane
d = sqrt((grid_center(num_grids,1)-grid_center(1,1))^2 +
(grid_center(num_grids,2)-grid_center(1,2))^2);
A_tot = (pi*R_grids(num_grids)^2); %R_grids(num_grids)

if ((R_grids(num_grids)+d)<= R_grids(1))
    A_int = A_tot;
else

    %Define angles between center of circles and points of intersection on
```

101

```matlab
    %circles
    alpha = 2*acos((R_grids(1)^2 + d^2 - R_grids(num_grids)^2) /
(2*R_grids(1)*d));
    beta = 2*acos((R_grids(num_grids)^2 + d^2 - R_grids(1)^2) /
(2*R_grids(num_grids)*d));

    %Define the total intersection area
    A_int = 0.5*alpha*R_grids(1)^2 - 0.5*R_grids(1)^2*sin(alpha) +
0.5*beta*R_grids(num_grids)^2 - 0.5*R_grids(num_grids)^2*sin(beta);
end

%This loop computes the transmission probability as a function of rotation
%angle k.

for k=1:num_pts

    [grid_center,Sx_mov,Sy_mov] =
rotate_source(num_grids,Sx,Sy,samp(k),M,N_samp);
    if (phi_crit > 0)

        if ((phi_phase >= 0) && (samp(k) > phi_phase && samp(k) <
phi_phase+phi_crit) || ((samp(k) > 180+phi_phase && samp(k) <
180+phi_phase+phi_crit)))

            T_prob(k) =
shift_RMCgrids_v5(grids_in(:,1:2),2,grid_size,grid_center(1:2,:),R_grids(1:2)
,grid_dim,Sx_mov,Sy_mov,Sz,samp(k)) ./ A_tot;

        elseif ((phi_phase < 0) && (samp(k) < (phi_phase+phi_crit)) ||
(samp(k) < phi_phase+180 && samp(k) > phi_phase+180+phi_crit) || ((samp(k) >
360+phi_phase && samp(k) < 360+phi_phase+phi_crit)))

            T_prob(k) =
shift_RMCgrids_v5(grids_in(:,1:2),2,grid_size,grid_center(1:2,:),R_grids(1:2)
,grid_dim,Sx_mov,Sy_mov,Sz,samp(k)) ./ A_tot;

        end

    else

        %calculates
        T_prob(k) =
shift_RMCgrids_v5(grids_in,num_grids,grid_size,grid_center,R_grids,grid_dim,S
x_mov,Sy_mov,Sz,samp(k)) ./ A_tot;
        T_prob(k) = T_prob(k) +
shift_RMCgrids_v5(grids_in(:,1:2),2,grid_size,grid_center(1:2,:),R_grids(1,1:
2),grid_dim,Sx_mov,Sy_mov,Sz,k)*(A_tot-A_int)/A_tot^2;
%         area(k) = mask_matrix_builder(R_grids,grid_center,mask_coord);
    end

end
% save('F:\Lab RMC\Results\Movies\mask_movie.mat','Mask8_16_0','area');
% T_prob = area./A_tot;
% plot(T_prob,'r.-');
```

102

```matlab
% pause;


if (num_pts == round(N_samp/2))
    T_prob(round(N_samp/2)+1:N_samp) = T_prob(1:round(N_samp/2));
end



A_out = T_prob;
```

A.7 Write_RMCLib.m
```matlab
function Write_RMCLib(lib_title,A,x,x_max,dx,y,y_max,dy,Home_Address)

%By: Ben Kowash
%Date: 17 Jun 08
%
%v 1.0
%Description: This function takes in data about a system run and writes a
%RMC system library based on the input information.

lib_path = [Home_Address,'RMCLib\System_Matrix\'];

lib_vol = [lib_path,lib_title,'.mat'];
save(lib_vol,'A','x','x_max','dx','y','y_max','dy')
```

A.7 shift_RMCgrids_v5.m
```matlab
function [T_out] =
shift_RMCgrids_v5(grids_in,num_grids,grid_size,grid_center,R_grids,grid_dim,x
p,yp,zp,pos_plot)

% Title: shift_RMCgrids
% By: Ben Kowash
% Date: 12 Dec 07
% Updated: 2 May 08
% version: 4
%
% Description: This function takes a vector of grids in and then shifts the
% grids with respect to the first grid dependent on the location of the
% source.  The function "get_proj" is used in this routine to calculate the
% center of the new shifted grid so that the new position can be computed.
%
% In this updated version I find the edges of the slits using Matlab's FIND
% command and then rather than computer the solid angle I just find the
% ratio between the area of the rectangles and the entire disk.  This gives
% me the % photons transmitted.
%
% Differences from v.3: Instead of searching the entire grid of Q1 =
% prod(masks), I now circshift Q1 and take the difference.  This then
% leaves only the points where the data changes from zero to 1.
%
% v.5 allows the function to compute the mask area of trapazoid slots.  This
% includes finding the right and left edge of every slot using a slightly
modified circshift
% method from previous versions.  It also finds the corners of the trapzoid
```

103

```matlab
% with two top edge (TE) points and two bottom edge points (BE).

grid_overlap = ones(num_grids,1);
grid = zeros(grid_size,num_grids);
grid(:,1) = grids_in(:,1);

for i=2:num_grids

    %Find the left & right edges to ensure the grids overlap
    LE = grid_center(i,1) - R_grids(i); %Left edge of grid i
    RE = grid_center(i,1) + R_grids(i); %Right edge of grid i
    if (LE > R_grids(1)) || (RE < -R_grids(1))
        grid_overlap(i) = 0;
    end

    if (grid_overlap ~= 0)
        %Shift grid 'i' based on the location of the grid 'i' center wrt grid
1
        shift = round(grid_center(i,1) / (2*R_grids(1)) * grid_size);
        if (shift >= 0)
            grid(shift+1:grid_size,i) = grids_in(1:grid_size-shift,i);
            grid(1:shift,i) = 0;
        elseif (shift < 0)
            grid(1:grid_size-abs(shift),i) =
grids_in(abs(shift)+1:grid_size,i);
            grid(grid_size-abs(shift):grid_size,i) = 0;
        end
    end

end


Q1 = prod(grid,2);
Q2 = abs(Q1-circshift(Q1,1));
% figure(3);
% subplot(1,2,1);plot(Q2,'b',Q1,'r');hold on;
% subplot(1,2,1);plot(Q1,'r');hold off;
first = find(Q2 ~= 0);
Q2 = round(Q2./min([Q1(first(1)) Q2(first(length(first)))]));
mask_area = 0;
rect_edges = find(Q2 ~= 0);

for i = 2:2:length(rect_edges);
    rect_edges(i) = rect_edges(i) - 1;
end;

rect_size = size(rect_edges,1);
j = 1;
% figure(4);
p(1:5,1:2,1:rect_size-1) = 0;
while j<=rect_size-1

    LE = grid_dim(1,rect_edges(j));
    TE(1) = min(grid(rect_edges(j),:) + grid_center(:,2)');
```

104

```matlab
    BE(1) = max(grid_center(:,2)' - grid(rect_edges(j),:));
%     if (Q2(rect_edges(j+1)) ~= 0)
    RE = grid_dim(1,abs(rect_edges(j+1)));
    TE(2) = min(grid(rect_edges(j+1),:) + grid_center(:,2)');
    BE(2) = max(grid_center(:,2)' - grid(rect_edges(j+1),:));
%     else
%         LE = 0;
%         RE = 0;
%         TE(:) = 0;
%         BE(:) = 0;
%     end

    p(:,:,j) = [LE BE(1); LE TE(1); RE TE(2); RE BE(2);LE BE(1)];

    mask_area = mask_area + (RE-LE)*(min(TE)-max(BE))+.5*abs(TE(1)-
TE(2))*(RE-LE)+.5*abs(BE(1)-BE(2))*(RE-LE);

    j = j+2;

end


% figure(1);plot(Q1);legend(num2str(mask_area));hold on;

% for j = 1:rect_size-1;
%     subplot(1,2,2);
%     plot(p(:,1,j),p(:,2,j),'b');hold on;
% end;
% hold off;

x=-5:.01:5;
% if num_grids > 2;
%     plot(grid_dim,grid(:,1),'r');axis([-5 5 -5 5]);
%     hold on
%     plot(x,sqrt(R_grids(1)^2-(x-
grid_center(4,1)).^2)+grid_center(4,2),'b');
%     plot(x,-sqrt(R_grids(1)^2-(x-
grid_center(4,1)).^2)+grid_center(4,2),'b');
%     plot(grid_dim,-grid(:,1),'r')
%     plot(grid_dim,grid(:,2) + grid_center(2,2));
%     plot(grid_dim,grid_center(2,2) - grid(:,2));
%     plot(grid_dim,grid(:,3) + grid_center(3,2),'g');
%     plot(grid_dim,grid_center(3,2) - grid(:,3),'g');
%     plot(grid_dim,grid(:,4) + grid_center(4,2),'m');
%     plot(grid_dim,grid_center(4,2) - grid(:,4),'m');
%     legend(num2str(mask_area))
%     pause(0.1)
%     hold off
% else
%     figure(2);
%     plot(grid_dim,grid(:,1),'r');axis([-5 5 -5 5]);
%     hold on
%     plot(grid_dim,-grid(:,1),'r')
%     plot(grid_dim,grid(:,2) + grid_center(2,2));
```

105

```matlab
%     plot(grid_dim,grid_center(2,2) - grid(:,2));
% %     plot(grid_dim,grid(:,3) + grid_center(3,2),'g');
% %     plot(grid_dim,grid_center(3,2) - grid(:,3),'g');
% %     plot(grid_dim,grid(:,4) + grid_center(4,2),'y');
% %     plot(grid_dim,grid_center(4,2) - grid(:,4),'y');
%     legend(num2str(mask_area))
%     pause(0.1)
%     hold off
% end;

if (prod(grid_overlap) == 0)
    T_out = 0;
else
    T_out = mask_area;
end
```

A.8 mask_matrix_builder.m

```matlab
function [open_area] = mask_matrix_builder(R_grids,grid_center,mask_coord)

%Mask Matrix Builder
%18 Jan 2011


r = R_grids(1);
step =.01;
M = R_grids(1)./R_grids;

grid_center(:,1) = grid_center(:,1)-grid_center(4,1);
grid_center(:,2) = grid_center(:,2)-grid_center(4,2);

x1 = -r:step:r;
% y1 = sqrt(r^2-x1.^2);
% y2 = -sqrt(r^2-x1.^2);
%
% y3 = -r:step:r;
% x2 = sqrt(r^2-y3.^2);
% x3 = -sqrt(r^2-y3.^2);

theta_step = .01;
theta = 0:theta_step:2*pi+theta_step;

[xy_coord(:,1,1),xy_coord(:,2,1)] = pol2cart(theta,r);


% xy_coord(:,1,1) = cat(2,cat(2,x1,x1),cat(2,x2,x3));
% xy_coord(:,2,1) = cat(2,cat(2,y1,y2),cat(2,y3,y3));

mask_coord = mask_coord(1:4,:,:);
slot_coord(:,:,:,1) = mask_coord;%*2.54;
[~,~,num_slots] = size(mask_coord);

for i = 1:4;
        xy_coord(:,1,i) = (xy_coord(:,1,1)./M(i))+grid_center(i,1);
        xy_coord(:,2,i) = (xy_coord(:,2,1)./M(i))+grid_center(i,2);
```

106

```
        slot_coord(:,1,:,i) = (slot_coord(:,1,:,1)./M(i))+grid_center(i,1);
        slot_coord(:,2,:,i) = (slot_coord(:,2,:,1)./M(i))+grid_center(i,2);
        xy_loc(:,1,i) = round(xy_coord(:,1,i)/step) + length(x1)+100;
        xy_loc(:,2,i) = length(x1)+100 - round(xy_coord(:,2,i)/step);
        slot_loc(:,1,:,i) = round(slot_coord(:,1,:,i)/step) + length(x1)+100;
        slot_loc(:,2,:,i) = length(x1)+100 - round(slot_coord(:,2,:,i)/step);
end;

% figure(3);plot(xy_coord(:,1,1),xy_coord(:,2,1),'r-');hold on;
% plot(xy_coord(:,1,2),xy_coord(:,2,2),'b-');
% plot(xy_coord(:,1,3),xy_coord(:,2,3),'g-');
% plot(xy_coord(:,1,4),xy_coord(:,2,4),'y-');

grid1(1:2*length(x1)+101,1:2*length(x1)+101)=0;
grid2 = grid1;
grid3 = grid2;
grid4 = grid3;

% plot(xy_loc(:,2,2),xy_loc(:,1,2));
    for i = 1:length(xy_loc);

        grid1(xy_loc(i,2,1),xy_loc(i,1,1))=1;
        grid2(xy_loc(i,2,2),xy_loc(i,1,2))=1;
        grid3(xy_loc(i,2,3),xy_loc(i,1,3))=1;
        grid4(xy_loc(i,2,4),xy_loc(i,1,4))=1;

    end;

% grid1 = imfill(grid1,'holes');
% grid2 = imfill(grid2,'holes');
% grid3 = imfill(grid3,'holes');
% grid4 = imfill(grid4,'holes');
% det = abs(1-grid4);

grid1 = roipoly(grid1,xy_loc(:,1,1),xy_loc(:,2,1));
grid2 = roipoly(grid2,xy_loc(:,1,2),xy_loc(:,2,2));
grid3 = roipoly(grid3,xy_loc(:,1,3),xy_loc(:,2,3));
grid4 = roipoly(grid4,xy_loc(:,1,4),xy_loc(:,2,4));
det = abs(1-grid4);



slots1 = 0;
slots2 = 0;
slots3 = 0;
slots4 = 0;

for i = 1:num_slots;
    slots1 = slots1 + roipoly(grid1,slot_loc(:,1,i,1),slot_loc(:,2,i,1));
    slots2 = slots2 + roipoly(grid2,slot_loc(:,1,i,2),slot_loc(:,2,i,2));
    slots3 = slots3 + roipoly(grid3,slot_loc(:,1,i,3),slot_loc(:,2,i,3));
    slots4 = slots4 + roipoly(grid4,slot_loc(:,1,i,4),slot_loc(:,2,i,4));
end;

grid1 = grid1-slots1;
```

107

```
grid2 = grid2-slots2;
grid3 = grid3-slots3;
grid4 = grid4-slots4;

c = ceil((grid1+grid2+grid3+grid4)./4);
composite = c + det;
composite = ceil(composite./max(max(composite)));
composite = abs(1-composite);
open_area = length(nonzeros(composite))*step^2;
grey = -(c+det.*.8);
figure(4);imagesc(grey(400:1500,200:1450));colormap('gray');axis
off;title(open_area,'FontSize',24);
%
figure(5);imshow(composite(341:1186,341:1186),'InitialMagnification',20);xlab
el(open_area,'FontSize',24);
% pause(.01);
```

A.9 Resample_RMC.m

```
function [T_out] = Resample_RMC(raw_file,home,num_resample)
%function [T_out] = Resample_RMC(pos,cnt,home,num_resample)

%Function for resampling RMC data for use in a bootstrap error analysis
%
% Ben Kowash
% Date: 24 Apr 08
%
% This function takes the raw data generated by the Continuous RMC
% Labview routine, and resamples it to generate 'N' independant
% realizations of the same modulation profile.  The output is a length PxN
% matrix, where P is the # of independent angles of rotation for the RMC.

    %Open the raw data file
    load(raw_file);
    cnt = cnt';
    pos = pos';
    pos_start = home;

    %Reformat the position data array into angular bins
    pos_size = size(pos,1);

    %First we must adddress the decoding counter overflow
%       gate = 1;
%       stop_ovfl = pos_size;
%       for i=2:pos_size
%
%           if ((pos(i) < pos(i-1)) && (gate==1))
%
%               gate = 0;
%               start_ovfl = i;
%               j=start_ovfl+1;
%               while ((pos(j) >= pos(j-1)))
%                   j = j+1;
%                   if (j==pos_size)
%                       break
%                   end
```

108

```
%              end
%              %The following conditional is used because sometimes the
overflow
%              %counter decrements on the final value... i.e. pos(i) = 6300
and
%              %pos(i-1) = 6400. Without this conditional the overflow counter
%              %would be off by one position.
%              if ((pos(j) > 3000) && j<pos_size)
%                   j = j+1;
%              end
%              %
%              stop_ovfl = j-1;
%              pos(start_ovfl:stop_ovfl) = 65535 + pos(start_ovfl:stop_ovfl);
%
%          end
%
%          if (i>stop_ovfl)
%              gate = 1;
%          end
%
%      end

    for i=1:pos_size

        if (pos(i) > pos_start)
            pos(i) = pos(i) - pos_start;
        else
            pos(i) = 72000 - pos_start + pos(i);
        end

    end

    ang_pos = 360 * pos / (18000 * 4);

    %Count # of total rotations in file
    num_rot = 1;
    for i=2:pos_size

        if (ang_pos(i) < ang_pos(i-1))
            num_rot = num_rot + 1;
        end
    end

    T_rot = zeros(360,num_rot);
    gap = zeros(pos_size-1,1);

    %Put the data into Q independent sampling vectors.  Each vector here
    %represents one complete rotation of the RMC.
    k=1;
    for i=2:pos_size

        incr = round(ang_pos(i));
        if (incr==0)
            incr = 360;
        end
```

109

```matlab
        prev = round(ang_pos(i-1));
        if (prev==0)
            prev = 360;
        end

        gap(i-1) = incr-prev;
        if (gap(i-1) <=2)
            T_rot(incr,k) = T_rot(incr,k) + (cnt(i)-cnt(i-1));
        else
            for j=prev:prev+gap(i-1)
                T_rot(j,k) = T_rot(j,k) + (cnt(i)-cnt(i-1))/gap(i-1);
            end
        end

        if (ang_pos(i) < ang_pos(i-1))
            k = k + 1;
        end

    end

    %Error check to make sure all vectors are statistically similar -- this
    %is important if the RMC only completed a partial rotation on the final
    %pass
    T_sum = sum(T_rot);
    T_mean = mean(T_sum);
    T_std = std(T_sum);
    gate = 0;
    while (gate == 0)

        T_min = min(T_sum);
        min_pos = find(T_sum == T_min);
        if (T_min < T_mean - 3*T_std)
            T_rot(:,min_pos) = [];
            T_sum(min_pos) = [];
            T_mean = mean(T_sum);
            T_std = std(T_sum);
        else
            gate = 1;
        end

    end

    num_rot = size(T_rot,2);
    T_out = zeros(360,num_resample);
    T_out(:,1) = sum(T_rot,2);

    for i=2:num_resample

        f = ceil(num_rot .* rand(num_rot,1));
        T_out(:,i) = sum(T_rot(:,f),2);

    end

end
```

110

A.10 get_LLRMC.m

```matlab
function [LL] =
get_LLRMC(T_in,A_in,x_max,y_max,epsRMC,act,bkg,tau,num_sys,N_samp)

%Compute the log-liklihood ratio for the source and for no source.
yn_bar = zeros(size(T_in,2),1);

tic
for i=1:x_max*y_max

    yn_bar = (A_in(:,i).*epsRMC(1).*act + bkg).*tau';
    LL(i) = sum(T_in .* log(yn_bar) - yn_bar);

end
```

A.11 get_FisherRMC.m

```matlab
function [F_act,F_x,F_y,CRLB_act,CRLB_x,CRLB_y] =
get_FisherRMC(A_in,x_in,y_in,x_max,y_max,N_samp,act,bkg,tau,epsRMC,num_sys,R_
det,Sz)

N_samp_holder = 1; %A Place holder to keep track of position in matrix A
tau_tot = tau(1,:);
for k=1:num_sys

    N_samp_holder = N_samp_holder + N_samp(k);

    if (k>1)
        tau_tot = [tau_tot,tau(k,:)];
    end

end

N_samp_tot =sum(N_samp);
d_alpha = zeros(N_samp_tot,x_max*y_max);
d_beta  = zeros(N_samp_tot,x_max*y_max);

N_samp_tot = 360;
for k=1:N_samp_tot

    A_sub = reshape(A_in(k,:),x_max,y_max);
    %figure(1)
    %subplot(3,1,1)
    %imagesc(A_sub)
    %colorbar
    %pause(0.01)
    [d_aSub,d_bSub] = gradient(A_sub);
    d_alpha(k,:) = reshape(d_aSub,1,x_max*y_max);
    d_beta(k,:) = reshape(d_bSub,1,x_max*y_max);
    %subplot(3,1,2)
    %imagesc(d_aSub)
    %colorbar
    %subplot(3,1,3)
  %imagesc(d_bSub)
   %colorbar
```

111

```
end

clear A_sub

h = waitbar(0,'Computing Fisher Information');
for i=1:(x_max*y_max)

    pn_vec = zeros(1,3);
    F = zeros(3,3);
    Q = zeros(3,3);

    for k=1:N_samp_tot

        if (A_in(k,i) < 0)
            A_in(k,i) = 0;
        end
        pn_vec(1,1) = (tau(k) * epsRMC(1) * A_in(k,i));
        pn_vec(1,2) = (tau(k) * act * epsRMC(1) * d_alpha(k,i));
        pn_vec(1,3) = (tau(k) * act * epsRMC(1) * d_beta(k,i));
        Q(1,1) = tau(k) * (act * epsRMC(1) * A_in(k,i) + bkg);
        Q(2,2) = Q(1,1);
        Q(3,3) = Q(1,1);
        F = F + pn_vec' * pn_vec / Q;
        if sum(F) < 0
            pause
        end

    end

    F_act(i) = F(1,1);
    F_x(i) = F(2,2);
    F_y(i) = F(3,3);
    sys_var = F^-1;
    CRLB_act(i) = sys_var(1,1);
    CRLB_x(i) = sys_var(2,2);
    CRLB_y(i) = sys_var(3,3);

    waitbar(i/(x_max*y_max))
end
close(h)
```

A.12 RMC_MLEM.m

```
function lam_new = RMC_MLEM(lam_old, A, y, b, a)

% Title: RMC ML-EM routine
%
% By: Ben Kowash
% Date: 15 Oct 07
%
% Description: This routine takes input data and computes the estimate
% lambda_new based on the properties of the system.  The method used is a
% maximum-liklihood expectation-maximum iterative algorithm.
```

112

```matlab
lam_new = lam_old .* (A' * (y ./ (A * lam_old + b))) ./ a;
```

A.13 RMC_Omega.m

```matlab
function g = RMC_Omega(R,z,rho)


% Ben Kowash
% 24 Sep 07

%Description: This function returns the solid angle of a point source
subtended by a
%circular disk (i.e. RMC front mask/detector).  The method used in this
%algorithm is provided by S. Tryka in the paper "A Method for Calculating
%the Average Solid Angle Subtended by a Circular Disk from Uniformly
%Distributed Points Within a Coaxial Circular Plane", Review of Scientific
%Instruments, Vol 70, #10, pg 3915-3920, Oct 1999.
switch rho>=0

    case rho==0
        g = 2.*pi.*(1-z./sqrt(R.^2+z.^2));

    case rho<R
        %Calc parameters for elliptic integrals of 1st & 3rd kind
        Pp_sq = -4.*R.*rho ./ ((R-rho).^2 + z.^2);
        qp = -4.*R.*rho / (R-rho).^2;

        %Calc elliptic integral of 1st kind
        fun_K = @(delta)(1./(1-Pp_sq.*sin(delta).^2).^0.5);
        K_Pp = quad(fun_K,0,pi/2,1E-6);

        %Calc elliptic integral of 3rd kind
        fun_PI = @(delta)(1./((1-qp.*sin(delta).^2).*(1-
Pp_sq.*sin(delta).^2).^0.5));
        PI = quad(fun_PI,0,pi/2,1E-6);

        %Calc Omega
        g = (2.*pi) - (2.*z./sqrt((R-rho).^2+z.^2).*(K_Pp+(R+rho)./(R-
rho).*PI));

    case rho==R

        Ppr_sq = -4.*R.^2 ./ z.^2;

        %Calc elliptic integral of 1st kind
        fun_K = @(delta)(1./(1-Ppr_sq.*sin(delta).^2).^0.5);
        K_Ppr = quad(fun_K,0,pi/2,1E-6);

        %Calc Omega
        g = (pi - 2.*K_Ppr);

    case rho>R
        %Calc parameters for elliptic integrals of 1st & 3rd kind
        Pp_sq = -4.*R.*rho / ((R-rho).^2 + z.^2);
```

113

```matlab
        qp = -4.*R.*rho ./ (R-rho).^2;

        %Calc elliptic integral of 1st kind
        fun_K = @(delta)(1./(1-Pp_sq.*sin(delta).^2).^0.5);
        K_Pp = quad(fun_K,0,pi/2,1E-6);

        %Calc elliptic integral of 3rd kind
        fun = @(delta)(1./((1-qp.*sin(delta).^2).*(1-
Pp_sq.*sin(delta).^2).^0.5));
        PI = quadl(fun,0,pi/2,1E-6);

        %Calc Omega
        g1 = -2.*z;
        g2 = sqrt((R-rho).^2+z.^2);
        g3 = (K_Pp+PI.*(R+rho)./(R-rho));
        g = g1.*g3./g2;

    otherwise
        g = -100;

end

end
```

A.14 RMC_raw.m

```matlab
function [T_dat] = RMC_raw(raw_file,RMC_file,home,plot_val)

%Continuous RMC Raw Data Converter
%
% Ben Kowash
% Date: 8 Aug 07
%
% This subroutine takes the raw data generated by the Continuous RMC
% Labview routine, and converts it into properly binned RMC data that can
% be processed in an appropriate routine (ie MLEM, detector algorithm, etc)

%Open the raw data file
load(raw_file);
cnt = cnt';
pos = pos';
pos_start = home;

%Reformat the position data array into angular bins
pos_size = size(pos,1);


for i=1:pos_size

    if (pos(i) > pos_start)
        pos(i) = pos(i) - pos_start;
    else
        pos(i) = 72000 - pos_start + pos(i);
    end
```

114

```matlab
end

ang_pos = 360 * pos / (18000 * 4);

if (plot_val == 'T')
    figure(1)
    plot(ang_pos(:),'g.')
end

T_dat = zeros(360,1);
gap = zeros(pos_size-1,1);
for i=2:pos_size

    incr = round(ang_pos(i));
    if (incr==0)
        incr = 360;
    end
    prev = round(ang_pos(i-1));
    if (prev==0)
        prev = 360;
    end

    gap(i-1) = incr-prev;
    if (gap(i-1) <=2)
        T_dat(incr,1) = T_dat(incr,1) + (cnt(i)-cnt(i-1));
    else
        for j=prev:prev+gap(i-1)
            T_dat(j,1) = T_dat(j,1) + (cnt(i)-cnt(i-1))/gap(i-1);
        end
    end

end

cnt = T_dat';
if (exist([RMC_file])==0)
    save([RMC_file],'cnt','pos')
    ['New File Written = ',RMC_file]
else
    ['The file "',RMC_file,'" already exists!']
end

if (plot_val == 'T')
    figure(2)
    plot(T_dat,'b-o')
end
```

A.15 rotate_source.m

```matlab
function [grid_center,Sx_mov,Sy_mov] =
rotate_source(num_grids,Sx,Sy,angular_pos,M,N_samp)

% Title: rotate_source
% By: Ben Kowash
```

115

```matlab
% Date: 12 Dec 07
%
% Description: This function takes in the position of the RMC system and
% the location of the source.  The location of the projected grid center
% for each grid is then output.

%Grid center contains the x & y coordinates of the projected mask center
grid_center = zeros(num_grids,2);


omega = 2*pi*angular_pos / N_samp;


%Define the source position for the k-th time step
if ((Sx > 0) && (Sy >= 0)) %For src in 1st quadrant
    Sx_mov = sqrt(Sx^2+Sy^2) * (cos(omega+atan(Sy/Sx)));
    Sy_mov = sqrt(Sx^2+Sy^2) * (sin(omega+atan(Sy/Sx)));
elseif ((Sx < 0) && (Sy >= 0)) %For src in 2nd quadrant
    Sx_mov = sqrt(Sx^2+Sy^2) * (cos(omega+atan(Sy/Sx) + pi));
    Sy_mov = sqrt(Sx^2+Sy^2) * (sin(omega+atan(Sy/Sx) + pi));
elseif ((Sx < 0) && (Sy < 0)) %For src in 3rd quadrant
    Sx_mov = sqrt(Sx^2+Sy^2) * (cos(omega+atan(Sy/Sx) + pi));
    Sy_mov = sqrt(Sx^2+Sy^2) * (sin(omega+atan(Sy/Sx) + pi));
elseif ((Sx > 0) && (Sy < 0)) %For src in 4th quadrant
    Sx_mov = sqrt(Sx^2+Sy^2) * (cos(omega+atan(Sy/Sx)));
    Sy_mov = sqrt(Sx^2+Sy^2) * (sin(omega+atan(Sy/Sx)));
elseif (Sx == 0) && (Sy >=0)
    Sx_mov = sqrt(Sx^2+Sy^2) * (cos(omega+pi/2));
    Sy_mov = sqrt(Sx^2+Sy^2) * (sin(omega+pi/2));
elseif (Sx == 0) && (Sy < 0)
    Sx_mov = sqrt(Sx^2+Sy^2) * (cos(omega-pi/2));
    Sy_mov = sqrt(Sx^2+Sy^2) * (sin(omega-pi/2));
end


%Next find new location of A2center
for i=2:num_grids

    [grid_center(i,1),grid_center(i,2)] =
backproj_RMC(Sx_mov,Sy_mov,0,0,M(i),0,0,0);

end
```

A.16 ssim.m

```matlab
%Image Quality Assessment
%This will compute a Structual Similarity Based Image Quality Assessment
%Index (SSIM) for an image compared to a truth image.

clear all;
close all;
clc;

%Build truth matrix
bk = 15; %cps
src = .330; %mCi
```

116

```matlab
x_loc = 10; %x pixel location
y_loc = -16; %y pixel location
num_pix = 40; %number of pixels in row or column
% loc = ((sqrt(num_pix)/2)+(x_loc)-
1)*sqrt(num_pix)+((sqrt(num_pix)/2)+(y_loc)); %find location in array
loc = [x_loc num_pix+y_loc];
truth(1:num_pix,1:num_pix)=bk/(3.7*10^7); %sets array to bk in mCi
truth(loc(1),loc(2))=src;

for j = 1:8;

    path='J:\Lab RMC\Results\Ex 100mlem 100bs\';
    file = ['Mask',num2str(j),'-20cm'];

    for i = 1:11;

        %load image data from figure for comparison
        if i == 11;
            time = 600;
        else
            time = 30*i;
        end;

        name=[path,file,num2str(time),'s.fig'];
        load(name,'-mat');
        img =
reshape(hgS_070000.children(1,1).children(1,1).properties.CData,1,num_pix);%c
onverts fig data into array

        %Sets parameters for SSIM
        mu_truth = mean(truth);
        mu_img = mean(img);
        var_truth = var(truth);
        var_img = var(img);
        sig_truth = sqrt(var_truth);
        sig_img = sqrt(var_img);
        cov_mat = cov(truth,img);
        cov_truth_img = cov_mat(1,2);

        alpha = 1;   %These are using to adjust importances between luminance,
constrast, and structure
        beta = 1;
        gamma = 1;

        c1 = 0;      %These constants compensate for instabilities for near
identical differnces in the denominator
        c2 = 0;
        c3 = 0;

        l = (2*mu_truth*mu_img+c1)/(mu_truth^2+mu_img^2+c1); %luminance
        c = (2*sig_truth*sig_img+c2)/(var_truth+var_img+c2); %contrast
        s = (cov_truth_img+c3)/(sig_truth*sig_img+c3);       %structure

        SSIM(i,j) = l^alpha*c^beta*s^gamma;
```

117

```
    end;
end;

semilogy(cat(2,30:30:300,600),SSIM,'.-');legend('Mask 1','Mask 2','Mask
3','Mask 4','Mask 5','Mask 6','Mask 7','Mask 8');
```

A.17 backproj_RMC.m

```
function [x_center,y_center,w_proj,a_proj,c_proj] =
backproj_RMC(Sx_mov,Sy_mov,Ax_pr,Ay_pr,M,w,a,c)

% Function backproj_RMC
%
% By: Ben Kowash
% Date: 24 Oct 07
% Technique by: Ziya Akcasu
% Version: 1.0
%
% Description: This function first takes a mask located at z=0 (i.e. a
% mask located at the detector plane) and backprojects it up to the plane
% of the first mask.  These coordinates are then used to compare against
% the first mask to determine the total detector area uncovered as the
% mask system rotates.

%Compute the location of the projected mask center
%x_center = Sx_mov + (Sx_mov-Ax_pr)*(Az-Sz)/(Sz);
x_center = Sx_mov - (Sx_mov-Ax_pr)/M;
%y_center = Sy_mov + (Sy_mov-Ay_pr)*(Az-Sz)/(Sz);
y_center = Sy_mov - (Sy_mov-Ay_pr)/M;

%Compute the magnitude of the projected w.
w_proj = (w/M);

%Compute the magnitude of the projected a.
a_proj = (a/M);

%Computer the magnitude of the projected c.
c_proj = (c/M);
```

A.18 isEven.m

```
function [TF] = isEven(val)

%By: Ben Kowash
%Date: 26 Feb 08
%
%Description: This function takes in a value and determines whether that
%value is odd or even. If the value is even a 1 is returned.  Otherwise a 0
%is returned for false.

for i=1:size(val)
    if ((mod(val(i),2)) == 0)
        TF(i) = 1;
```

118

```
    else
        TF(i) = 0;
    end
end
```

A.19 Splice.m

```
function [] = Splice(RMC_file,home,desired_time)

%This allows for a long RMC measurement to be spliced into shorter
%measurements to look at the time dependency of reconstruction.  It
%requires that the RMC_file index be a three digit collected time
%identifier. eg. 'C:\RMCout\RMC_450 - Mask5-20cm.mat' would be for a 450
%second measurement with Mask5-20cm being the title entered into the RMC
%Continuous VI in labview or from the RMC command txt file. It also usese
%the raw data file associated with the collection time index.


collected_time = str2double(RMC_file(23:25));
RMC_file_name = RMC_file(26:length(RMC_file));
raw_file = ['F:\Lab RMC\RMCout\data_',num2str(collected_time),'.mat'];
load(raw_file);

%Pulls the data taken during the desired time

cnt = cnt(1:round(length(cnt)*(desired_time/collected_time)));
pos = pos(1:round(length(pos)*(desired_time/collected_time)));


new_raw_file = ['F:\Lab RMC\RMCout\data_',num2str(desired_time),'.mat'];
new_RMC_file = ['F:\Lab
RMC\RMCout\RMC_',num2str(desired_time),RMC_file_name];


save([new_raw_file],'cnt','pos');

RMC_raw(new_raw_file,new_RMC_file,home,'F')
```

A.20 Time_Detect.m

```
function [t_mean,t_std] = Time_Detect(cnt_bk,cnt_s_bk,collection_time)

%This computes time to detect based on one activity measurement for a
%specific channel window in the MCA base on the resolution of the detector
%for a specific energy level.  A detection threshold of photo-peak height
%above background is used.

% clear all;
% clc;
% close all;

%standard deviation for counts
cnt_s_bk = sum(diff(cnt_s_bk));
cnt_s_bk_std = sqrt(cnt_s_bk);
```

119

```matlab
cnt_bk_std = sqrt(cnt_bk);



%activity
s_bk_mean = cnt_s_bk/collection_time;
s_bk_std = cnt_s_bk_std/collection_time;
bk_mean = cnt_bk/collection_time;
bk_std = cnt_bk_std/collection_time;

src_mean = s_bk_mean - bk_mean;
src_std = sqrt(s_bk_std^2 + bk_std^2);

det_res = 7.5; % detector resolution in percent at specific energy level,
122.10 keV for NaI
energy = 122.10; % [keV]
FWHM = (det_res/100)*energy;
peak_std = FWHM/(2*sqrt(2*log(2)));


energy_window = 94:134;
peak_height = 500;


time = 20:.05:120;

for k = 1:1000;
    src = src_mean + src_std*randn(1,1);
    bk = bk_mean + bk_std*randn(1,1);

    for i = 1:length(time);
        y =
(bk*time(i))+(src*time(i))*normpdf(energy_window,energy,peak_std);

        %This it the histogram of the photopeak growth through time
        bar(energy_window,y);axis([min(energy_window) max(energy_window) 0
1600]);
        pause(.05);

        if max(y)-min(y) > peak_height;
            t(k) = time(i);
            break
        end;
    end;
end;
t_mean = mean(t);
t_std = sqrt(var(t));

% time_title = ['Mean=',num2str(t_mean),'+-',num2str(t_std)];
% hist(t,100);title(time_title);
```

120

Appendix B. Experimental Setup and System Settings

B.1 List of Equipment and Commonly used settings

Equipment List:
        NIM bin: Ortec 4001A
        Detector/PMT: Bicron 3x3" NaI
        High voltage power supply: Tennelec 952A
        Pre-Amplifier: Ortec 113
        Shaping Amplifier: Ortec 572
        Single Channel Analyzer: Ortec 550
        Mulit-Channel Analyzer: Ortec 926 ADCAM
        Data Acq. Board: National Instruments 6111 E-PCI using a SCB-68 interface
        Stepper Motor: Applied Motion HT23-297
        Motor Driver: Applied Motion Si 3540
        Rotatary Table: Velmex B4836TS
        Motor Controller:
        Optical Encoder Ring: Renishaw RESR R20-115
        Encoder Read Head: RGH 20
        Decoder: Avago HCTL-2016 on National Instruments USB interface 6008
        Source Positioning System: Velmex Bi-slide

Commonly Used NIM settings:
        HVPS: +800 volts
        Pre-Amp: 200 µF
        Amplifier:
            Course Gain: 100
            Fine Gain: 12.76
            Shaping Time: 2 µs
        SCA:
            Mode: Normal
            Lower Window: 0.92 volts
            Upper Window: 1.31 volts
        MCA:
            Resolution: 1024

Source Information
        Co-57 disk source with 1 cm diameter
        Activity Calibrated on 20 Oct 2009 at 0.84 mCi
        AFIT Source ID: T-121

121

Commonly Used Driver Motor settings:
    Motor Resolution: MR13
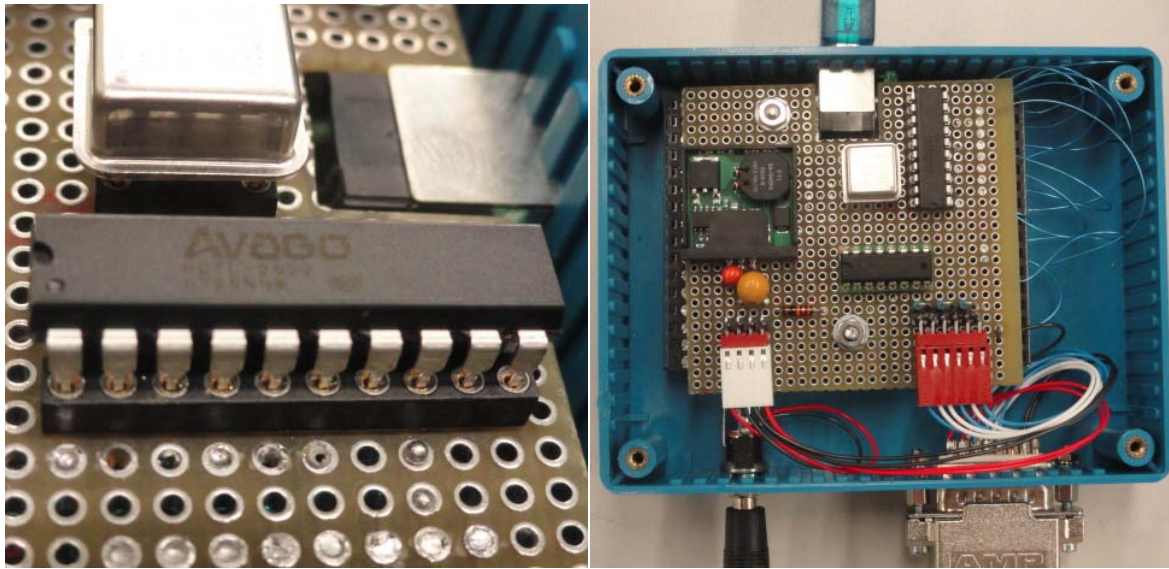   Velocity: VE0.1365
    Acceleration: AC360
    Deceleration: DE360
    Motor Current: CC1.5
    Step size: DI327

B.2 Decoding circuit with 32-bit chip installed

These photos show the installation of the Avago HCTC-2022 32-bit decoder chip installed to enable the processing of all of the positional data without having to compensate for the 16-bit chip.

Bibliography

[1] J. Yardley, "New York Times," *Indian University is Deemed Source of Radiation Exposure*, April 2010.

[2] B Johns. (2008, July) Domestic Nuclear Detection Office. [Online]. http://aapa.files.cms-plus.com/SeminarPresentations/2008PortSecurity/08SECURITY_Johns_Bob.pdf

[3] B. Kowash, "A Rotating Modulation Imager for the Orphan Source Search Promblem," Ann Arbor, 2008.

[4] D. Smith, "Rotating Modulation Collimator Imagers," *New Astronomy Reviews*, pp. 209-213, 2004.

[5] Z. Wang, "Image Quality Assessment: From Error Visibility to Structual Similarity," *IEEE*, pp. 600-612, 2004.

[6] Y. Chen, "Direct demodulation technique for rotating modulation collimator imaging," *Astronomy and Astrophysics Supplement Series*, pp. 363-368, 1998.

[7] A. Wilmore, "The imaging Properties of the Rotation Collimator," *Monthly Notices of the Royal Astronomical Society*, pp. 387-403, 1947.

[8] A. Sharma, "Non-invasive Estimation of Potassium in Bovine Liver Using Neutron Stimulated Emission Computed Tomography (NSECT)," *IEEE*, pp. 2076-2078, 2006.

[9] B. Budden, "Noise-Compensated Algebraic Reconstruction for a Rotational Modulation Gamma-Ray Imager," *IEEE Tansactions on Nuclear Science*, pp. 1-8, 2010.

[10] G. Hurford, "The RHESSI Imaging Concept," *Solar Physics*, vol. 210, no. 1-2, pp. 61-86, September 2002.

[11] G. Knoll, *Radiation Detection and Measurement*. Hoboken: John Wiley and Sons, 2000.

[12] N. Boyce, "Thermal Neutron Point Source Imaging using a Rotating Modulation Collimator (RMC)," Air Force Institute of Technology, Wright Patterson Air Force Base, 2010.

[13] S. Kay, *Fundamentals of Statistical Signal Processing Estimation Theory vol. I*.: Prentice Hall Signal Processing Series, 1993.

[14] A. Poulkou, "On sampling Expansions of Kramer Type," *Abstract and applied Analysis*, vol. 2004, no. 5, pp. 371-385, May 2002.

[15] Brook Haven National Lab. (2010, December) National Nuclear Data Center. [Online]. http://www.nndc.bnl.gov/

[16] K. Krane, *Introductory Nuclear Physics*. New York, US: John Wiley and Sons, 1988.

[17] F. J. Anscombe, "Graphs in Statistical Analysis," *American Statistician*, vol. 27, 1973.

[18] Motor Driven Rotatry Table. (2010, September) Velmex, INC. [Online]. http://www.velmex.com/pdf/rot/Motor%20Rotary%20Section.pdf

[19] E. Candes, "People Hearing without Listening: An Introduction to Compressed Sampling," *IEEE ASSP Magazine*, pp. 21-27, 2008.

[20] D. Donoho, "Reflections on COmpressed Sensing," *IEEE Theory Newsletter*, pp. 18-23, 2008.

[21] S. Kay, *Fundamentals of Statistical Signal Processing Detection Theory, vol. II*.: Prentice Hall Signal Processing, 1993.

[22] P. Marziliano, "Reconstruction of Ireegularly Sampled Discrete-Time bandlimited Signals with Unknown Sampling Locations," *IEEE Transactions on Signal Processing*, pp. 3462-3471, 2000.

[23] G. Apostolopoulos, "On-line statistical processing of radiation detector pulse trains with time-carying count rates," *Nuclear Instruments and Methods in Physics Research A*, pp. 464-473, 2008.

1. REPORT DATE (DD-MM-YYYY) 24-03-2011	2. REPORT TYPE Master's Thesis	3. DATES COVERED (From – To) Jun 2010 – Mar 2011

4. TITLE AND SUBTITLE **Adaptive Imaging Methods using a Rotating Modulation Collimator**	5a. CONTRACT NUMBER
	5b. GRANT NUMBER
	5c. PROGRAM ELEMENT NUMBER

6. AUTHOR(S) **LT Daniel T. Willcox United States Navy**	5d. PROJECT NUMBER
	5e. TASK NUMBER
	5f. WORK UNIT NUMBER

7. PERFORMING ORGANIZATION NAMES(S) AND ADDRESS(S) Air Force Institute of Technology Graduate School of Engineering and Management (AFIT/EN) 2950 Hobson Way WPAFB OH 45433-7765	8. PERFORMING ORGANIZATION REPORT NUMBER AFIT/GNE/ENP/11-M20

9. SPONSORING/MONITORING AGENCY NAME(S) AND ADDRESS(ES) Defense Threat Reduction Agency CSU ATTN: COL Mark Mattox 1900Wyoming Blvd SE Kirtland AFB, NM 87117-5669	10. SPONSOR/MONITOR'S ACRONYM(S) DTRA-OP/CSU
	11. SPONSOR/MONITOR'S REPORT NUMBER(S)

12. DISTRIBUTION/AVAILABILITY STATEMENT
APPROVED FOR PUBLIC RELEASE; DISTRIBUTION UNLIMITED

13. SUPPLEMENTARY NOTES

14. ABSTRACT
The Rotating Modulation Collimator (RMC) belongs to a larger class of radiation imaging systems that rely on either temporal or spatial modulation of incident radiation through collimation to map the location of the incident radiation source. The strengths of these detection systems include their low cost and simplicity. A major drawback is the collection time required for low radiation intensities due especially to the loss of radiation information resulting from collimation. One method of addressing this drawback for the RMC is by applying an adaptive imaging approach. As with most system design theory, there are inherent design tradeoffs for the RMC. By using different RMC configurations for the same radiation environment observation, these tradeoffs can be wagered against one another to improve overall performance. This research explores the effect of RMC configuration changes, specifically by changing the mask design, sampling method, and the angle between the image plane and the RMC centerline.

15. SUBJECT TERMS
Gamma Imaging, Rotating Modulation Collimator, Gamma Detection

16. SECURITY CLASSIFICATION OF:			17. LIMITATION OF ABSTRACT	18. NUMBER OF PAGES	19a. NAME OF RESPONSIBLE PERSON Benjamin Kowash , Maj., USAF
a. REPORT U	b. ABSTRACT U	c. THIS PAGE U	UU	140	19b. TELEPHONE NUMBER (Include area code) 937.255.3636 x4571 (benjamin.kowash@afit.edu)

Standard Form 298 (Rev. 8-98)
Prescribed by ANSI Std. Z39-18